University of Bath

UNIVERSITY OF BATH

PHD

Porous membrane phase contactor for gas-liquid homogeneous catalytic reactions. Direct hydration of propene

Lapkin, Alexei A.

Award date:
2000

Awarding institution:
University of Bath

Link to publication

Porous membrane phase contactor for gas-liquid homogeneous catalytic reactions.
Direct hydration of propene.

Submitted by Alexei A.Lapkin

for the degree of Doctor of Philosophy

of the University of Bath

2000

Signature of the author:

Alexei A.Lapkin

UMI Number: U601829

UMI U601829

ProQuest LLC
789 East Eisenhower Parkway
P.O. Box 1346
Ann Arbor, MI 48106-1346

Acknowledgements

The objective of this study is to investigate the feasibility of a high-pressure porous membrane phase contactor reactor applied to gas-liquid homogeneous catalytic reactions. The membrane has several functions in the phase contactor reactor. The primary function is to generate high interfacial area in order to provide a significant area of mass transfer between gas and liquid or two immiscible liquid phases. The secondary function is the continuous removal of the products of a reaction which potentially can shift equilibrium limited reactions towards a higher yield of a desired product. This work specifically addresses the problems of operation and performance of high-pressure membrane phase contactor reactors in the case of gas-liquid equilibrium limited reactions. Direct hydration of olefins was studied as a test reaction.

Industrial direct hydration processes are based on (1) homogeneous catalysis with heteropolyacid based catalysts, (2) trickle-bed reactors with solid acidic resin catalysts and (3) supported liquid phase (SLP) catalysts using aqueous phosphoric acid catalyst. It is the SLP technology that the membrane phase contactor is intended to improve. The major drawbacks of the SLP process are: (1) leaching of phosphoric acid and corrosion of downstream equipment, (2) low conversion of the vapour phase process and (3) low concentration of the product stream. Membrane phase contactors should, in principle, remove these limitations. An effective separation of the gaseous and liquid phases by a porous membrane should prevent loss of acid whilst enabling more flexibility in terms of operational conditions, i.e. mixed or separated feed of reagents, gas and liquid flow rates and the optimum concentration of the liquid phase acid catalyst.

Direct hydration of olefins is performed at high pressures (1.5-6.0MPa in the case of propene), which makes the stability of the gas-liquid interface within a membrane a primary concern for the operation of a contactor reactor. This issue was addressed by tailoring the membrane structure and developing an on-line process control system. Carbon membranes were used in this project because of the mechanical strength and chemical stability of carbon in strong acids. Porous carbon membranes were prepared using the technology and precursors developed by MAST Carbon Ltd, a partner company in this research project. Membranes with pore diameters in the range 0.45-0.75μm were

found to provide sufficient resistance in order to control the transmembrane pressure within ca. ±0.02MPa. This allowed experiments to be performed at 2MPa pressure over 50 hours. The on-line pressure control system utilising a specially designed fuzzy algorithm ensured the stability of the transmembrane pressure during all stages of the reactor operation: start-up, shut-down and steady state.

An experimental rig was designed and constructed for two-phase catalytic experiments. The membrane reactor was studied in the semi-continuous mode. Therefore, the yield of the main product exhibited a maximum. The best performance of the reactor is comparable with that of industrial SLP catalyst based reactors. The yield of propan-2-ol in the membrane reactor reached ca. 200 $kg/m^3_{(acid)}/hr$, with an alcohol concentration in the gaseous stream of ca. 25wt% (yield is calculated in relation to the membrane pore volume). The higher product concentration in the gaseous stream is observed in the case of the membrane reactor used in this project, due to separate feeding of reagents on each side of the membrane.

The reactor was operated in the fully-wetted mode. It was found that the reactor is limited by liquid phase mass transfer, although periodic pulsation of pressure invoked by a piston pump significantly reduced the diffusional mass transfer resistance. It is suggested that operation of the reactor with non-wetted membranes having an asymmetric porous structure would improve the performance of this reactor.

The kinetics of the propene hydration reaction was studied in a batch reactor. The kinetic model was developed on the basis of literature data on the mechanism of the liquid phase acid catalysed direct hydration of olefins. The model was implemented in the ODE solver and was fitted to the experimental data. The model was extended to include mass transfer across the porous membrane phase contactor. This reactor model was used extensively to evaluate the potential performance of the phase contactor reactor and to test the hypothesis on the mass transfer limitations of the reactor.

List of Figures

List of Tables

Contents

Homogeneous catalysis in the liquid phase plays an important role in the chemical industry. Because the number of chemicals capable of forming solutions is much greater than the number of chemicals stable in the gas phase, there is a considerably greater variety of chemical reactions and products that can be obtained in the liquid phase [1]. The same is valid for catalysts, which is well illustrated by the increase in homogeneous catalytic processes with the advent of organometallic chemistry [2, p.3]. The general characteristics of liquid phase homogeneous catalytic processes are the large number of molecules in unit of volume, consequently producing fast reaction rates, while ionic and redox reaction mechanisms, are responsible for high selectivities when compared to radical gas phase reactions. The selectivity of homogeneous catalytic processes can be modified by tailoring the complex structure of a catalyst to a specific reagent [3]. The comparatively low temperature of liquid phase processes is also an important factor, therefore reducing the capital cost of such industrial processes. As more attention is paid to the environmental efficiency of chemical processes (this includes energy and pollution) [4], the role of homogeneous catalysis in chemical industry will increase. High reactivity, selectivity and low temperatures together with great variety of chemical products comes at the price of necessary downstream separation of the homogeneous catalyst from the reaction mixture.

The problem of "decoupling the residence time of a homogeneous catalyst and reactants" [2, p.832] becomes more important as the cost of the reagent tailored homogeneous catalysts increases. It is desirable to retain and reuse homogeneous catalysts and several approaches to this problem have been developed, the benefits and disadvantages of which are listed in Table I-1.

Immobilisation of homogeneous catalysts can be achieved by covalent or ionic bonding, physical adsorption, impregnation of the porous solid support with the liquid catalyst or by containing the homogeneous catalyst within the porous solid matrix. The main aim of such exercises is to achieve continuous operation and easy catalyst recovery, which characterise heterogeneous catalytic processes. At the same time, all of these techniques mean that reactants have to diffuse to active sites also characteristic of

heterogeneous catalysis. The activity of a heterogenised catalyst is almost exclusively lower than that of the corresponding homogeneous catalyst. Activity remains unchanged only in the case of supported liquid phase (SLP) and supported aqueous phase (SAP) catalysts i.e. when the catalyst phase remains unaltered. The SLP catalytic direct hydration of alkenes is described in detail in section II.3. Most of the heterogenised catalysts also suffer from leaching. Immobilisation by physical adsorption has been applied to enzyme catalytic systems in an attempt to improve the recovery and stability of enzymes. It was also proposed to adsorb enzymes onto the surface of membranes in order to shift the reaction equilibrium by selectively removing one of the products through a membrane [5,6]. Imbedding oxygen-sensitive hydroformylation catalysts in a polymer matrix also increases the stability of the catalyst [7].

Table I-1. Approaches to retaining and reuse of homogeneous catalysts

Method	benefits	disadvantages
Immobilisation on solid support		
covalent bonding	separation and reuse of catalyst, continuous process	loss of activity, catalyst leaching, additional mass transfer resistance
physical adsorption	reuse of support, regeneration of catalyst, continuous process	
SLP/SAP	retaining catalyst activity, reuse of catalyst, continuous addition of catalyst, continuous process	catalyst leaching, mass transfer resistance
imbedded in solid matrix	continuous operation, increased catalyst stability	catalyst leaching, mass transfer resistance
Ligand modification with soluble polymers	retaining catalyst activity, separation by membrane filtration	discontinuous two-stage process
Membrane separation	homogeneous catalysis	two-stage process
Extraction	homogeneous catalysis	two-stage process, loss of catalyst
Biphasic operation	homogeneous catalysis	two-stage process, strict operating temperature range
Membrane phase contacting	homogeneous catalysis, shift of reaction equilibrium, continuous operation, modular reactor design	small scale reactors, danger of flooding and cross contamination

Homogeneous catalysts, having large molecules such as live cells, enzymes and some organometallic complexes with large ligands, can be successfully separated from the reaction mixture by membrane separation methods using the membrane commensurate with the molecular dimensions of the catalyst molecule. Ultrafiltration is used on an industrial scale for the separation of biocatalysts [2, p.833]; reverse osmosis and nanofiltration separations have been proposed for some organometallic complexes [8] and cofactors in biocatalysis [9]. In these cases there is no loss of catalyst activity and almost 100% catalyst recovery can be achieved. For catalysts with smaller size molecules it was proposed to modify the catalyst by introducing large inert ligands [10] or soluble polymers [11]. The enlarged molecule can be easily separated by ultrafiltration. This method of increasing the size of catalyst molecules involves chemical modification which can result in a decrease in activity. Alternatively, the size of catalyst molecules can be increased by encapsulating them within emulsified droplets [12].

Another class of two-step processes, involving homogeneous catalytic reaction and consecutive separation of catalyst, is based on phase separation and extraction. Several conceptually different processes have been developed some of which were successfully commercialised. The basic idea is to separate catalyst and reaction products in different phases. This can be achieved by extraction of products after completion of reaction [13], temperature induced phase splitting [14] or continuous phase separation when the products of catalytic reaction are insoluble in the catalyst phase. An example of the latter process is the hydroformylation process using a water soluble Rh-based catalyst, first commercialised in 1984 [2, p.592]. Catalytic processes in supercritical CO_2 or other sc-solvents offer an elegant method of homogenising catalyst for the duration of reaction. In some cases solubility of catalyst in supercritical solvent depends on the concentration of a reagent [15].

Recent developments in membrane technology have resulted in the emergence of a new method of separation of homogeneous catalysts. In the case of liquid phase reactions involving a gaseous reagent, such as hydrogenation, oxidation, hydroformylation, etc., a porous membrane contactor can provide not only a high contact area but also an extremely high area-to-unit-volume ratio.

Membrane contactors were originally developed for such applications as saturation of liquids with gases, gas stripping, removing of volatile organics from water, aeration of fermenters, extraction of metal ions etc to replace conventional scrubbers [16,17]. For most of these applications hydrophobic polymeric hollow fibre membrane modules were used. In the case of liquid-liquid systems, hydrophilic membranes were used [18,19].

5

Another interesting application of porous membrane contactors is controlled drug release [20]. Contactors offer considerable advantages over conventional methods of gas-liquid contacting. One of the most important features of membrane contactors manufactured in the form of hollow fibres, is their extremely high specific area – up to 8000 m^{-1}, which accounts for a high efficiency of interface mass transfer. The high specific area of hollow fibre contactors often compensates for the additional mass transfer resistance introduced by the membrane itself [21].

Membrane contactors offer dispersion-free methods of mass transfer between two phases and this has several important consequences. Flow streams of the two fluids on the sides of a membrane contactor are completely independent. Hence, there is more flexibility in optimising flow rates and stream composition. There is no danger of entrapment of droplets of one phase in another which may be important in extraction and some chemical reactions with complex reaction pathways. It was also noted that due to very low liquid hold-up in membrane contactors, more expensive tailored solvents or catalysts could be used.

To the best knowledge of the author there are only three examples of the application of membrane contactors to homogeneous catalytic gas-liquid reactions. A two-membrane reactor comprising a supported liquid phase hydroformylation catalyst sandwiched between the membranes is described in [22]. Such a reactor configuration was developed to overcome the major drawback of SLP catalysts i.e. leaching of the liquid catalyst. Although complete catalyst retention was achieved, introduction of two mass-transfer barriers had a detrimental effect on the product yield. Another concept of a membrane hydroformylation catalyst is proposed in [23]. The catalyst comprises ceramic hollow spheres with porous walls with the homogeneous hydroformylation catalyst synthesised in situ. The role of the ceramic catalyst armour is to contain the homogeneous catalyst as well as to generate an additional mass-transfer resistance for carbon monoxide. In this particular case, mass transfer resistance to carbon monoxide is beneficial due to negative order of reaction with respect to CO [2, p.51]:

$$r = k \cdot [substrate] \cdot [catalyst] \cdot [P_{H_2}][P_{CO}]^{-1} \qquad \text{Eq. I-1}$$

A two-membrane reactor was developed for the partial oxidation of ethylene to acetaldehyde using soluble aqueous Pd chloride – Cu chloride catalyst [24]. Two bundles of hollow fibre membranes were used to supply oxygen and ethylene to the aqueous catalyst solution. Such a configuration provides a feed of separate reagents which for reasons of safety is essential for oxidation of hydrocarbons with pure oxygen, flexibility for optimising flow rates of gases as well as recovery of the gaseous product from the

6

liquid phase. Polypropylene hollow fibres were used which placed limitations on the operating temperature and pressure.

A phase-transfer catalyst in a membrane reactor has also been introduced [25]. In phase transfer catalysis, the reaction between two immiscible fluids is promoted by a catalyst, two forms of which have preferential solubilities in the different fluids. They are formed in the reactions between reagent and by-product of the main catalytic reaction. The catalyst, moving between the two phases brings the reagent into the reactive phase and the by-product into the non-reactive phase. The process is usually achieved by creating an emulsion with a high interfacial area. An alternative arrangement is to use non-dispersive phase contacting by immobilising the interface within the porous structure of a membrane. It was shown [25] that in the case of an organic phase reaction, the use of a hydrophobic membrane is preferable. Organic filled hydrophobic membranes present an active volume, whereas in the case of a hydrophilic membrane, filled with non-reactive aqueous solution, the membrane volume acts as an additional mass transfer barrier.

Current work described in this thesis represents a new development in the application of membrane contactors to gas-liquid homogeneous catalytic reactions. Recent advances in inorganic membrane materials provided the basis for the development of this new method which comprises the hydration of propene in a porous membrane contactor reactor. The very corrosive nature of the catalyst used (phosphoric acid) and the high operating pressure and temperature are additional complications of the process. Preparation of membrane contactors, development of the reactor control system, results of reaction studies and simulations are described in the following chapters. These are preceded by a description of prior art in the production of propan-2-ol via the direct hydration of propene and the application of membranes in catalysis.

II.1. Application of membranes in catalysis

Historically, the first membrane reactor is believed to have been be patented by Snelling in the USA in 1915 [26]. The reactor comprised a packed-bed dehydrogenation catalyst enclosed in a platinum or palladium tube. Palladium is known for its ability to dissolve hydrogen in the form of palladium hydrides [27]. Reaction between hydrogen and palladium is relatively fast and reversible, which allows for a considerable flux of hydrogen across the dense palladium barrier under the gradient of a hydrogen concentration. The mechanism of hydrogen transfer ensures almost 100% selectivity for these dense metal membranes.

Selective removal of one of the products of reversible catalytic reaction allows a shift in thermodynamic equilibrium which results in an increase in conversion. Theoretical analysis of a catalytic reactor with selectively permeable walls is given in [28]. It was shown that the maximum increase in conversion in such a reactor depends on the rate of back permeation of products, recycle of reagents and the ratios between reaction rates and permeabilities. A similar reactor configuration is modelled in [29] with the aim of obtaining the radial concentration profile for the tube-in-tube reactor configuration.

Reactors with selective membranes containing packed-bed or fluidised bed catalyst have received much attention in the literature. Early reports of reactors comprising dense palladium or palladium alloy membranes containing various catalysts (Pt on Al_2O_3, acidic zeolites) are summarised in [30]. A report on the pilot plant study of a palladium membrane steam reformer by the Japanese companies was given in [31].

Palladium itself is one of the most widely used heterogeneous catalysts. It is apparent that catalytic and separation functions of the same material can be utilised simultaneously. Most of the earlier work on palladium based catalytic membranes was done by V.M.Gryaznov [32]. The two major limitations of dense noble metal membrane technology are the cost of materials and their structural stability. Pure palladium membranes tend to become brittle and non-selective under high temperature reaction conditions. Much more stable Pd-containing alloys were developed, which also enables the use of thinner membranes to give a higher hydrogen flux at lower cost. Recent developments in Pd-based membranes are summarised in [32].

Increasing attention to selective oxidation processes [4] has had an effect on the development of inorganic oxygen selective membranes. The mechanism of oxygen transfer through solid oxide membranes is ionic which ensures high selectivity towards oxygen. Transfer of the oxygen ion from one side of the membrane to the other requires transfer of two electrons in the opposite direction to account for electroneutrality. Research has focused on solid electrolytes which possess effective ion and electron properties to give a high oxygen flux. The materials for these membranes are usually based on stabilised oxides of Zr, Th or Ce and oxides with a perovskite structure (La, Sr, Mn mixed oxides). A number of reviews give a good summary of the literature [33] and a mixed oxide membrane based on bismuth is described in [34].

The membrane reactors described so far have only one or two functions, i.e. selective separation that can be used for reagent feed or product removal and catalysis on the active surface of a membrane. In the case of mixed oxide membranes, the material should also possess an electrical conducting function. Other membrane materials with a catalytic function that have been actively investigated are zeolites and acidic resins (such as Nafion). But, as it was shown in a recent review [35], there are many other functions that membranes can have in a chemical reactor (see Table II-1).

Table II-1. A list of membrane functions in a chemical reactor [35].

No	Function
1.	Separation of products from reaction mixture
2.	Separation of a reactant from a mixed stream for introduction in a reactor
3.	Controlled addition of a reactant/reactants
4.	Nondispersive phase contacting
5.	Segregation of a catalyst in a reactor
6.	Immobilisation of a catalyst in/on a membrane
7.	Membrane as a catalyst
8.	Membrane as a reactor
9.	Electric conductor
10.	Heat conductor
11.	Immobilisation of liquid reaction medium

Nondispersive phase contacting and immobilisation of the liquid reaction medium (Table II-1 4&11) are the two functions specific to the application of membrane contactors to gas-liquid and liquid-liquid systems described in the Introduction section. Similar devices with heterogeneous catalysts were proposed.

A cross-flow reactor with a ceramic membrane supported Pd catalyst was developed for liquid phase hydrogenation reactions [36]. The reactor is effectively a gas-liquid contactor module with a catalytically active membrane which has a high packing density. Hydrogenation of nitrobenzoic acid was performed in the reactor and it was shown that the cross-flow configuration of the membrane module allowed complete utilisation of the available catalyst surface. In this particular case the membrane module itself is the reactor, giving structured fluid flow, catalyst support, immobilisation of the gas-liquid interface and product removal.

A similar reactor is reported in [37]. A zeolite catalyst (titanium silicalite) was imbedded into the glassy polymeric membrane (polydimethylsiloxane) (PDMS) and used as a contactor between the organic phase containing n-hexane and the aqueous phase containing hydrogen peroxide. The thickness of the resulting catalytic membrane was between 250-600 μm but no data on catalyst distribution across the polymeric film was given. The problem with this approach is that imbedding the catalyst into the dense polymeric matrix would inevitably create a large diffusional barrier and considerably decrease the catalyst efficiency. Unfortunately, no data on catalyst efficiency are given in [37]. Experiments [38] show that imbedding the homogeneous $[Co(CO)_3(PPh_3)_3]_2$ catalyst in thin (<50μm) films of glassy polyphenyleneoxide resulted in a non-uniform distribution of the catalyst and a partial loss of the triphenylphosphin stabilising ligand. This led to oxidation of the catalyst. A more detailed investigation of the effect of a polymer membrane thickness on the effectiveness of a composite embedded catalyst was given in [39]. A zeolite catalyst (zeolite-encapsulated iron-phtalocyanine) was imbedded into the PDMS membranes of different thickness. The membrane catalysts having a thickness less than 200 μm were operating in the kinetic regime. It was found that an increase in zeolite loading into the PDMS membranes results in a linear increase in the catalyst turnover. Simultaneously, an increase in the solids loading has an adverse effect on the tortuosity of a composite catalyst and therefore increases the diffusional limitation.

A gas-liquid membrane reactor was proposed for the denitrification of water [40]. Commercial ceramic membranes were used in a single unit as a catalyst support and nondispersive liquid saturator. A similar reactor was described earlier for reactions of volatile organic compounds, e.g. hydrogenation of α-methylestyrene to cumene [41]. The main advantage of the membrane reactor in both cases is the elimination of any gas-phase resistance. This considerably improves performance of the membrane catalyst in comparison with packed-bed catalyst configurations.

The catalytic denitrification of water aided by the membrane reactors was also described in the two recent publications [42,43]. The reaction of nitrate hydrogenation proceeds via the nitrite intermediate towards the formation of nitrogen or ammonia. It was shown in both quoted papers that the reaction is limited by internal diffusion of dissolved hydrogen. At the same time a decrease in the dissolved hydrogen concentration has a favourable effect on the selectivity towards nitrogen formation. The two papers explore different configurations of a membrane reactor. A membrane contactor type reactor is proposed in [42] with the aim of controlled addition of hydrogen in order to improve the reaction selectivity. It was shown that although the membrane reactor showed a comparable activity to that of a powder catalyst, the diffusion limitation regime attainable in a conventional batch reactor allows to achieve much higher selectivity values. A flow-through membrane reactor is proposed in [43] in order to decrease the internal diffusion limitations. It was shown that the activity of a membrane catalyst is higher in the flow-through regime than that in the batch regime. No data on the effectiveness factor and the selectivity of a membrane catalyst were given.

A membrane can be considered as a mass transfer barrier. It was shown, at least on a conceptual basis, that introduction of an additional mass transfer barrier can be beneficial (in the case of negative reaction order for CO in hydroformylation [23] and as stabilisation of air sensitive metal-carbonyl complexes [7]). The mass transfer resistance of porous ceramic membranes was utilised to control the stoichiometry of the reaction mixture near the catalyst in order to improve reaction selectivity: this was achieved by impregnating a tubular membrane with catalyst and controlling the flow rates and pressures of gaseous reagents fed from the opposite sides of a membrane [44]. Provided that reaction is diffusion limited (fast kinetics), the reaction plane is formed along the length of a membrane at a certain depth.

The concept of a flow-through reactor was proposed for reactions requiring strict control of contact time. The reactor comprising a stack of flat-sheet ultrafiltration polymeric membranes with dispersed metal Pd catalyst was tested for the hydrogenation of polyunsaturated liquid oils [45]. Better selectivity towards cis-mono unsaturated oils was obtained. The same concept was applied to lean combustion processes [46,47]. An advantage is gained due to uniform distribution of reactants over the area of the flat membrane combustor which eliminates hot-spots and allows effective utilisation of radiated heat for preheating the reactants.

Several novel functions, not listed in Table II-1, that membranes might potentially have in chemical reactors are proposed in [48]. Combination of high surface area and

electric conductivity may lead to the development of membrane based sensors. Conducting membranes could also be used in the electrocatalytic processes. A conductive membrane could be used as a semipermeable electrode to separate the products of an electrocatalytic reaction produced near catode and anode [49]. A reactor was proposed in [50] to couple the two reactions having a positive and a negative potentials using a catalytically active conducting membrane. Membranes produced from semiconducting materials such as TiO_2, ZnO, CdS could be used in photocatalytic reactions. If the selective layer of a membrane contains particles with diameters less than 5 nm, then this layer can be used as a guide for laser beams. This opens many new potential applications for membrane reactors.

II.2. Direct hydration of olefins

II.2.1. Reaction mechanism and kinetics

Homogeneous liquid phase hydration of olefins was discovered in the early 19th century [51,52]. Hydration provides the route to synthetic production of alcohols – one of the most important industrial chemical processes of the 20th century. Synthetic ethanol production was introduced in the USA in 1930s and has steadily grown from 10% of all ethanol produced in 1934 to ca. 90% in 1958 [53]. Early patent literature on the hydration reaction covers the two-step reaction in sulphuric acid [54] and the direct vapour phase reaction with the phosphoric acid catalyst supported on carbon [55].

It is generally accepted that the hydration reaction involves formation of a carbocation, but whether the carbocation exists as a stable intermediate is disputed. One of the first mechanisms proposed for the hydration reaction involves formation of an open structure (as opposed to a bridged structure) carbocation, the rate limiting step being the bimolecular reaction between the carbocation and water [56,57]:

$$C_3H_6 + H^+ \rightleftharpoons C_3H_7^+ \qquad \text{fast} \qquad \textbf{Eq. II-1}$$

$$C_3H_7^+ + H_2O \rightleftharpoons C_3H_7OH + H^+ \qquad \text{slow}$$
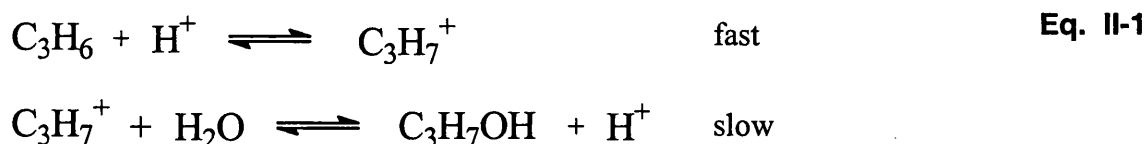
This mechanism corresponds to a bimolecular electrophilic substitution mechanism, which is characterised by possible skeletal isomerisations while retaining the structure of the substrate [58]. A similar mechanism was proposed in [59] to explain the kinetics of propene hydration over a thin film phosphoric acid catalyst. The rate equation in this case is given by the equation:

$$W = AKK_g \frac{a_{H^+} f_{C_3H_6}}{f_{C_3H_7^+}} P_{C_3H_6} = AKK_g h_0 P_{C_3H_6}$$

Eq. II-2

where A – rate constant of limiting reaction; K – equilibrium constant of carbenium ion formation; K_g – Henry coefficient; h_0 – Hammett acidity function and $P_{C_3H_6}$ – partial pressure of propene.

Note that the rate of reaction is directly proportional to the Hammett acidity function, rather than to the activity of the proton. This is supported by many experimental observations of the apparent rate of the acid catalysed hydration reaction [56,57,58,59].

Stability of free carbocations of aliphatic hydrocarbons decreases from tertiary to primary due to a decrease in electron donor effect of the side groups [58]. This implies that if the mechanism described above (Eq. II-1) is correct and the rate limiting reaction is between the carbocation and the water molecule, there is an equilibrium concentration of highly unstable species present in the reaction mixture. It is quite unlikely that carbenium ions may exist in aqueous solution as a stable intermediate. Some kinetic data indicates that water is probably playing an important role in the formation of the reaction intermediate [60]. The mechanism presented by Taft [61] includes the formation of the carbenium ion as a rate limiting step and its fast transformation into an oxonium ion:

Eq. II-3
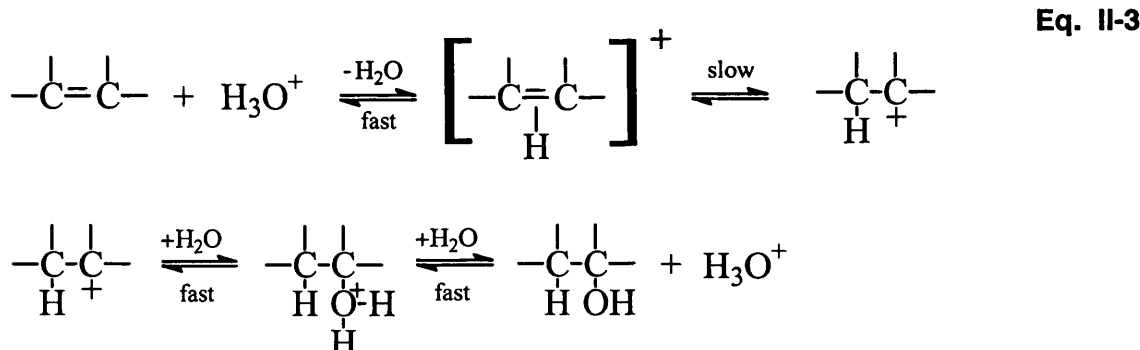
A similar mechanism was later proposed on the basis of nonempirical quantum chemical calculations [62]. The initial π-complex is speedily transformed into a more covalent oxonium ion and carbocation may only appear as an activated complex. The most likely structure of the solvated carbenium ion includes three water molecules as shown for the case of the methyl ion in Figure II-1.

$$\begin{array}{c} H_{\diagdown}O^{\diagup}CH_3 \\ \vdots \\ H \delta+ \\ | \\ O \\ H_{\diagdown}H^{\diagup O^{\diagdown}}H_{\diagdown}O^{\diagup}H \\ O \qquad O \\ | \qquad | \\ H \qquad H \end{array}$$
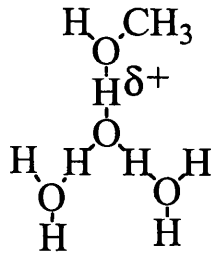
Figure II-1. Solvated methyl carbenium ion [62].

It was therefore suggested that the acid catalysed hydration reaction correspond to a bimolecular nucleophilic substitution S_N2 mechanism [62]. It was also suggested in [57] that a solvent molecule might form a covalent bond with the α carbon, coupled with protonation at the β carbon. However, no firm experimental proof was found to support this hypothesis. The rate equation for this mechanism was derived in [63] and given by:

Eq. II-4

$$\upsilon_1 = kK_1 s \frac{f_\pi}{f_{C_2H_4} f^{\neq}} P_{C_2H_4} h_0 ,$$

where k – rate constant of the limiting reaction; K_1 – equilibrium constant of π-complex formation; f – activity coefficients; s – solubility coefficient of ethylene in phosphoric acid (s = $a_{ethylene}/P_{ethylene}$); h_0 – acidity of phosphoric acid ($h_0 = a_{H^+} f_B / f_{BH^+}$).

Assuming constant solubility (s) and activity coefficients (f) the observed reaction rate, including the reversible reaction, is given by:

Eq. II-5

$$\upsilon = k_1 h_0 \left(P_{C_2H_4} - K_P^{-1} \frac{P_{C_2H_5OH}}{P_{H_2O}} \right)$$

As one can see, given either the free carbenium ion mechanism or the hydrated carbenium ion mechanism, the rate equation has the same general form. It should be noted that all kinetic studies on the direct hydration of olefins catalysed by liquid acids were based on the measurements of the change of pressure in the reactor. The rate of formation of alcohol was assumed to be directly proportional to the rate of change of pressure [59] and the formation of by-products was not considered. The only true kinetic study of the liquid phase kinetics of the hydration reaction was performed with a solid acidic resin catalyst [64]. The results of this study can not be directly transferred to the liquid acid catalysts.

II.2.2. Reaction equilibrium

Equilibrium of the hydration reaction has been studied extensively both experimentally and computationally. One of the early attempts to estimate the equilibrium constant K_p of

the ethylene hydration on the basis of thermal data resulted in the conclusions that such a calculation was not possible due to the lack of accurate thermal data and the equilibrium constant should always be determined experimentally [65]. In later papers it was shown that the two important parameters that must be taken into consideration to give a realistic estimate of the equilibrium constants are the formation of ether and high temperature binary VLE data [66,67]. Only recently, with advances in computer technology and methods of VLE modelling, relatively accurate calculations of the hydration equilibrium became possible. Two examples of such calculations are given in [68,69] for the liquid phase hydration of propylene. In both cases the Peng-Robinson-Stryjek-Vera cubic equation of state was employed, although with different mixing rules. Computational methods of determination of equilibrium constants and composition have limited power in the case of catalytic reactions with liquid acids. It was shown in [70] that the equilibrium constant of the hydration reaction catalysed by phosphoric acid depends on the concentration of acid.

An extensive study of the equilibrium composition of the direct hydration of propene was reported in [71]. The effect of pressure and temperature on the equilibrium conversion was studied and the results are represented in Figure II-2.

It is apparent from these results that high pressures and low temperatures favour the formation of 2-propanol. This is consistent with Le-Chetalier's principle as the hydration reaction proceeds with a decrease in mole numbers and is exothermic.

Temperature dependencies of equilibrium constants of alcohol and ether formation are shown below. Figure II-3 shows equilibrium constants of alcohol formation according to the overall reaction:

$$C_3H_6 + H_2O \leftrightarrow C_3H_7OH \qquad \qquad \textbf{Eq. II-6}$$

$$K_p = \frac{[C_3H_7OH]}{[H_2O][C_3H_6]} \qquad \qquad \textbf{Eq. II-7}$$

Thermochemical data for pure substances in the ideal gas state, including temperature coefficients for heat capacity are presented in [67]. The solid line in Figure II-3 was calculated on the basis of thermochemical data. The dotted line was calculated on the basis of the data presented in [76].
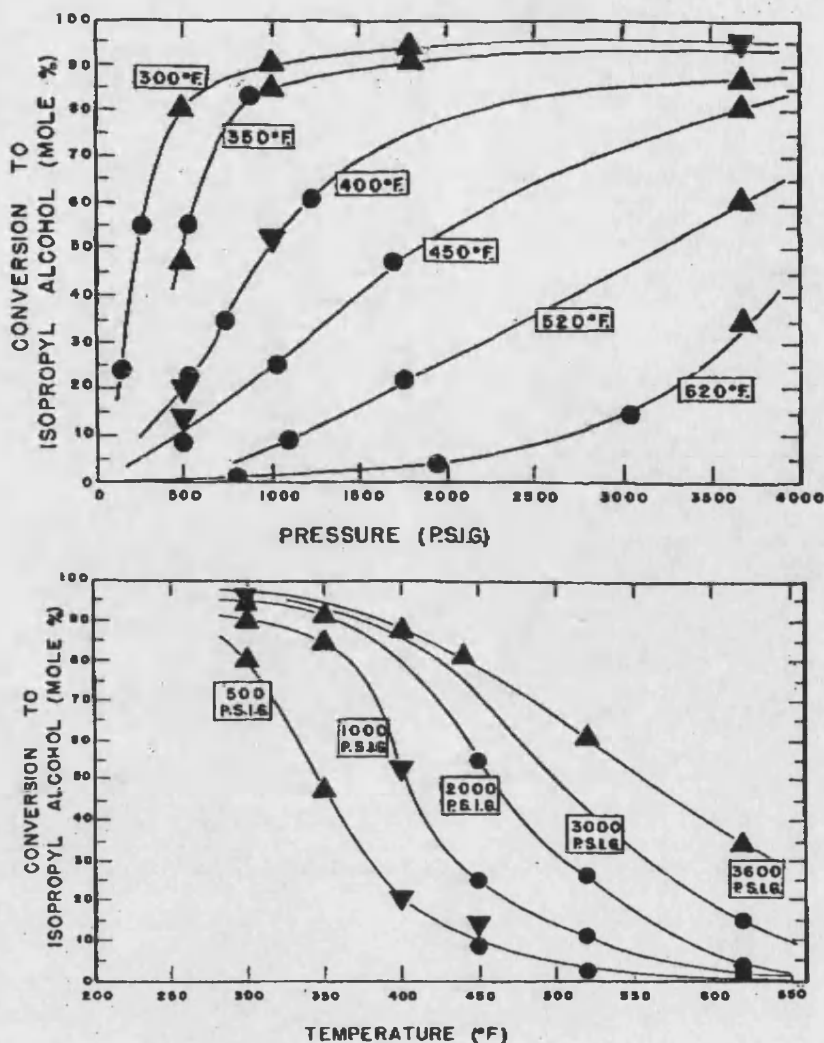
Figure II-2. Equilibrium conversion in propylene hydration vs. pressure and temperature.
Adapted from [71].

Reaction of ether formation is usually represented by Eq. II-8:

$$2C_3H_7OH \leftrightarrow C_6H_{14}O + H_2O \qquad\qquad \textbf{Eq. II-8}$$

$$K_p = \frac{[C_6H_{14}O][H_2O]}{[C_3H_7OH]^2} \qquad\qquad \textbf{Eq. II-9}$$

The gas phase equilibrium constant shown in Figure II-4 was calculated on the basis of thermochemical data [67]. The liquid phase equilibrium constant was calculated on the basis of the data presented in [64]. In the same work, liquid phase data for the propan-2-ol equilibrium constant were presented. Values of Kp were normalised to the water concentration to give dimensionless numbers. The numerical values of the liquid phase equilibrium constants obtained in [64] are shown below:

$$K_p = \frac{[C_3H_7OH]_l}{[C_3H_6]_l} = 5.29 \cdot 10^{-6} e^{55000/RT} \qquad\qquad \textbf{Eq. II-10}$$

16

$$K_p = \frac{[C_3H_7OH]^2_l}{[C_6H_{14}O]_l[H_2O]_l} = 8.55 \cdot 10^{-2} e^{10800/RT}$$

Eq. II-11
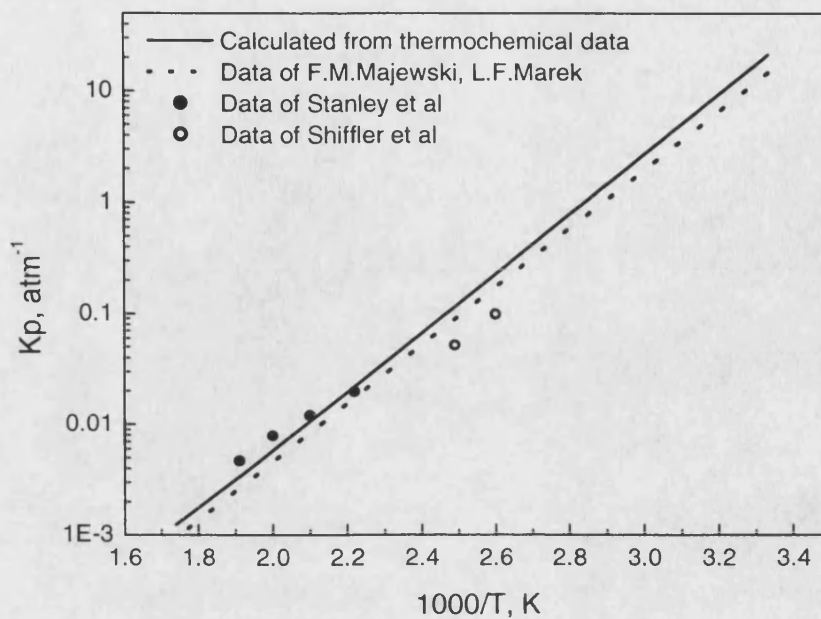
Figure II-3. Gas phase equilibrium constant of propan-2-ol formation.
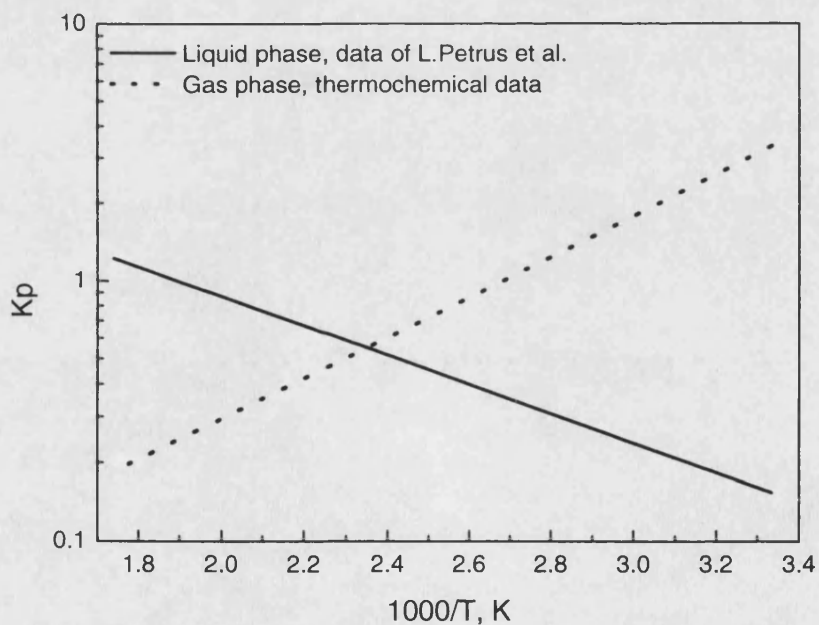
Figure II-4. Equilibrium constant of DIPE formation.

II.3. Catalysts, kinetics and reactors

Sulphuric Acid – indirect process. In the presence of sulphuric acid the olefin is first absorbed in acid with the formation of the alkyl ester which is subsequently hydrolysed with water. This process is mostly described in the early literature on the hydration process and was, in fact, the first large scale petrochemical process dating back to the 1920-s [72,73]. Indirect hydration is not an attractive process due to the large quantities of dilute sulphuric acid that have to be re-concentrated. Reaction is also not very selective due to a range of intermediate species formed upon absorption of the olefin in sulphuric acid, e.g. ester, ether, polymers etc. The step of olefin adsorption was studied in detail in [74]. The fact that the two-step hydration process is not selective was later exploited to shift the reaction towards the production of di-isopropyl ether, which is now considered as a possible new additive for reformed petrol [75].

Phosphoric acid – direct process. Phosphoric acid is known as one of the most active catalysts for olefin hydration. An early paper describes high pressure propylene hydration in diluted phosphoric acid solutions with the acid concentration up to 12.1wt% [76]. A commercial phosphoric acid catalyst is prepared by impregnation of a suitable porous support with the aqueous solution of phosphoric acid of 55-54 wt% concentration, followed by drying at 100°C which brings the concentration of acid on the support to 85 wt%. Reaction takes place in the film of phosphoric acid and is dependent on a number of operational parameters: feed steam/olefin ratio, feed volumetric velocity, total pressure, temperature, acid loading, acid concentration. Phosphoric acid catalysis is described in a number of publications, but the most explicit description of phosphoric acid catalysis is given in [77].

The acid is supported on a porous material such as celite, kieselghur or one of several synthetic alumosilicates. One of the best synthetic supports contains SiO_2 (78.7%), Al_2O_3 (16.7%), CaO (1.23%), Na_2O (1.21%), Fe_2O_3, MgO, SO_3. The support is activated by sulphuric acid prior to impregnation with phosphoric acid. Such a procedure increases the activity of the catalyst compared to a non-activated one. The activation results in a change of the SiO_2 /Al_2O_3 ratio in the support in favour of SiO_2 (89%).

A modification of this catalyst is proposed in [78]. After impregnation of the porous support with phosphoric acid, the catalyst is calcined at 700-1100°C which results in the formation of silicophosphates of various composition, depending on temperature. The new catalyst is characterised by an improved selectivity towards the main product compared to the original catalyst. It was shown in a number of publications that the

active species in the aforementioned catalyst is liquid phosphoric acid formed on the surface of the porous support and crystalline silicophosphates such as $Si_3(PO_4)_4$, due to the hydrolysis of the latter [79,80,81]. The reaction takes place in a very thin film of free acid spread on a porous support. It is shown in [82] that phosphoric acid catalysts are only active if there are no strong interactions between acid and support which would prevent formation of free acid under reaction conditions.

A model catalyst mimicking the one described above was studied in detail for the dehydration of dimethylvynilcarbinol [83], the hydration of ethylene [63] and propylene [59]. In all instances the model catalyst was prepared by impregnation of phosphoric acid onto quartz particles.

In the case of propylene, if the observed reaction rate is expressed in the most general form (Eq. II-12) the reaction constants at 84.3 wt% acid concentration are given by [59]:

Eq. II-12

$$v = \frac{dP_{C_3H_7OH}}{dt} = k_1 P_{H_2O} \cdot P_{C_3H_6} - k_2 P_{C_3H_7OH},$$

$$k_1 = 6.3 \cdot 10^3 \cdot e^{-11400/RT} \quad [min^{-1} \, atm^{-1}] \quad k_2 = 4.9 \cdot 10^9 \cdot e^{-20200/RT}$$

The activation energies are given in cal/mol in the above equation.

The observed reaction rate was found to be proportional to the Hammett acidity function. Therefore a high acid concentration benefits the reaction rate. It was found experimentally that acid concentrations above 83wt% are required for ethylene hydration [77]. It was also shown in [59] that both the reagent and the product influence the acidity function and hence lower the reaction rate.

The supported liquid phase catalyst described above has several drawbacks. The major problem is catalyst leaching. In the case of a pure supported phosphoric acid catalyst the loss of acid may reach 1 kg of acid per 200-400 kg of alcohol produced. In the case of a silicophosphate catalyst the loss of acid is similar – 2.5-3.0 kg of acid per 1000 kg of alcohol produced and the interval between acid addition to the catalyst is 500-600 hours [77].

Leaching of free acid in the course of reactor operation requires both catalyst support and reactor material to be acid resistant. It is known that all ceramic-based porous supports for this catalyst have a limited lifetime and have to be replaced regularly. To prevent the reactor corroding, industrial reactors are usually copper-lined. It was suggested that additional lining with porous carbon bricks benefit the corrosion resistance of reactor wall [84]. In this case the corrosion resistance originates from the fact that porous carbon bricks generate an additional reservoir for acid and prevents free acid flow against the reactor wall.

Because of the nature of the catalyst the feed steam/olefin ratio is very important. A high steam ratio favours reaction but will dilute the acid and result in catalyst leaching. A low steam ratio results in dehydration of the catalyst and a high rate of formation of di-isopropyl ether and polymerisation. The optimum ratio of steam to olefin was found to be in the range of 0.6 to 0.75. It was also found that the optimum contact time for the phosphoric acid catalyst is 18-20 sec for ethylene hydration.

Heteropoly acid based catalysts. Liquid phase direct hydration of propylene was in fact the first industrial catalytic application of heteropoly acids (HPAs), commissioned in 1972 [85]. Both liquid phase and vapour phase [86,87] options for the hydration reaction using heteropoly acids and their salts were investigated.

Heteropoly acids are defined as condensates of different oxoacids. A heteroatom is placed in the centre of the molecule and surrounded by metal-oxygen octahedral units. Several structures of heteropoly acids are known, the most important being the Keggin structure, having a generic formula $XM_{12}O_{40}{}^{x-8}$ (X=Si^{4+}, P^{5+} etc, M=Mo^{6+} or W^{6+}) and represented in Figure II-5 [88]. The importance of this particular structure of heteropoly acids stems from its temperature and chemical stability, allowing for harsh conditions of industrial catalytic processes.
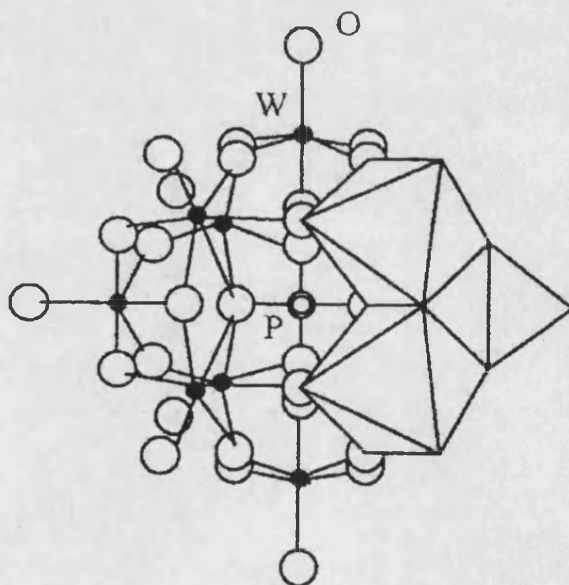
Figure II-5. Structure of Keggin-type heteropoly anion.
Reproduced from [88]. Letters represent the positions of atoms of oxygen, phosphorus and tungsten.

Heteropoly acids are, perhaps, the most unique catalysts known up to date. HPAs are strong Brönsted acids, generally stronger than mineral acids such as sulphuric or perchloric acids. Solid HPAs possess a discrete ionic structure with highly mobile

protons as well as polyanions. Because of the relatively open structure of polyanion, small polar molecules can access the bulk of the molecule. Hence, internal protons are accessible for catalytic reactions and responsible for the high activity of HPAs in acid catalysis. It was shown that internal protons in HPAs are fairly uniform [89]. This property results in the notion of a "pseudo liquid state" of solid HPA catalysts [90].

Apart from their acidic properties, HPAs are efficient oxidants due to fast reversible multielectron redox transformations. Heteropoly acids are considered as one of the most promising catalysts for liquid phase partial oxidations. This is due to the flexibility of the chemistry of HPAs, allowing for inclusion of the second transition metal atom without loss of structure and stability. This property provides an opportunity for tailoring a catalyst to a specific process as it has been demonstrated in [3] for the case of the homogeneous partial oxidation of saturated hydrocarbons.

The third important property of HPAs as catalysts is the possibility of bi-functional catalysis. The catalytic activity of HPAs in the hydration reaction was found to be significantly higher than that of strong acids like sulphuric or perchloric acids [88]. The factors responsible for high catalytic activity of HPAs compared to strong inorganic acids are: increase in the solubility of olefins, increase in acidity and activation of olefins by coordination with the polyanion of the heteropoly acid [91]. As it was shown by quantum chemical calculations [62], the mechanism of the hydration reaction requires stabilisation of the transition-complex which is achieved by formation of covalent intermediates. In the case of heteropoly anions, the anion itself is a perfect coordination agent. Furthermore, it was shown that an increase in the basic properties of polyanions might result in an increase in catalytic activity of the resultant molecule. In case of heterogeneous acid catalysis, the Cs salt of tungstophosphoric acid ($H_3PW_{12}O_{40}$) – $H_{0.5}Cs_{2.5}PW_{12}O_{40}$ – showed an increase in catalytic activity in ester decomposition reactions by a factor of 2.5, compared to the parent acid [92].

The reason for coordination of organic intermediates by heteropolyanions is believed to be related to the softness of HPAs [93], i.e. the polarizability and mobility of the heteropolyanion.

It is generally accepted that the mechanism of olefin hydration by heteropoly acids involves two parallel stages i.e. the reaction of formation of the carbocation and the reaction of formation of complex with polyanion of heteropoly acid [88], Eq. II-13.

This mechanism was derived from the observation that at low HPA concentration the reaction is first order for the catalyst, but at high concentration the order is increasing up to two. The same phenomenon can be explained by a strong salt effect due to the

heteropolyanion [90]. It is shown in [94], that the rate of isobutene hydration catalysed by HPAs is directly proportional to the Hammett acidity function as it is in the case of catalysis by mineral acids (see above). This implies that there is no difference in the mechanism of liquid phase hydration by mineral acids or heteropoly acids. As it was underlined in [90] the argument whether the increase in the reaction order in case of concentrated HPA solutions is the result of a parallel mechanism or a salt effect is rhetoric as on the molecular level it is exactly the same.

Eq. II-13

$$RC\overset{H}{=}CH_2 + H^+ \xrightarrow{\text{slow}} R\overset{H}{\underset{+}{C}}-CH_3 \xrightarrow{H_2O} RCH(OH)CH_3 + H^+$$

$$+H_2O \uparrow - HPA^{n-}$$

$$RC\overset{H}{=}CH_2 + H^+ + HPA^{n-} \xrightarrow{\text{slow}} R\overset{H}{\underset{+}{C}}-CH_3\cdots HPA^{n-}$$

The resulting expression for reaction rate is given by:

$$v = k_1 \overline{P}_{alkene}\left[H_3O^+\right] + k_2 \overline{P}_{alkene}\left[H_3O^+\right]\left[HPA^{n-}\right],$$

Eq. II-14

where k_1 and k_2 are reaction constants for the two reaction pathways.

Strong acidic resin catalysts. The first propylene hydration plant using an acidic resin catalyst was commissioned by Deutsche Texaco in 1972 [71]. The acidic resin catalyst is a solid catalyst, characterised by high concentration and uniform distribution of acidic sites. The resins most commonly studied for the hydration process are Amberlist-15 and IR-120, activated with strong mineral acids prior to reaction [71,95]. The other resins proposed for the olefin hydration are perfluorinated sulfonic superacid catalysts such as Nafion 501 polymer [96] and sulfonic polyorganosiloxane polymers [97].

The peculiarities of these catalysts are best summarised in [71]. The industrial processes using ion-exchange resins are three-phase trickle-bed processes. Hence, mass transfer effects play a major role in the overall process performance. The process steps include absorption of olefin into water, transfer of dissolved olefin to the surface of the catalyst, reaction on the surface of the catalyst, transport of unreacted olefin and products away from the catalyst surface and desorption of products, the last step being the least important as the product alcohol is highly soluble in water.

It was found that the resin catalyst particles must be fully wetted by water to prevent adsorption of olefin onto the catalyst particle internal surface. In the case of propylene,

olefin adsorbed onto acidic resin particles reacts speedily to form polymeric by-products. The reaction kinetics were shown to be independent of the particle size. This implies that all protons are accessible to the reagent. Accessibility of the acidic sites depends on the size of the reagent molecules and the properties of the polymer. It was noted that macroporous resins perform better than those of a gel type; the more rigid structure of Amberlist-15 allowing this resin to sustain its structure under operating pressure.

Zeolite and other solid hydration catalysts. A number of heterogeneous catalysts were investigated for the direct hydration of low olefins. In an early paper [65] the following materials were studied for the hydration process: aluminium oxide, thorium oxide, tungstic acid (WO_3), thorium phosphate, aluminium phosphate, the ammonium salt of phosphotungstic heteropoly acid, mixed aluminium chromium oxide and some other combinations of oxides. A WO_3-SiO_2 catalyst was used in one of the first kinetic studies of the vapour phase direct hydration process [98]. A range of slurried mixed oxide catalysts was reported in the patent [99]. It was noted that the presence of surface active agent is beneficial for good mixing in the reactor. The acidic zeolite catalysts ZSM-5, ZSM-23, ZSM-35, ferrierite, mordenite and different pentasils were studied in vapour-phase, liquid phase and mixed-phase hydration processes [100,101,102].

Among the above catalysts, only zeolite based catalysts offered comparable yields and selectivities to propanol with the commercial phosphoric acid catalyst. In the case of the vapour phase reaction, zeolites were found to be sensitive to the water content, the optimum water:propylene feed ratio being 0.05 to 0.5 [102]. The liquid phase reaction allows for higher conversions. The patent [101] claims that ZSM-35 is active both in the vapour phase and liquid phase reactions.

The high selectivity of zeolite catalysts in hydration processes is due to product size exclusion, as large oligomeric by-products cannot be formed in the intermediate pore-size zeolites such as ZSM-5, -23 and -35.

II.4. Process improvements, patent literature

A range of process improvements was proposed to the basic hydration schemes described above. In the case of vapour phase reactions over solid or supported liquid phase catalysts conversions do not exceed 5-8%. If conversion is higher than 20% the reverse reaction of dehydration becomes significant. The major drawback, however, is the need for re-circulation of large quantities of unreacted olefin. In the case of liquid-phase reactions the conversion per pass may reach as high as 75% but the resulting liquid

product contains no more than 10-30% of alcohol. Inventions described below tackle these problems in significantly different ways.

In order to increase conversion per pass and avoid reverse reaction it was proposed to use a series of hydration reactors with intermediate removal of alcohol. The patent [103] describes the vapour phase hydration of ethylene-propylene mixtures, obtained from a fluid catalyst cracking unit, catalysed by perfluorinated ion-exchange resins where the reactants stream passes through a series of reactors each having separate removal of product alcohol. A similar claim was made in [104] for the case of liquid-phase reactions, the main difference being the counter-current flow of olefin and water through the series of reactors. The patent claims that in such a configuration, the reagent flows are co-current in each of the reactors and counter-current in the series of the reactors which allows maintenance of high selectivity (91mol%) and high conversion. The summary of the processes performances is shown in the Table II-2.

In the patent [105] the first in the series of hydration reactors is dedicated to conversion of the by-product diisopropyl ether to isopropanol by reacting with excess water. Hence, the by-product of the main hydration stage is recycled, maintaining an equilibrium concentration of ether and preventing further formation of ether. A similar approach was exploited in [106] with the difference that it was proposed to feed all by-products, including polymerisation products, back to the reactor inlet. The separation of the effluent in a hydration reactor is a key issue. It is said that the separation is achieved partially due to formation of organic and aqueous liquid phases containing heavy hydrocarbon by-products and a corresponding propan-2-ol solution. The two liquid phases are separated in a decanter and by-products are re-circulated.

An alternative method of enhancing the yield of alcohol is the use of an inert organic solvent in the reaction zone which would affect the distribution of products and shift the reaction equilibrium. The patent [107] describes a process in which glycol diether solvent was used as a second liquid phase. It was shown that the product alcohol was distributed approximately equally between aqueous and organic phases, but ether and other by-products were concentrated in the organic phase. Therefore, continuous removal of alcohol from the organic phase shifted the equilibrium towards higher alcohol production. The remaining constituents in the organic phase, ether and by-products, effectively suppress further formation of by-products. A total alcohol yield as high as 99 per cent was demonstrated with an alcohol concentration in the product stream about 15wt%.

A number of patents deal with the problem of increasing the concentration of product alcohol in order to reduce the down-stream cost of distillation and purification. Several

approaches have been proposed. The use of saturated hydrocarbons C_3-C_4 under supercritical conditions, as extraction agent is described in [108]. The extraction agent is applied to the liquid effluent of a hydration reactor in its supercritical state. Subsequent withdrawal of the extract and decrease of pressure below the critical pressure of the extracting agent, leaves the concentrated alcohol solution with an average concentration of ca. 88wt%. The patent [108] describes earlier attempts of a similar kind where extracting agents, being either supercritical saturated hydrocarbon or supercritical CO_2, were applied to the vapour effluent of a hydration reactor. In these cases the volumetric ratio of the extraction agent to the extracted fluid is considerably higher than that in the case of extraction from the liquid phase. A much earlier patent describes extractive distillation as a down stream separation process with the extraction agent being diisopropyl ether – a by-product in the hydration process [109]. The separation process is split into two stages. In the first stage, most of the water is removed in a simple condenser column. The effluent of the condenser column with the alcohol close to its azeotrope concentration is passed into the second column where the ether is used as a withdrawal agent. The alcohol stream after the second column is essentially water free with the alcohol concentration 95.5%, residual components being di-isopropyl ether and by-products. The earlier patent [110] describes a reactor in which liquid water is reacted with supercritical propene and the alcohol produced is withdrawn from the top of the reactor together with unreacted olefin. Subsequent depressurisation of the part of the effluent stream leaves an 80% alcohol solution. The total space-time yield of this reactor was reported to be 210 kg/hr/m^3 [110].

The patent [111] describes an integrated dehydrogenation-hydration process in which the feed contains saturated hydrocarbons and the resulting products are isopropanol and tertiary butyl alcohol. As it was shown above in the patent [103], the feed stream of a hydration reactor may be an effluent of a hydrocarbon cracking unit. In this case the feed contains saturated as well as unsaturated hydrocarbons, the latter being concentrated and re-circulated in the hydration unit. A pressure swing or temperature swing adsorption separation technique was proposed in [112] as an intermediate stage in the vapour phase hydration process. The adsorption stage allows removal of excess saturated hydrocarbons from the feed stream.

Until recently di-isopropyl ether has been considered an undesirable by-product of the hydration process. Following an increase in concerns about the safety of the main additive of reformed petrol, methyltertbutylether (MTBE), alternative additives were sought. Di-isopropyl ether is considerably less soluble in water compared to MTBE and

therefore carries much less risk of water contamination in urban areas. A number of recent patents is related to the formation of di-isopropyl ether by the direct hydration of propene.

Conditions in the hydration reactor which favour the formation of di-isopropyl ether are a high concentration of alcohol and minimum of water. Ether may be formed through reaction of alcohol with propene or through dehydration of alcohol:

Eq. II-15

$$CH_3CH{=}CH_2 + CH_3\overset{OH}{\underset{|}{C}}HCH_3 \rightleftharpoons CH_3\overset{|}{\underset{CH_3}{C}}H{-}O{-}\overset{|}{\underset{CH_3}{C}}HCH_3$$

Eq. II-16

$$2\,CH_3\overset{OH}{\underset{|}{C}}HCH_3 \rightleftharpoons CH_3\overset{|}{\underset{CH_3}{C}}H{-}O{-}\overset{|}{\underset{CH_3}{C}}HCH_3 + H_2O$$
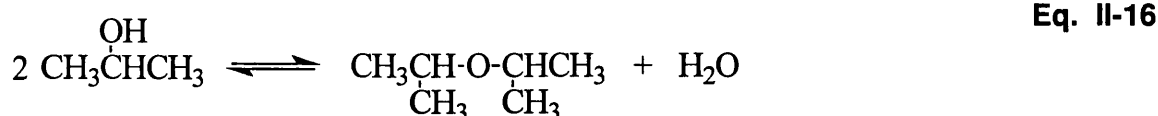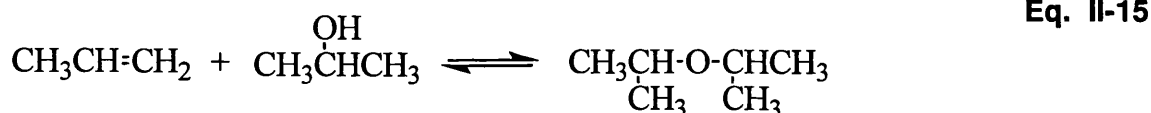
The patent [113] describes a two-stage process in which the first step is a trickle-bed hydration reactor with an ion-exchange resin catalyst, and the second stage is a catalytic distillation column using the same catalyst. It is believed that reaction (Eq. II-15) allows for a higher use of reagents and is therefore preferable.

A process for converting a mixed feed, containing C_3 and C_2 hydrocarbons, into di-isopropyl ether is described in [114]. The advantage of the proposed flow-sheet consists in using a vertical stripper column for removing the C_2 feed impurities and re-circulation of the C_3 feed. A two-stage process disclosed in [115] avoids re-circulation of the olefin feed by adjusting the water:olefin ratio and employing different catalysts in two consecutive hydration reactors. The first reactor contains a zeolite catalyst and the feed stream has minimum water. The second reactor contains acidic resin catalyst and the feed stream has an excess of water. The recycled product in this two-stage reactor is propan-2-ol which is recovered from both reactors as an aqueous azeotrope, concentrated by distillation and extraction and re-circulated to the reactors. Recycle of propan-2-ol was also proposed in [116], where a series of four hydration reactors with different water:olefin feed mole ratios, progressively increasing from 0.4 in the first reactor to 1.2 in the last, was used in such a way that the indirect propene hydration with propan-2-ol (Eq. II-15) preferably occurs. The reactor operation conditions were chosen so that a single non-aqueous liquid phase was sustained in the fixed bed of catalyst. Zeolite catalysts are said to be more efficient in reaction (Eq. II-15) than acidic resins.

Table II-2. Direct ethylene and propylene hydration reaction with different catalysts

Reagent	Gas phase / aq. phase	Catalyst	Pressure, MPa	Temperature, K	H_2O:olefin mole ratio	Feed rate, $kg\ l^{-1}\ hr^{-1}$	Conversion, % per pass	Yield of alcohol, $kg\ m^{-3}\ hr^{-1}$	Reference
Ethylene	G	H_3PO_4 /silica gel	8.7	558	0.67	2060	4.9	207	77
Propylene	A	$Cu_{1.5}HSiW_{12}O_{40}$	25	553	27	0.26 (C_3H_6) 3.0 (aq)	71	86.3	85
Ethylene	G	$H_4SiW_{12}O_{40}$ /Nb	6.8	533	0.3	1200	0.9	22	86
Propylene	G	$H_4SiW_{12}O_{40}$ /SiO_2	3.7	493	2.8	2000-11000	1.3-6.2	120-530	87
Propylene	A	Ion-exchange resin	20.7	422	11.8	0.6 (aq)	72.9	-	71
Propylene	G	ZSM-5	4.9	466	0.18	8.42[**]	-	0.66[*]	102
Propylene	G/A	ZSM-35	6.8	466	2.7	0.23[**] 0.26(aq)	40.75	-	101
Propylene	A	Ion-exchange resin	10	423	25.4	-	78	92.4	104

[*] $kg\ kg^{-1}\ hr^{-1}$
[**] weight hourly space velocity (WHSV)

III. _____ Experimental

III.1. Membrane preparation

Membranes and membrane precursors were kindly provided by MAST Carbon Ltd. All membranes used were based on NOVOLAC™ phenolic resin. The following procedure was used for manufacturing the precursor discs. Phenolic resin particles were milled to a desired particle size and sieved to provide a narrow particle size distribution. The shape of the milled particles depends upon the type of a mill used and has a strong effect on the further processing of the resin pastes. The paste consisting of phenolic resin powder, methylcellulose, polyethylene oxide and water was well mixed and placed in a mould in the shape of a disk. A hot pressing technique was used, the temperature gradually raised to 110°C in 5 minutes followed by cooling for 2 minutes. For most of the membranes used in this study the pressure was set at 10kN.

The precursor discs were cured at 523K in air for ca. 6 hours followed by carbonisation in a flow of nitrogen at 1073K for ca. 8 hours. It was noted that the curing process resulted in slight deformation – dishing – of the precursor discs manufactured from small resin particles (ca. 5μm). In order to minimise such a deformation, the precursor discs were sandwiched between two sheets of stainless steel mesh and placed under a weight (approximately 1kg). Temperature was increased from ambient to 523K at a rate of ca 1°K/minute.

Carbonisation was performed in a cylindrical quartz reactor equipped with flat quartz inserts accommodating up to 8 precursor discs per batch. The temperature of the quartz reactor was gradually increased from ambient to 1073K at approximate rate 5°K/min.

Despite all the precautions taken, the resulting disks were slightly deformed, i.e. dish-shaped. Following carbonisation, all membranes were cleaned with ethanol to remove any deposit of residual organic material from the surface. Membranes were polished using sandpaper to produce flat surfaces for better sealing in the membrane cell, rinsed with distilled water and dried in vacuum at 100°C for at least 12 hours.

The majority of membranes used in this study were carbonised in a flow of nitrogen. Carbonisation in carbon dioxide and hydrogen was also performed to investigate the

effect of environment on the surface properties of the resulting membranes. Among the three gases used, nitrogen is inert to carbon, carbon dioxide potentially oxidises the surface to make it more hydrophilic, hydrogen reduces the surface and makes it more hydrophobic. The average weight loss after carbonisation is shown in Table III-1.

Table III-1. Weight loss during carbonisation

Carbonisation environment	Weight loss, %
N_2	28.1 ± 3.7
H_2	33.5 ± 3.1
CO_2	29.4 ± 3.4

Several membrane samples were brominated with pure bromine at 410°C in a flow of argon for 7 hours. The reaction was performed in a three-neck pyrex flask equipped with a drop funnel, two stop-valves, a flow regulator and a wash bottle. The weight increase after reaction was found to be 32 ± 1 per cent.

Each batch of membranes used in this study is listed in Table III-2.

Table III-2. Carbon membranes batch description

Batch No	Precursor particle size, μm	Pressure, kN	Carbonised in	Further treatment
1	30	10	N_2	-
2	4.89	10	N_2	-
3	4.89	10	CO_2	-
4	4.89	10	H_2	-
5	4.89	10	N_2	bromination
6	<5	10	N_2	-
7	<5	40	N_2	-

III.2. Membrane characterisation

Membranes which are suitable for application as interphase contactors should possess a certain pore structure and surface chemistry [17]. The porous structure of an interphase contactor should provide a large interfacial area and easy control of the position of the interface. In the case of a high-pressure contactor the control of the interface within a membrane becomes the most important and difficult problem.

It follows from the literature on membrane distillation that, for a process in which the position of the gas-liquid interface within the membrane is of vital importance, the maximum pore size range ensuring the process pressure and its fluctuation does not result in complete membrane wetting is ca. $0.5 - 0.6\mu m$ [117]. This range of pore sizes was taken as a rough guide to the development of a high-pressure carbon membrane contactor.

A number of membranes were tested in a simple fluid displacement test rig in order to evaluate the dependence of the entering pressure on the pore size. The test rig consisted of a copper cell, nitrogen cylinder, a precision pressure regulator, a test gauge and a set of precision Gillmont rotameters (see Figure III-1). An Ashcroft test gauge was used, with the maximum pressure 50psi = 345kPa and accuracy 0.05psi = 0.345kPa. The minimum detectable flow rate was 0.0453ml/min, using the Gillmont micro-tube flowmeter.

The experimental procedure was as follows. A membrane was placed in the cell and sealed using two o-rings. The upper compartment of the cell was filled with liquid and tightly closed. A forward pressure regulator was used to increase the pressure in the upper compartment of the cell and flow readings were taken directly from the rotameters. A bleed valve was used for better pressure regulation. Gillmont calibration charts were used to calculate the flow rates. The same rig was also used to measure permeability of nitrogen through dry carbon membranes.
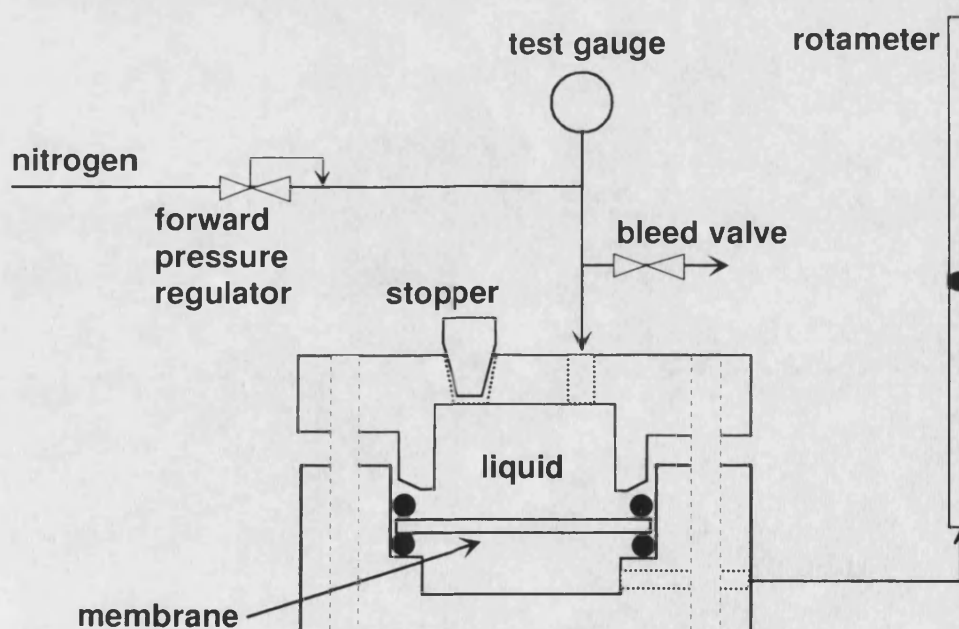
Figure III-1. Schematic diagram of the fluid displacement test rig.

A similar method of fluid displacement measurements is described in [118] for the determination of the pore-size distribution in ceramic membranes. Two immiscible fluids

are used: a wetting fluid is allowed to fill the pore volume of a membrane and a non-wetting fluid is pressed into the pores. In the present work water and aqueous phosphoric acid solution were pressed into the pores of a membrane to determine the entering pressure. Entering pressure is given by equation:

$$\Delta P_{interface} < \Delta P_{entry} = \frac{-2B\gamma_L \cos\theta}{r_{max}},$$ **Eq. III-1**

where B – geometrical factor related to the pore structure (B=1 for cylindrical pores); r_{max} – maximum pore radii; θ - liquid-solid contact angle; γ_L – liquid interfacial tension; ΔP_{entry} – entry pressure for liquid [119].

An example of the flow vs. pressure graph obtained in the experiments with the membranes from batch 1 is shown in Figure III-2. The membrane was tested "as received" i.e. no cleaning treatment was done prior to the measurement. The graph is typical for such fluid displacement experiments. It shows an initial non-linear region below the entering pressure followed by a linear increase in flow above the entering pressure. The value of entering pressure found for this particular membrane sample – ca. 8psi = 55.2kPa. Following this experiment the membrane was cleaned with ethanol and water and dried in vacuum at 100°C overnight. This resulted in the membrane becoming fully wetted by water.
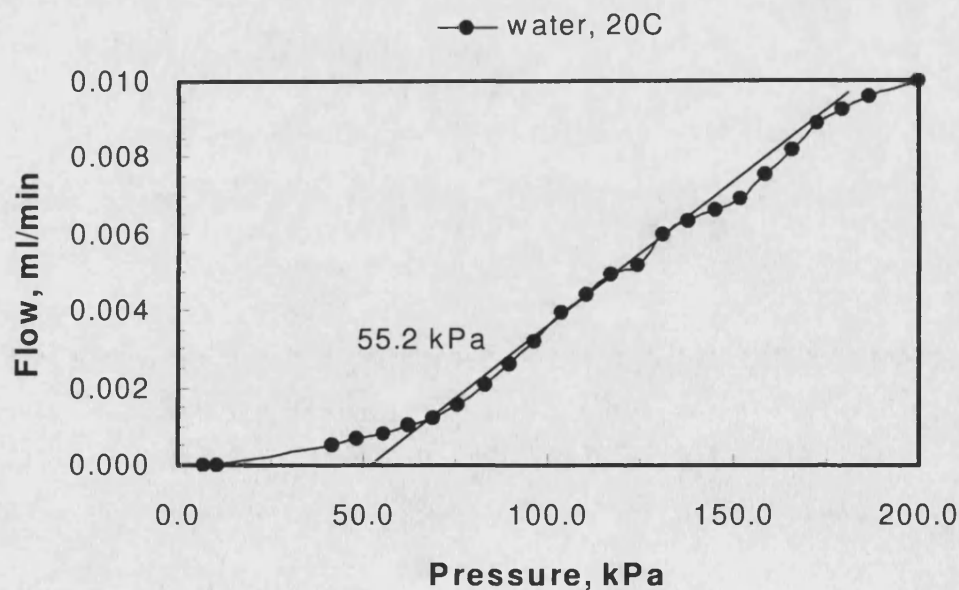
Figure III-2. Fluid displacement experiment.
Membrane from batch 1. Flow of water displaced by nitrogen.

It is apparent that in the initial experiment the hydrophobicity of the membrane was a result of impurities on the membrane surface. However, the clean surface of these carbon membranes is hydrophilic.

The porosity of these membranes (batch 1) was calculated from measurements of gas permeation as a function of pressure. The Blake-Kozeny equation gives the functional relationship between the superficial velocity of gas flowing through a porous body composed of particles of mean diameter D_p [120]:

$$\upsilon_0 = \frac{\Delta P}{L} \cdot \frac{D_p^2}{150\mu} \cdot \frac{\varepsilon^3}{(1-\varepsilon)^2}$$

Eq. III-2

where ΔP – pressure difference across the membrane; L – membrane thickness; ε - porosity and μ - viscosity.

The results of nitrogen permeation experiments were fitted to Eq. III-2 giving a mean particle diameter ca. 4.5μm and porosity ca. 46% (see Figure III-3). According to [121] the porosity of this carbon material should generally be around 40% i.e. close to the porosity of random packing of spheres; linear dimensions decrease approximately by a factor of 5 as a result of carbonisation. The values found for the membrane (batch 1) are in good agreement with literature empirical rules.
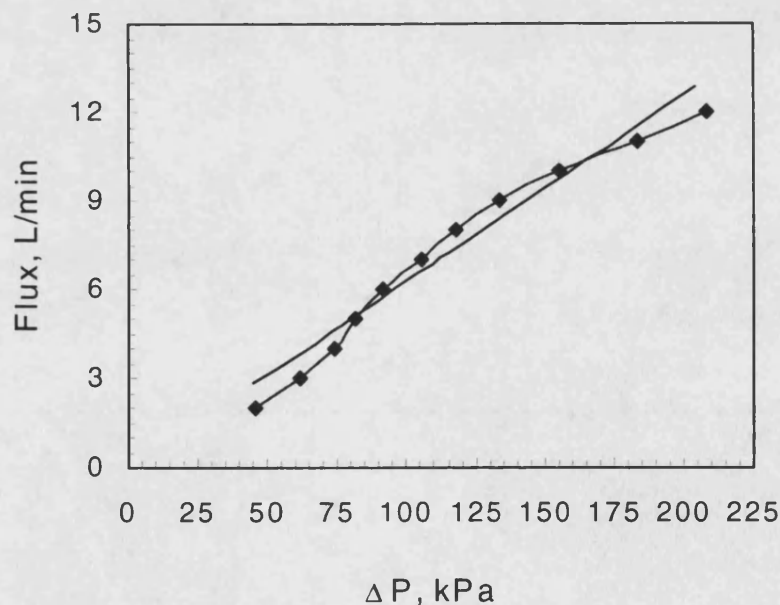
Figure III-3. Permeability of nitrogen through porous carbon membrane.
Membrane prepared using 30μm precursor particles (batch 1). Solid line - fit to Eq. III-2.

Although it seems that the clean surface of the carbon membranes is hydrophilic, it is possible that in the membranes with smaller pore sizes the entering pressure for the solutions of phosphoric acid will be higher. It is likely that the residual organic matter

within the membranes with smaller pores will have a permanent effect on the interphase behaviour.

Smaller pore sizes can be achieved using smaller particles of the resin precursor. A number of membranes were prepared using 4.89μm[*] particles (batch 2). Nitrogen permeability and entering pressure of aqueous solution of phosphoric acid were measured.

One of the results of the nitrogen permeability experiments is shown in Figure III-4. The two membrane samples measured gave similar values of particle size (1.81 and 1.92 μm) and porosity (14.0 and 14.3%). The value of porosity seems to be low, whereas the value of particle size seems to be too large. It was shown that this is due to the way the membranes are produced (see below).
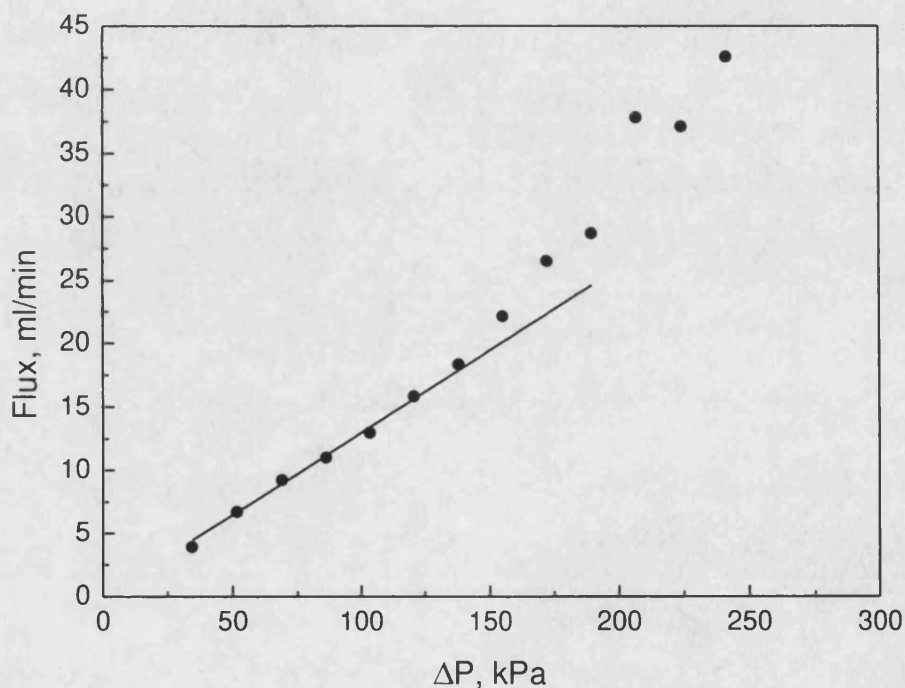
Figure III-4. Permeability of nitrogen through porous carbon membrane
Membrane prepared using 4.89μm precursor particles (batch 2). Ambient temperature.

Measurements of entering pressure were performed with 85wt% solution of phosphoric acid. Membrane samples were cleaned as described before. No flow was detected at a pressure of 241.5kPa = 2.38atm. The 2mm membrane sample broke at 310.5kPa. It seems that at ambient temperature the entering pressure of the 85wt% phosphoric acid solution is higher than 3atm. An attempt was made to measure the contact angle between these membranes and phosphoric acid solution and water.

Contact angles were measured using the sessile drop method [122] on a Ramé-Hart NRL goniometer. It was found that both water and phosphoric acid solution wet the surface of the studied membranes. Experimentally it means that a drop placed on the surface of a carbon disc would quickly disappear making the contact angle measurements nearly impossible.

A significant hysteresis of contact angle was observed when advancing and receding angles were measured. The most probable cause of the hysteresis in this particular case is the roughness of the surface [122]. In order to make a qualitative comparison, all values of contact angles were measured with approximately the same size of droplets on the freshly cleaned and dried membrane surfaces, with the rate of drop disappearance being considerably lower than that of the actual measurement.

The size of droplets was estimated from an approximation of a spherical cap, i.e.

$V = \frac{1}{6}\pi \cdot h \cdot \left(3r_b^2 + h^2\right)$, where r_b – radius at the base of a cap and h – height of a cap,

measured. Regardless of the carbonisation media (membrane batches 2,3,4) the average contact angle for all discs was found to be approximately 50° for phosphoric acid solution (85% wt). It seems that the carbonisation environment has little effect on the wetting of carbon membranes. This may be the result of oxidation of the carbon surface upon exposure to air. As indicated in [123], oxygen accumulation takes place even at room temperature regardless of the nature (natural or synthetic) of a carbon. The simplest way to modify permanently the surface chemistry of carbon is to use C-halide bonds to achieve strong covalent chemical bonding.

Contact angle measurements of the brominated membranes (membrane batch 5) revealed a broad hysteresis (see Figure III-5). The real contact angle lies between the values of advancing and receding contact angles, i.e. between 50 and 100. Therefore it is concluded that bromination of carbon membrane results in a decrease of wettability by phosphoric acid solution.

---

* The value of the precursor mean particle size as quoted by the material producer.
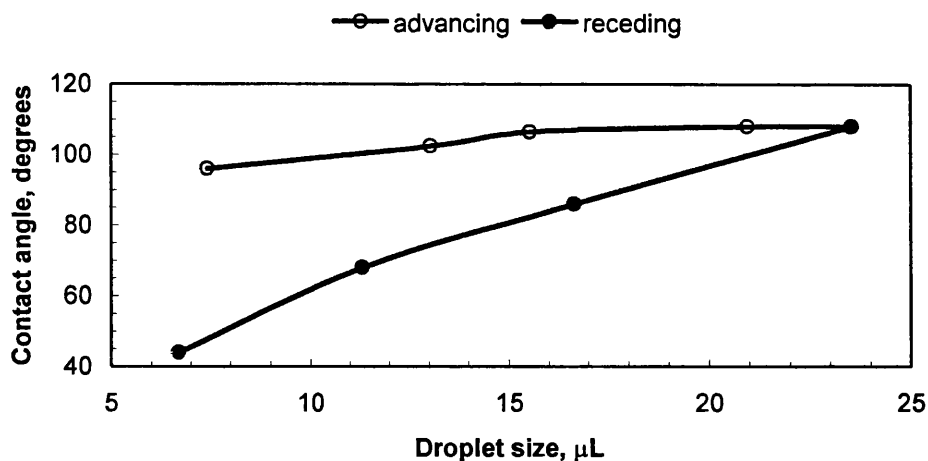
Figure III-5. Contact angle hysteresis.
Phosphoric acid 85wt% on Br-carbon membrane (batch 5)

Data on the contact angle between a phosphoric acid solution and porous carbon membranes can be used to estimate the entering pressure using Eq. III-1. Additional information on surface tension and pore size is required for this purpose. The surface tension of the phosphoric acid solution was measured using a WITE DB2KS microbalance equipped with a platinum ring. Measurements were performed at 19°C over a range of acid concentrations.

The experimental data are shown in Figure III-6. The data point at zero acid concentration was measured with demineralised water. The measured surface tension of water 70.6mN/m is close to the literature data 72.8mN/m at 20°C [147]. The slightly lower value is most likely due to the impurities in water. The measured value of surface tension of 85.4wt% phosphoric acid is 82.2mN/m. The increase in acid concentration results in an almost linear increase in surface tension until 96wt% of acid. Further increase in acid concentration results in a decrease in surface tension.
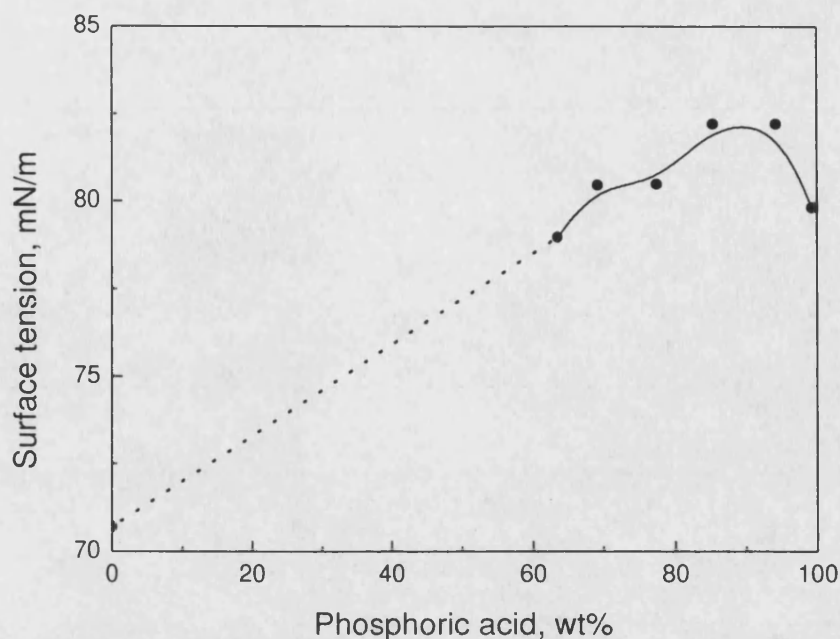
Figure III-6. Surface tension of phosphoric acid solutions at 293K.

The pore structure of the carbon membranes was characterised using low temperature nitrogen sorption, mercury porosimetry and scanning electron microscopy. Mercury intrusion experiments were performed with the samples from batches 2, 5-7. The results of calculations of porosity are given in Table III-3. The values of porosity were calculated for the total mercury intrusion volume measured, as well as for the volume of mercury in the pores of the listed median diameter. The latter gives the actual value of the volume of pores of this diameter.

Prior to comparing the results between samples it should be stressed that each membrane is unique in that sense that it is prepared individually i.e. pressed one at a time. It is therefore possible that the observed deviations in porosity and mean pore diameters are due to the manufacturing process only. Hence, there is no reason to attribute the differences in porosity to either bromination or catalytic reaction.
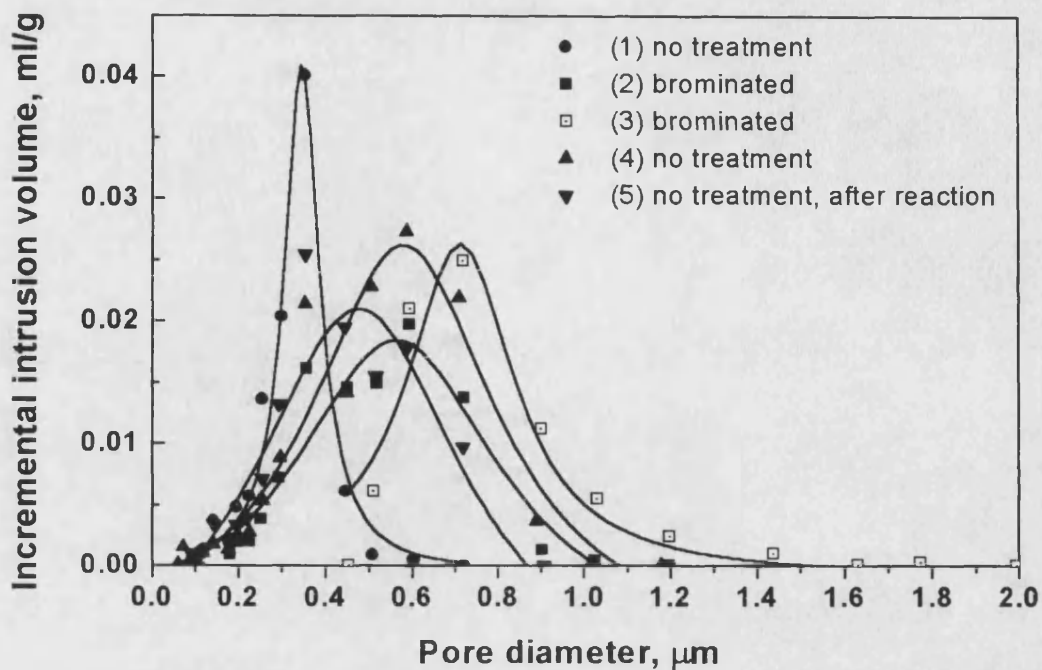
Figure III-7. Mercury porosimetry of membrane samples

Table III-3. Results of mercury porosimetry

Sample	Batch	Mean pore diameter, μm	Porosity, %	Total porosity recorded, %
1	2	0.35	11.74	24.21
2	5	0.56	14.16	19.49
3	5	0.71	8.04	24.73
4	2	0.58	14.90	22.70
5	2	0.45	10.74	39.60

Average apparent (skeletal) density: 1.47 g/cm^3

Average porosity: 12%

Average pore volume: 0.08 cm^3/g

Average pore diameter: 0.5 μm

Tortuosity of carbon membranes was estimated using the relationship between observed (D_{eff}) diffusivity in the porous sample and diffusivity in the absence of spatial constraints of the porous structure (D^0):

$$D_{eff} = D^0 \frac{\varepsilon}{\tau}$$

Eq. III-3

where ε is porosity and τ is tortuosity.

Steady-state Wicke-Kallenbach method of measuring diffusivity in porous solids was used [124]. Measurements were performed with the membrane sample (batch 2) glued into a 3mm thick stainless steel washer which was sealed in the cell between two silicon rubber washers. Design of the Wicke-Kallenbach cell is shown in Appendix B. Measurements were performed at 293K and flow rate of gases in the range of 650 ml/min. It was checked that at this flow rate there is no effect of boundary layer on the diffusivity [125]. Methane and nitrogen were used in these experiments. Measured effective diffusivity of methane in the carbon membranes was:

$$D^{eff}_{methane/nitrogen} = 1.58 \times 10^{-3} \text{ cm}^2/\text{sec} .$$

Diffusivity in the porous body with the average pore diameter of ca. 0.5μm is likely to be in the transitional regime, i.e. both bulk and Knudsen diffusivity should be considered [124]. The reference diffusivity is, therefore, calculated using equation III-4.

$$\frac{1}{D^0} = \frac{1}{D^0_{ab}} + \frac{1}{D^0_K}$$

Eq. III-4

The corresponding value of bulk (molecular) diffusion coefficient (D^0_{ab}) was calculated using Equation VII-8 shown in Chapter VII.1:

$$D^0_{methane/nitrogen} = 0.172 \text{ cm}^2/\text{sec} .$$

The corresponding value of Knudsen diffusion coefficient (D^0_K) was estimated using Equation III-5 [124]: $D^0_K = 1.04 \text{ cm}^2/\text{sec}$

$$D^0_K = 9700 \cdot r \cdot \sqrt{\frac{T}{M}}$$

Eq. III-5

where r is effective pore radius [cm] and M is molecular weight.

Using Equation III-4 diffusivity of methane is $D^0=0.147$ cm^2/sec, i.e. molecular diffusion dominates over Knudsen. Using the value of porosity and measured effective diffusivity, the tortuosity factor is $\tau=12.1$. The obtained value of tortuosity factor is just outside the most common range between 3 and 10 [124].

An SEM picture of a membrane from batch 2 (carbonised in N$_2$ flow, no further treatment) is shown in Figure III-9. It reveals considerable deformation of originally spherical resin particles and large areas of compressed impermeable matter, thus confirming the low porosity values measured by mercury porosimetry. Surprisingly,

further increase in pressure during the manufacturing the precursor discs seems to have little effect on the macropore structure of the material (see Figure III-8).

Values of porosity found using the mercury intrusion method correspond well with the values found earlier using the nitrogen permeation technique (see Figure III-4 and discussion above). It seems that membranes produced from resin particles of approximately 5µm diameter are significantly deformed during the hot pressing procedure. According to the manufacturer, carbonisation of the NOVOLAC™ resin results in a decrease in linear dimensions by a factor of five. For batches 2-5 of the membranes used in this work the size of the carbonised particles should therefore be approximately 1µm. Measurements of nitrogen permeability, mercury intrusion and the SEM image show the size of carbonised particles of ca. 2µm and porosity of membranes of ca. 12%.
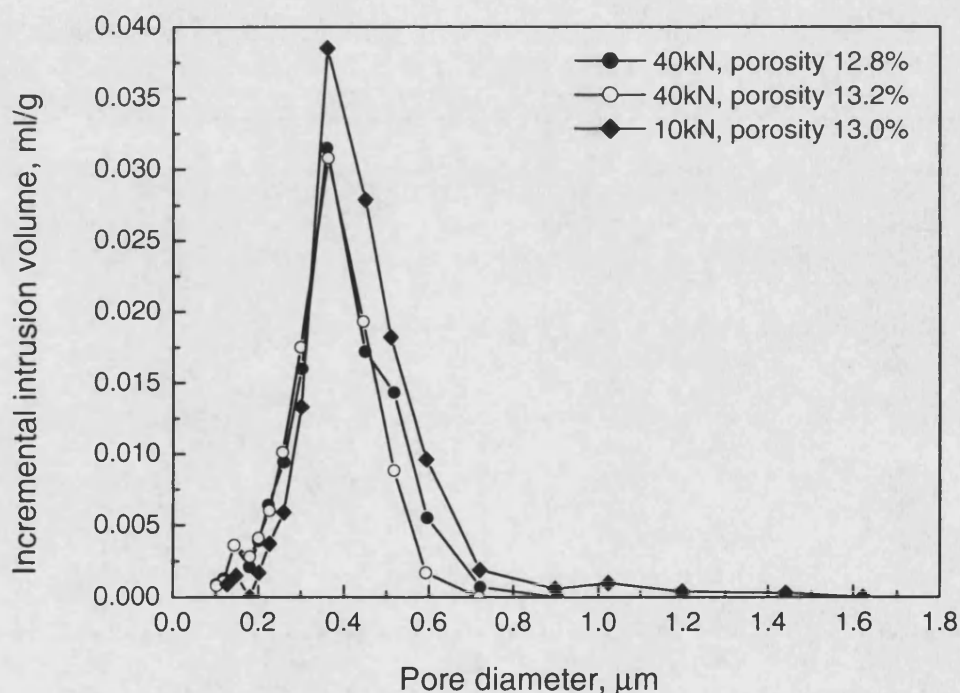
Figure III-8. Mercury porosimetry of carbon membranes
Membranes pressed at 10 and 40kN. Batches 6 & 7.

Using the data on the pore size of the membranes (batch 2,5), surface tension of phosphoric acid solutions and contact angle between the surface of the membranes and phosphoric acid, the entering pressure of 85wt% phosphoric acid solution at ambient temperature can be estimated using Eq. III-1. For a contact angle 50° and an average pore diameter 0.5µm, the capillary pressure within the porous carbon is approximately

400kPa. For a contact angle 100°, measured for the brominated membrane the entering pressure is approximately 100kPa. Neither of these estimates corresponds to the experimental observation that no flow of acid through the membrane was detected at 300kPa pressure at ambient temperature (see above). It is suggested that the contact angle between the acid solution and the inside surface of carbon membranes is considerably different from that on the outer surface. This could be due to deposits of residual organic material produced during carbonisation. Hence, the membranes exhibit the behaviour of a hydrophobic material. Further discussion of the effect of the contact angle and surface tension on the position of the interface within a porous contactor is given in Chapters VI and VIII.
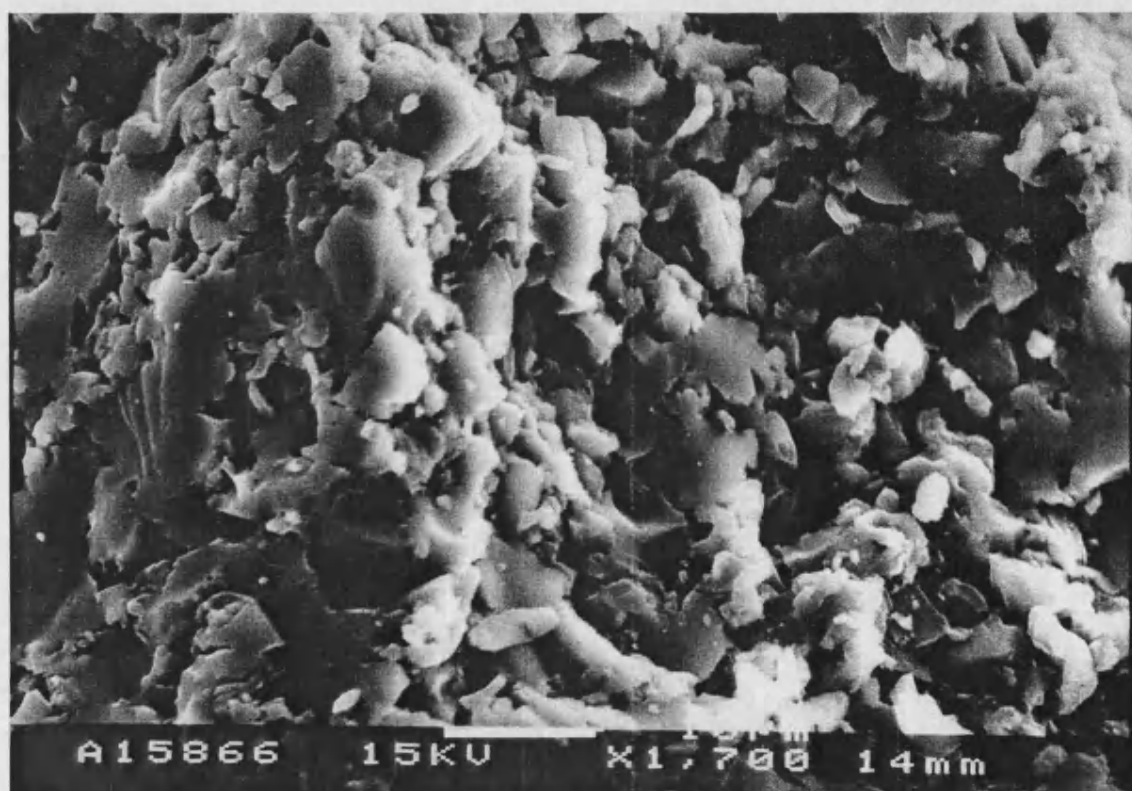
Figure III-9. SEM of carbon membrane.

To complete the investigation of the porous structure of the carbon membrane contactors, the adsorption-desorption isotherms of nitrogen were measured for one of the carbon membranes (batch 2). The isotherm at 77K was measured using an ASAP 2010 instrument (Micromeritics). The equilibration time per point was ca. 20-30min for low pressures (P/P_s < 0.5) and 8-10min for higher relative pressures. The shape of the isotherm shown in Figure III-10 is characteristic of solid materials with pore sizes in the range of ultramicropores, i.e. less than 0.8nm [126]. A similar nitrogen sorption isotherm

for NOVOCARB™ carbon was reported in [121]. The results of analysis of the isotherm showed a high micropore surface area and volume.

Results of the mercury porosimetry study and measurements of low temperature nitrogen adsorption showed that the pore structure of the carbon membranes used in this work consists of two distinct pore sizes (see Figure III-11). The macropore region is formed by the random packing of near spherical precursor particles of ca. 5μm diameter. Compression of resin particles under a force of 10kN at 110°C resulted in deformation of particle shape and decrease of intraparticle distances. The average pore diameter of the macropore region is ca. 0.53μm and pore volume ca. 0.081cm³/g. After carbonisation the precursor particles become microporous with an average pore diameter of 0.7nm and micropore volume 0.222cm³/g.
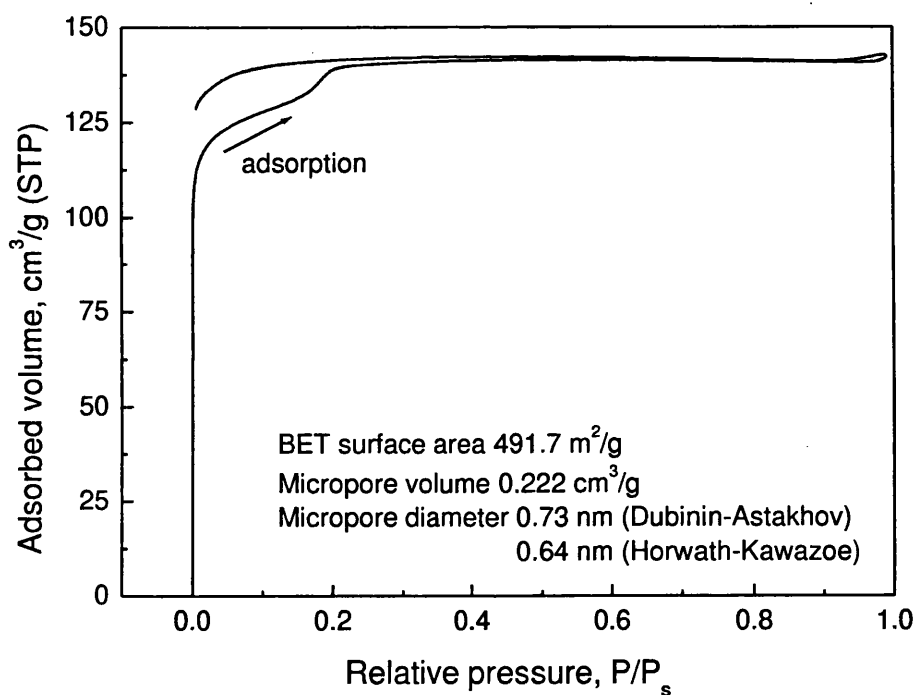
Figure III-10. Isotherm of nitrogen adsorption onto carbon membrane, 77K. Membrane produced from 5μm precursor particle size (batch 2).

micropores   macropores   carbonised particle
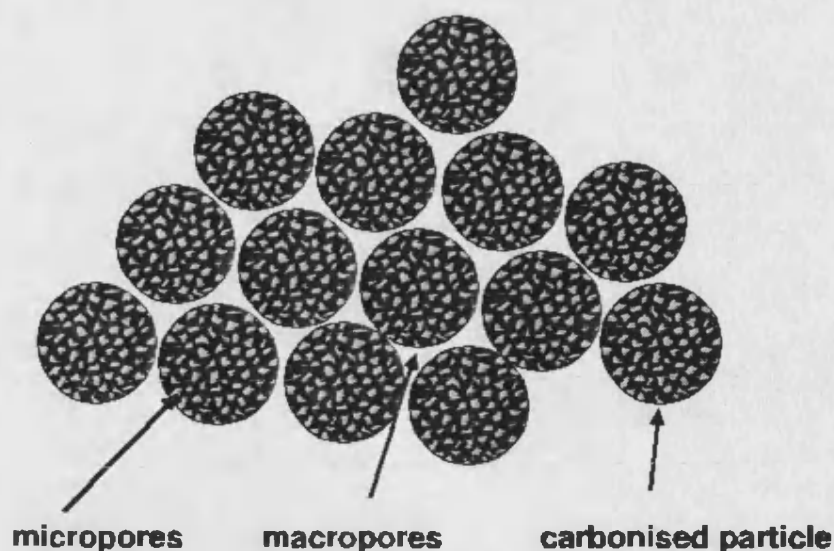
Figure III-11. Schematic representation of bi-porous structure of NOVOCARB™ membranes

III.3. Batch reactor

A conventional autoclave batch reactor was used for equilibrium and kinetic studies. The reactor used was a Baskerville 350ml autoclave equipped with a magnetic stirrer. The volume of the autoclave was calibrated by measuring the pressure change upon expansion of nitrogen from the autoclave into a calibrated volume assuming ideal gas behaviour.

Maximum operational conditions of the autoclave were 50bar and 200°C. A glass lined reactor, PTFE stirrer and PTFE lined thermocouple sleeve were used to prevent corrosion of the reactor. Sampling of the gas phase was achieved via a heated stainless steel line. Analysis was performed using a gas chromatograph as described in the Analysis section of this chapter (page 58). The gas sampling valve was evacuated between taking samples.

III.4. Semi-batch low pressure reactor

A low pressure semi-batch glass reactor was used for screening of surfactants. The reactor comprised a 500ml Pyrex three-neck flask, a heating mantel with magnetic stirrer, a mass-flow controller and a wash-bottle to ensure a constant back-pressure in the flask. A schematic diagram of the reactor is shown in Figure III-12.
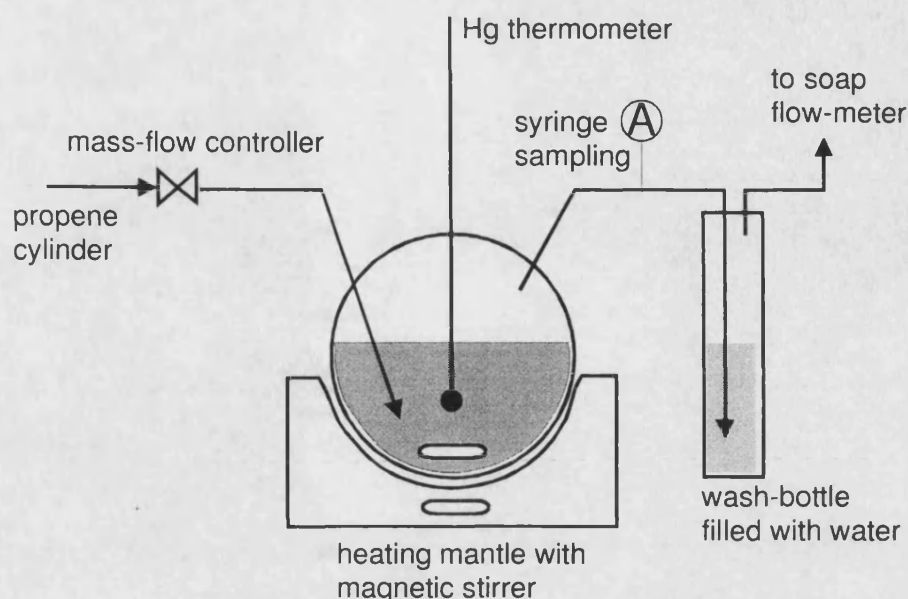
Figure III-12. Schematic diagram of the low-pressure semi-batch reactor.

All surfactants used were obtained from Sigma. In each experiment a weighted amount of surfactant was introduced to a weighted amount of acid in the flask and heated to a required temperature. The reaction was started after the surfactant was completely dissolved. A mild agitation regime was used to ensure that no foam was formed at the gas-liquid interface. The gas-phase samples were taken with a syringe from silicone tubing connecting the flask with a wash-bottle. The gas-phase samples were manually injected into the GC and analysis was performed using the method described in the Analysis section (page 58).

III.5. Experimental apparatus for membrane reactor studies

The apparatus was designed and constructed to perform the catalytic experiments in a membrane reactor. The apparatus was designed to operate at temperatures up to 205°C and pressures up to 3.0 MPa. Maximum temperature was limited by the thermal stability of the polyamide diaphragm of the pressure regulator used. The maximum pressure was limited by the operating range of the transducers used. The ranges of operating temperatures and pressures used in commercial propene hydration processes are 150-200°C and 1.0-6.0 MPa. The range of pressures and temperatures used in this study is therefore representative of that used in the commercial applications. A schematic diagram of the reactor system is shown in Figure III-14. A photographic image of the reactor is shown in Appendix A together with the details of the membrane cell design.

Initially, the reactor, liquid reservoir and all liquid feed lines were made of copper. Copper is used in the commercial supported liquid phase hydration process to reduce the corrosion effect of phosphoric acid. Significant corrosion of all copper parts was observed and the reactor and most of the liquid circulation lines were replaced with stainless steel parts. The most common grade – grade 316 stainless steel was used. No significant corrosion of steel components was observed at temperatures below 100°C. At 130°C corrosion became significant. Leached metals were qualitatively analysed by atomic absorption spectroscopy (Perkin-Elmer) which showed high concentrations of chromium and nickel, both being present in the stainless steel. No copper was determined in the liquid phase and this indicates that the remaining copper parts of the reactor were passive. It is likely that initially strong corrosion of copper was due to contact between copper and stainless steel compression fittings. Strong corrosion of the stainless steel parts was also observed in the batch reactor. Comparison of the results of the batch kinetic experiments obtained in the glass lined reactor and the steel reactor showed no difference. Therefore it was concluded that the presence of metal ions could be ignored in the analysis of the results of the membrane reactor experiments.

The apparatus was enclosed in a heat-insulated cabinet equipped with a 3kW heater and a fan to provide a uniform temperature distribution inside the cabinet. Liquid tank was heated by a stirrer-plate equipped with a Pt-100 temperature probe and a controller. All the gas lines between the reactor and the flow-meter were insulated and heated to prevent condensation of the vapour products. The gas flow was monitored using Gillmont precision rotameters which were in turn checked against a bubble flow-meter. Because the flow measurements were performed at atmospheric pressure and temperature different from that in the reactor, the flow rate was later re-calculated to the conditions inside the reactor. Compressibility factors for given (P,T) were obtained graphically (see Figure III-13) using literature data [127].
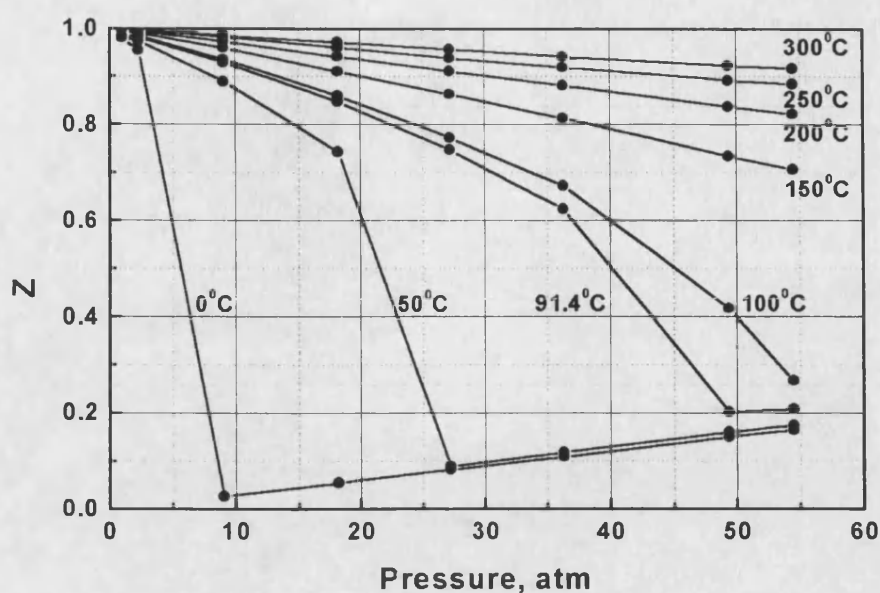
Figure III-13. Compressibility factor for propylene.
Reproduced from [127].

Two high-temperature transducers (XTE-190M, "KULITE Ltd.") were installed in the gas and liquid lines close to the reactor to enable accurate pressure measurement. Both transducers operated in gauge mode and were connected to a PC via a PCL 812 PG data acquisition card (Advantech Ltd.) and LabVIEW^{TM} (National Instruments Inc.) software.

Regulation of pressure was performed automatically with the aid of the custom developed software described later. The hardware part of the pressure regulation system consisted of two proportional servo valves PPR-1 and PPR-2 (QBT-1 "Proportion Air") (see Figure III-14). Valve PPR-2 was used directly to admit nitrogen to the liquid reservoir and thus pressurise the liquid phase. Because the high temperature of the gaseous feed prohibits direct use of servo valves, the valve PPR-1 was used to regulate the gaseous pressure via a mechanical proportional valve (MPR).

A conductivity sensor was installed in the membrane cell on the gas side of the membrane. The sensor was connected to a relay device and, in turn, to the PC and provided an alarm signal to indicate the presence of any liquid on the gas side of a membrane. This could happen in the event of membrane flooding or membrane breakage.

A duplex-head plunger pump was used for the circulation of liquid. Two pulse dampers were installed immediately before and after the pump in order to reduce the pressure pulsation. For an operating pressure of 2MPa the maximum liquid pressure deviation did not exceed 0.01 and 0.04MPa, with and without pulse dampers respectively.
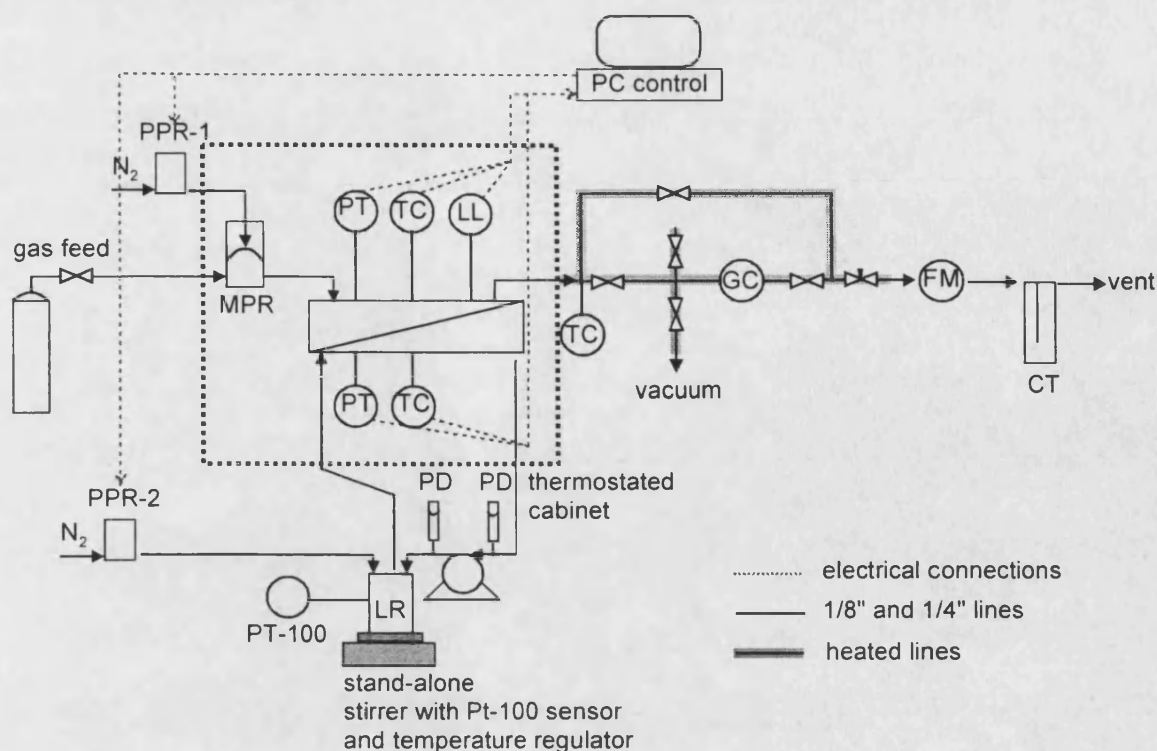
CT: cold trap   MPR: mechanical pressure regulator
FM: flowmeter   PT: pressure transducer
GC: gas chromatograph sampling valve   PD: pulse damper
LL: liquid level sensor   PPR: servo pressure regulators
LR: liquid reservoir   TC: thermocouple

Figure III-14. Experimental apparatus for two-phase membrane catalysis studies

III.6. Control system

Because of the narrow range of transmembrane pressures that had to be maintained, an automatic control system was developed. As shown in the previous sections, the maximum allowed transmembrane pressure depends on membrane pore size, liquid-solid wetting and gas-liquid interfacial tension. All three parameters may vary between experiments and even during the course of an experiment. Solid-liquid wetting and gas-liquid interfacial tension both depend on the chemical composition of the gas and liquid phases. Hence, these latter two parameters will inevitably change during start-up of the reactor until steady state operation is reached. Hence, the ultimate goal of the control system is to adjust the transmembrane pressure according to the behaviour of both the reaction mixture and equipment.

During the stages of start-up and shut-down, when pressure in the gas and liquid containing parts of the reactor system have to be changed from zero to a desired pressure (reverse on shut-down), the non-linear behaviour of the equipment is of major

importance for maintaining the transmembrane pressure within a desired range. Changes of pressure and transmembrane pressure during this stage of the experiment or reactor life are far greater in magnitude than during steady-state operation. Hence, the main development in the control system was dedicated to the start-up and shut down of the reactor system to prevent membrane flooding and destruction. It was also discovered that using some specific features of the designed control software and equipment a periodic pressure oscillation pattern could be achieved.

Non-linear behaviour of equipment

For the first stage in development of the of control system, the behaviour of all pieces of equipment used was recorded over the operating range of pressures and temperatures. The equipment that is directly involved in pressure regulation consists of two pressure transducers and two pressure regulators.

The pressure transducers used ("KULITE XTE-190M") are miniature high temperature sensors equipped with a metal membrane to withstand aggressive fluids. To the author's knowledge these devices were the only pressure transducers available at the time of this research project which could operate at temperatures as high as 300°C. Being semiconductor devices, the transducers showed significant non-linearity with temperature and slight non-linearity of response at different temperatures. Temperature shifts from zero-line, i.e. the signal of the pressure transducers at atmospheric pressure, is represented in Figure III-15, the two transducers being marked as "gas" and "liquid".

In order to compensate for non-linear behaviour of the pressure sensors, extensive calibration data obtained with a Budenberg dead-weight tester over a 2.5MPa pressure and 200°C temperature range were fitted with a polynomial of the form

$$P(atm) = \frac{Volt}{k(T)} + \alpha(T) \pm \sigma_{n-1}$$, where $k(T)$ and $\alpha(T)$ are cubic polynomials and σ_{n-1} is the

standard deviation.

The standard quadratic deviation of the pressure measurements was found to be $\sigma_{n-1,l}$ =0.09, $\sigma_{n-1,g}$=0.12 (subscripts l,g refer to liquid and gas respectively) over the whole range of pressures and temperatures. These polynomials were used in the data acquisition and control software to obtain the pressure readings at any temperature. Because of direct contact with phosphoric acid, one of the two transducers significantly changed its response curve after ca. 6 months. Both devices were re-calibrated using a DRUCK DPI 603 portable pressure calibrator. A new set of coefficients was then calculated for both

pressure transducers. The calculated deviation of pressure after re-calibration was found to be $\sigma_{n-1,l}=0.08$, $\sigma_{n-1,g}=0.04$ over the range of temperatures between 15-150°C and pressures between 0-2.0MPa gauge.
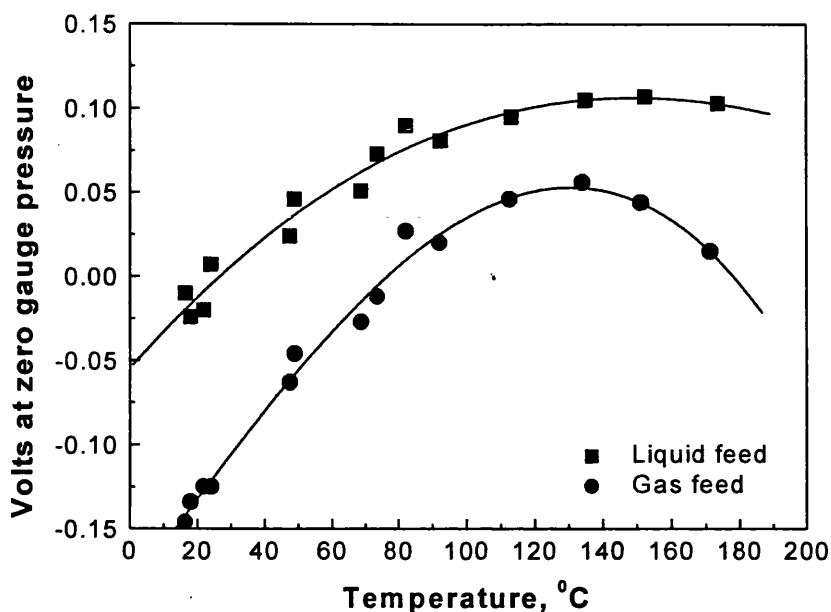
Figure III-15. Temperature shift from zero-line of pressure transducers

The two proportional pressure regulators (PPR1&2), each equipped with two servo valves and an internal pressure transducer, showed excellent linearity over a 2.5MPa pressure range ($\sigma_{n-1}=0.02$). However, due to their temperature limitations these regulators could not be used at temperatures above 70°C. Hence, a mechanical proportional forward reducing regulator was used in the gas stream. This regulator was equipped with a polyamide membrane which allowed a maximum operational temperature of 205°C. The regulator was installed directly inside the heating cabinet. One of the two servo regulators was used to open and control the membrane of the mechanical regulator. The mechanical regulator was found to be extremely non-linear, with too low a response at low pressures and too high a response at high pressures. It also had a tendency to slow oscillations at high pressures.

Another piece of equipment that may affect the pressure in the reactor is the liquid circulation pump. A duplex-head plunger pump was used in this study. It was found that at high pressures the pulsation of liquid pressure invoked by the pump reached 0.04MPa. An example of liquid pressure pulsation recorded is shown in Figure III-16. Pulsation of the transmembrane pressure was suppressed by using pulse dampers immediately before

and after the pump. One of the dampers was specifically designed to provide 2% damping at 2.0MPa gauge pressure. This was achieved by an 1.8MPa air cushion separated from the liquid stream by a PTFE membrane. The second damper was a 300ml cylinder, providing dead-volume on the suction port of the pump. Combination of the two pulse dampers significantly increased the period of pulsation, giving more regular and long pulses compared to operation without damping. The shape of the pulse obtained with both dampers installed indicated that the custom-designed damper was more efficient than the dead-volume damper. This is probably the main reason for a very modest reduction in the amplitude of pulsation.
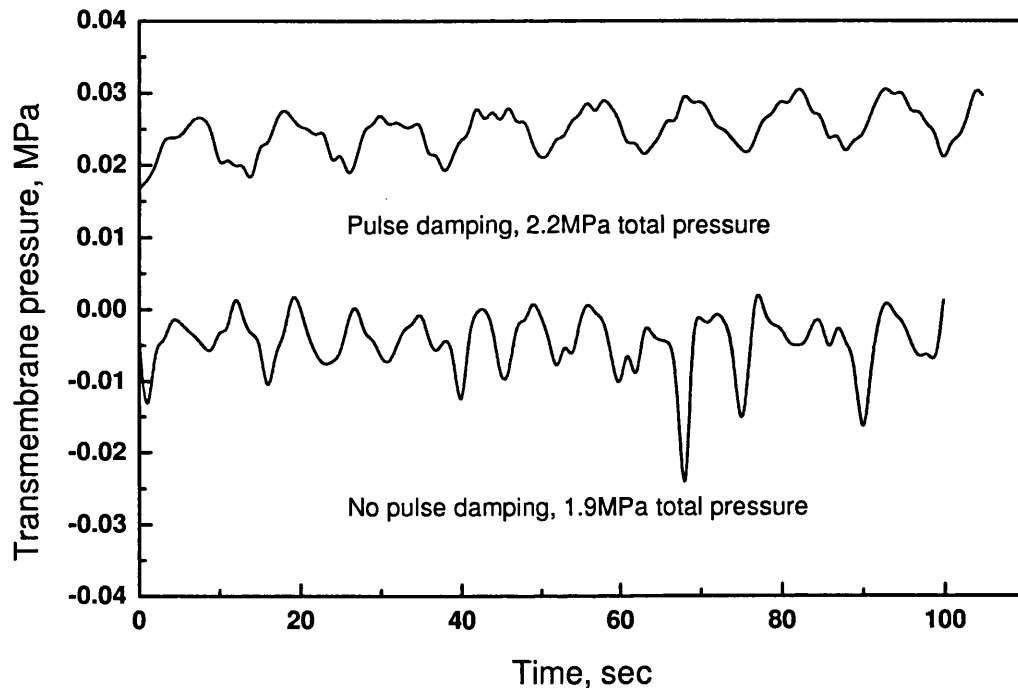
Figure III-16. Liquid pressure pulsation

To summarise the results of this section, the control system to be designed must be able to respond adequately to the non-linear behaviour of the instruments used and be capable of adapting to spontaneous changes in the system behaviour. Such a task limits the choice of control methods to fuzzy control, the most important feature of which is adaptability to non-linear variation of parameters.

A review of applications of fuzzy control in chemical engineering

Fuzzy set theory was first introduced by Lotfi A. Zadeh in 1965 [128]. Since then the theory has been developing so fast that, by the end of 1990-s, devices based on fuzzy

mathematics could be found in many household appliances, electrical plants, robots etc. Its astonishing success is due to the unique nature of fuzzy sets, allowing one to account for vagueness and the imprecise nature of real objects in rigid mathematical terms.

There is very little literature available on the application of fuzzy mathematics in chemical engineering. A self-adaptive algorithm for pH control is described in [129]. The controller uses fuzzy reasoning for altering the scaling coefficients (coefficients c_i in Eq. III-6) employed for calculating the control output, on the basis of the results of the previous control actions. This allows the algorithm to learn the behaviour of a given system and alter the control output parameters. In the study reported in [129] the need for alternative to PID control system arises from highly non-linear and irregular behaviour of the system. An additional difficulty is presented by the time-lag between the action (addition of acid or base) and the result (change of pH), which is due to the mixing of solutions and depends on many parameters i.e. temperature, viscosity and volume of liquid, stirrer speed. It is obvious that the time-lag is generally unpredictable, therefore using the model-based or derivative-based control would be a disadvantage. It was found experimentally that the fuzzy controller was more efficient compared to a conventional PID controller.

A similar problem of control in a system with considerable time-lag was addressed in [130] where a fuzzy controller for a tubular separation plant is described. The system describer in this paper [130] is analogous to a membrane filtration plant. The control parameter, being the concentration of a desired component in the retentate or permeate, depends on the total flow, pressure and membrane fouling characteristics. The main feature of the system is the time delay between the change in the total flow or other parameter and its effect on the system. This time lag is a function of membrane properties and stream properties and varies significantly. This is the reason for conventional control systems to be rather ineffective when applied to systems with long and erratic relaxation behaviour. The fuzzy controller developed in [130] consists of a simple rule-base fuzzy inference part and a predictive part that utilises a linear equation for approximation. Efficiency of the designed predictive fuzzy controller was gauged against a conventional PID controller. The fuzzy controller showed significantly better set-point tracking and less oscillation compared to the PID controller.

The efficiency of the simple fuzzy controllers that are model-free or use a combination of linear models with variable scaling factors in chemical processes was demonstrated experimentally in [129,130,131]. As it was discussed at length in [132], the so-called Sugeno fuzzy controller that utilises linear rules with adaptive scaling factors

are very efficient and could be used for most chemical engineering applications (in fact for *any* control applications as it was demonstrated theoretically in [133]):

$$IF \quad x_1 \text{ is } B_1 \text{ AND}...\text{AND } x_n \text{ is } B_n \quad THEN$$

$$y = c_0 + c_1 x_1 + c_2 x_2 + ... + c_n x_n$$

<div align="right">**Eq. III-6**</div>

Here x_i are the fuzzy functions describing deviation of a control parameter from its optimum value; y – is the control action.

A modification of this approach is an adaptive algorithm that modifies fuzzy functions instead of fuzzy rules. This is by far a more complex problem because of the number of fuzzy membership functions usually used and the shape of these functions. Despite these problems a successful development was described in [134], where generic algorithms were used to modify the functions of a fuzzy controller.

An original fuzzy controller was developed for optimum control of a pyrolysis pilot plant for ethylene production [135]. The task of the designed controller was to perform global optimisation of the process, i.e. to achieve the longest possible reactor life-time and optimum product yield. Such parameters as the number of reactors, links between inlets and outlets of the reactors and age and performance of each reactor were taken into account. In order to obtain the control model the authors developed new mathematical equations based on fuzzy mathematics. The performance of the resulting control model was tested on pilot plant and compared with a traditional manual control and control with "crisp" equations. It was found that optimisation by crisp models gives rise to a 1.2% increase in product yield and a 3.8% increase in the reactor life-time. Fuzzy optimisation resulted in a 4.0% increase in the lifetime of the reactor and a 1.0% increase in the product yield. As one can see, in the case of very complex reactor optimisation problem, optimisation with fuzzy equations and crisp equations give similar results. The modest performance of the fuzzy controller may have been a result of using non-adaptive non-predictive model.

Control of high pressure membrane contactor

The main objective of the development of the control system for the high-pressure membrane contactor is to provide smooth start-up, operation and shut-down of the reactor. Because the gaseous pressure regulator used was less sensitive than the liquid pressure regulator it was not feasible to achieve fast pulsation of the gas pressure to compensate for the pulsation in liquid flow. Therefore during the normal operation the necessary two controllers (the liquid pressure controller and the gas pressure controller) were made independent.

A schematic diagram of the developed control system is shown in Figure III-17. It represents a closed-loop non-adaptive control system, in which the human operator can play an active role by switching from normal operation to shut-down or by switching off the adjustment of the liquid pressure near the set-point.

The controller utilises a weighted average equation to calculate fuzzy implications [136]:

$$y = \frac{\sum_i R_i \cdot \mu_i(x)}{\sum_i \mu_i(x)},$$

Eq. III-7

where R_i is the value of the i-th rule, $\mu_i(x)$ is the value of i-th membership function corresponding to the input crisp number x.

The first control block is the liquid pressure controller. Its first action at the start of the reactor may be considered as feed-forward control (see Table III-4 rule 1). The fuzzy implications of the liquid controller were designed as polynomials with scaling factors directly related to the difference between the actual pressure and the set pressure. In order to decrease the influence of the pressure pulsation on the performance of the control system the operator can switch to a mode in which the control output of this part of the system is constant (Table III-4 rule 8'). This method proved to be sufficiently robust to perform experiments as long as 56 hours.
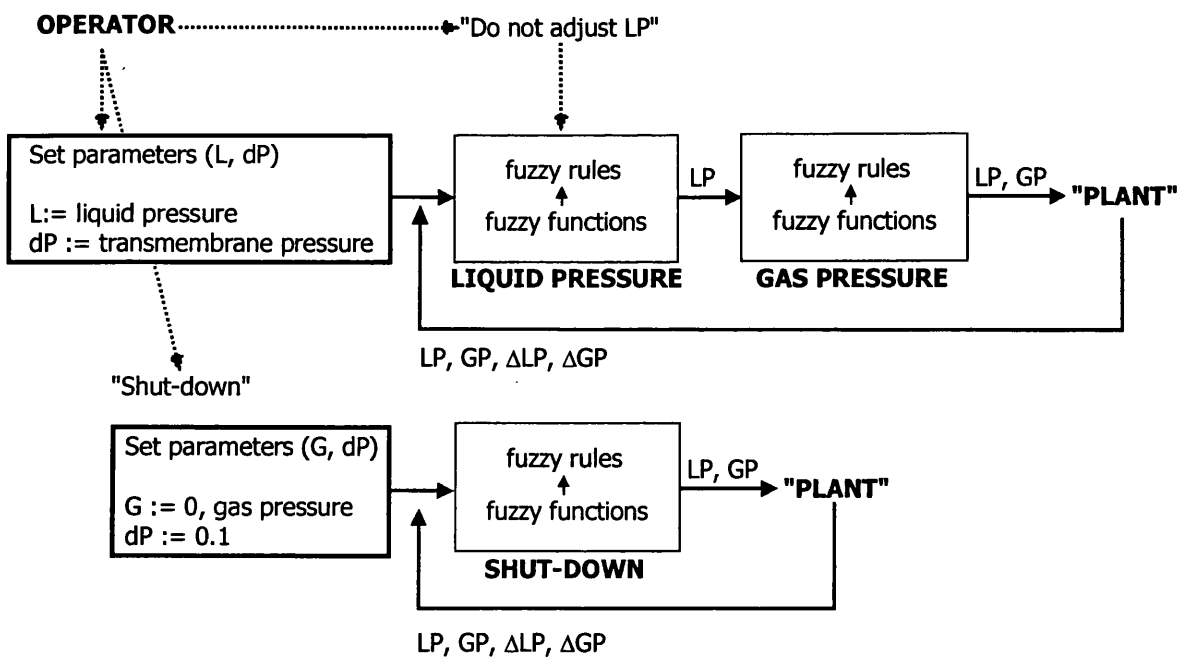
Figure III-17. Diagram of the control system for high pressure membrane contactor

L — set pressure for the liquid-filled part of the reactor; LP — pressure in the liquid-filled part of the reactor; GP — pressure in the gas-filled part of the reactor; dP — transmembrane pressure; ΔLP(GP) — difference between measured pressure before and after action.

On start-up the output of the gas pressure controller is directly related to the output of the liquid pressure controller. As the gas pressure approaches the set-point the output of the gas pressure controller gradually becomes independent of the liquid pressure (Table III-4 rules 4-6). The corresponding fuzzy membership functions are shown in Figure III-18 and Figure III-19. Figure III-20 shows the shapes of membership functions and the calculation procedure for the value of a membership function.

The performance of the control system was first tested in simulation runs, i.e. in the programming environment assuming ideal conditions (no action-response delay, no oscillations, linear response). The simulation of the start-up of the reactor is shown in Figure III-21.

The shut-down procedure is performed by a dedicated controller in which the gaseous pressure is adjusted according to the actual rate of pressure decrease and the liquid pressure is adjusted to give constant transmembrane pressure. In the actual experiments shut-down was usually performed manually, i.e. the rate of decrease of gas pressure was regulated manually using a back-pressure regulating needle valve. The role of the control system was to maintain the transmembrane pressure at a constant level by adjusting the liquid pressure.

At set-point, the active functions – function 8 in the liquid pressure controller and function 5 in the gas pressure controller – were given a certain tolerance, reflected in the trapezoidal shape of the functions (width of "bc", see Figure III-20). There was significant effect of the tolerance of the gas pressure control on the performance of the system. This effect was the result of a combination of the set pressure tolerance and the peculiarities of the response of the pressure regulating hardware used. At one per cent gas pressure tolerance, the gaseous pressure was stable. Therefore any fluctuations in the transmembrane pressure were those invoked by the liquid circulation pump. At two per cent of the pressure tolerance the gaseous pressure began to oscillate. The resulting oscillations of the transmembrane pressure are shown in Figure III-22. The amplitude of these oscillations was controlled by the tolerance of the set gas pressure which is given by the fuzzy function 5 of the gas pressure controller.

Data shown in Figure III-22 were recorded during actual catalysis runs. The performance of the control system was strongly dependent on the rate of system response. It was possible to regulate the rate of response by adjusting pressure increments in fuzzy implications and rate of data acquisition. The latter parameter characterises the time interval between reading and writing data to an AD/DA interface card. The best results in terms of smoothness of start-up were achieved with a very slow pressure

increase. It is apparent from Figure III-23 that the time required for start-up is of no importance and depends on the actual performance of the system. In all further experiments much larger pressure increments were used, resulting in faster start-up with high transmembrane differences. This was possible due to the high mechanical strength of carbon membranes and the narrow pore sizes of membranes used. The performance of the control system was monitored during catalysis experiments and is shown along with the results (see Chapter VI).

The control system was programmed using the graphical object-oriented environment in LabVIEW™ v5.0. Listings of the programs are shown in Appendix C.

Table III-4. Rule-base for the pressure controller (start-up and normal operation)

№	Rule	№	Rule
	Liquid pressure controller (LC)		Gas pressure controller (GC)
1	$P_{in}+\Delta P_1$	1	LC_{out}
2	$0.5\cdot(0.05P_{set}+P_{in}+\Delta P_2)$	2	$LC_{out}-\Delta P_{set}\cdot\dfrac{P_{in}}{P_{set}}$
3	$0.5\cdot(0.1P_{set}+P_{in}+\Delta P_3)$	3	$LC_{out}-\Delta P_{set}\cdot\dfrac{P_{in}}{P_{set}}$
4	$0.5\cdot(0.475P_{set}+P_{in}+\Delta P_4)$	4	$\max(GC_{out},P_{in})+\Delta P_4$
5	$0.5\cdot(0.85P_{set}+P_{in}+\Delta P_5)$	5	GC_{out}
6	$0.5\cdot(0.925P_{set}+P_{in}+\Delta P_6)$	6	$\min(GC_{out},P_{in})-\Delta P_6$
7	$0.5\cdot(0.95P_{set}+P_{in}+\Delta P_7)$		
8	$0.5\cdot(P_{set}+P_{in})$		
9	$P_{in}-\Delta P_9$		
10	$P_{in}-\Delta P_{10}$		
8'	P_{set}		

Notation in the table:

P_{in} – pressure measurement in liquid or gas phases

P_{set} – set pressure in liquid or gas phases

ΔP_{set} – set transmembrane pressure

ΔP_i – pressure increment

LC_{out} – output of liquid pressure controller

GC_{out} – output of gas pressure controller on the previous iteration
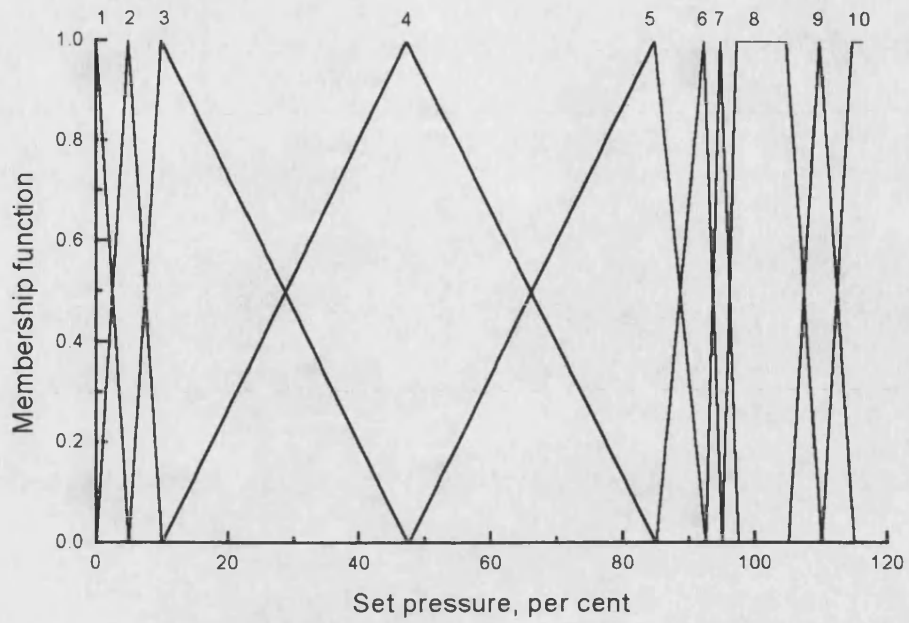
Figure III-18. Membership functions for the liquid pressure controller
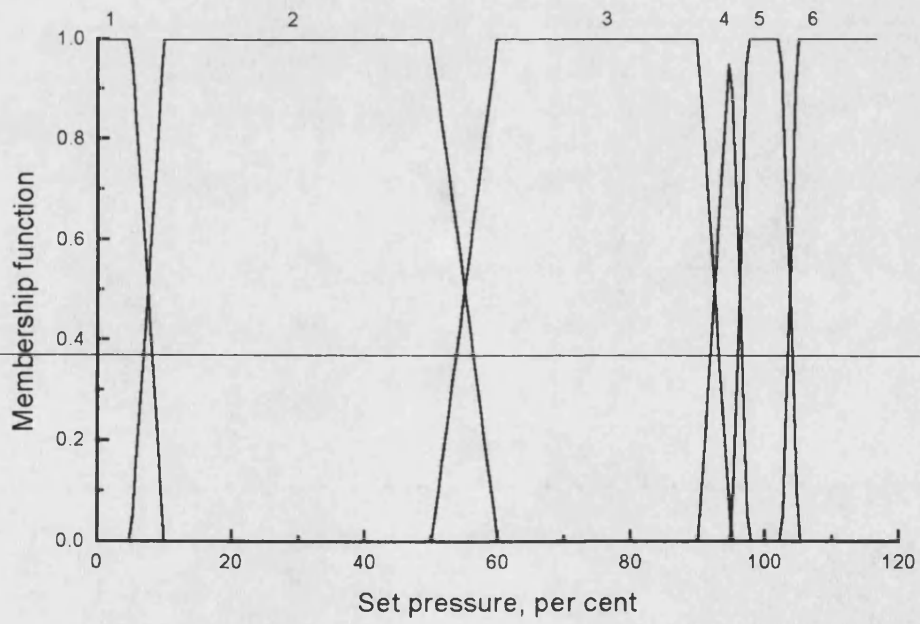
Figure III-19. Membership functions for the gas pressure controller
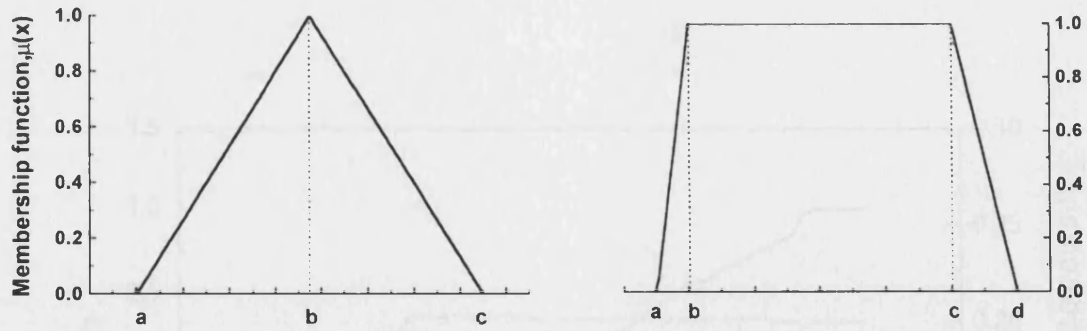
Figure III-20. Membership functions: triangular and trapezium

$$\mu_{triang}(x) = \max\left\{\min\left[\frac{x-a}{b-a}, \frac{c-x}{c-b}\right], 0\right\}$$

$$\mu_{trapezium}(x) = \min\left\{\max\left[0, \min\left(\frac{d-x}{d-c}, 1\right)\right], \max\left[0, \min\left(\frac{x-a}{b-a}, 1\right)\right]\right\}$$

Eq. III-8

Figure III-21. Simulation of reactor start-up and shut-down.
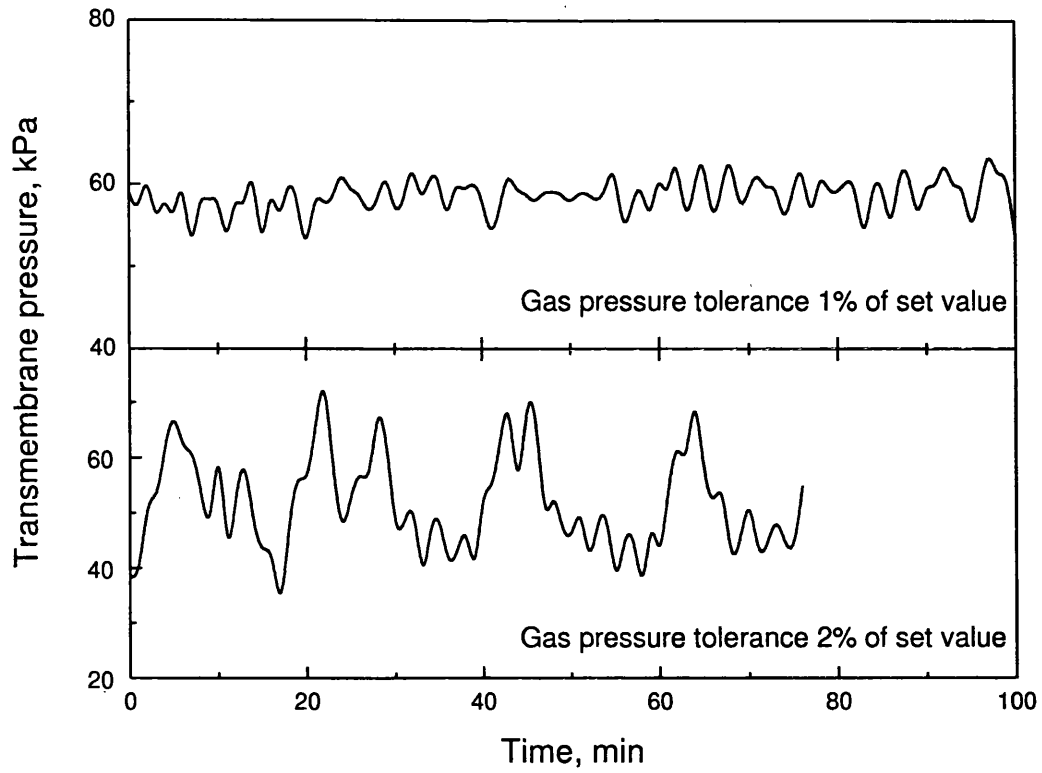
Figure III-22. Oscillations of the transmembrane pressure due to variance in gas pressure tolerance
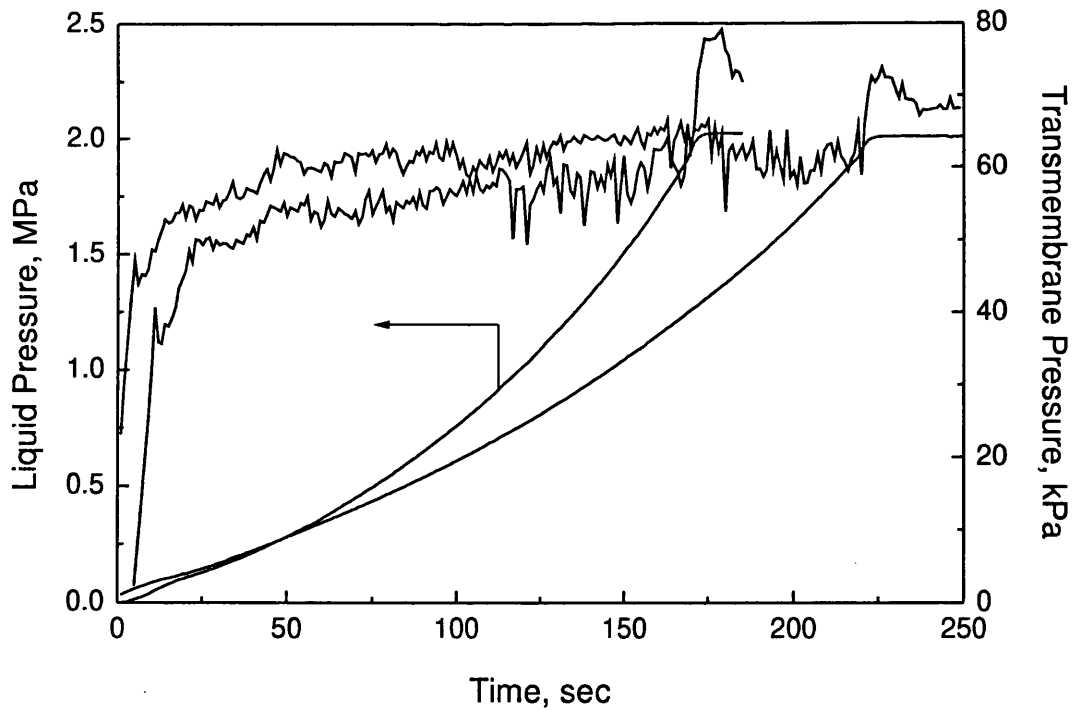
Figure III-23. Start-up of membrane contactor

III.7. Analysis

III.7.1. Analysis of vapour phase

Composition of the vapour phase was determined using an on-line gas chromatograph (Perkin-Elmer Autosystem GC) which was connected to the batch and membrane reactors via a heated valve assembly. The heated sampling loop of the gas chromatograph was evacuated between samples. The gas chromatograph was equipped with TCD and FID detectors connected in series. Analysis conditions are given below:

packed column "Poropak-S" 2m; temperature program: 50 °C 2 min, ramp 30 °C/min to 150 °C, hold 1 min, ramp 40 °C/min to 200 °C, hold 6.42 min.

The GC was calibrated for the four main components, i.e. propene, water, propan-2-ol and diisopropyl ether. All sensitivity coefficients were calculated to give mole numbers. Calibration of propene was obtained by syringe injection of pure propene at ambient pressure and temperature. The average error of calibration in the range of $0 \div 6.2 \times 10^{-5}$ mole was found to be 7.15%. The average error is defined as $Error, \% = 100 \times \dfrac{\sigma_{n-1}^{C}}{\Delta C}$,

where ΔC – is the range of concentration in moles and σ_{n-1}^{C} – is the standard deviation in the determination of concentration [137]. Concentration of propene was calculated in the assumption of ideal gas behaviour. Propan-2-ol was calibrated by syringe injection of an aqueous solution of alcohol. In the range of concentrations between $6.5 \times 10^{-8} \text{-} 3.9 \times 10^{-7}$ mole, the calibration curve of propan-2-ol was approximately a straight line (see Figure III-24), with an average error of 3.44%. At higher concentrations $(1.6 \times 10^{-6} \text{-} 5.2 \times 10^{-6}$ mole) different calibration coefficient was used. The average error of analysis at these concentrations was 3.76%. Calibration of water was obtained by syringe injection of pure water or solution containing water and propan-2-ol. In the latter case the water concentration was determined independently by Karl-Fisher titration as described further in this section. Calibration of DIPE was obtained by syringe injection of a solution of DIPE in propan-2-ol, the estimated error of calibration is ca. 9.5%.

Five typical chromatographs are shown in Figure III-25A-E. The propene and water peaks were registered by the thermal conductivity detector (TCD). Propan-2-ol and DIPE were detected by the flame ionisation detector. It is clear from Figure III-25 that the higher the acid concentration the more by-products are formed in the reaction mixture. Reaction catalysed by 55wt% solution of phosphoric acid (Figure III-25A) shows no peaks other than those of the four main components, whereas reaction catalysed by 95wt% acid (Figure III-25D) reveals eight more peaks. Note that in the membrane reactor experiment (Figure

III-25E), the formation of by-products other that DIPE is negligible. Attempts were made to identify as many by-products as possible (see page 63).
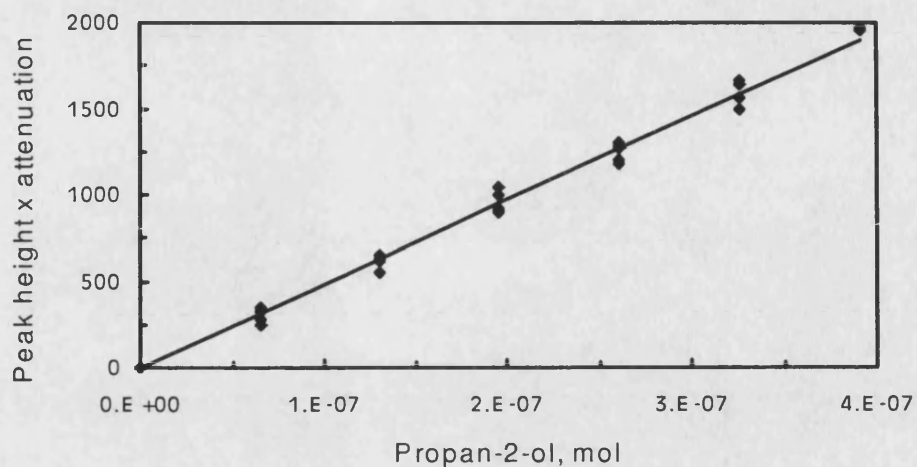
Figure III-24. An example of the calibration curve for propan-2-ol, FID detector
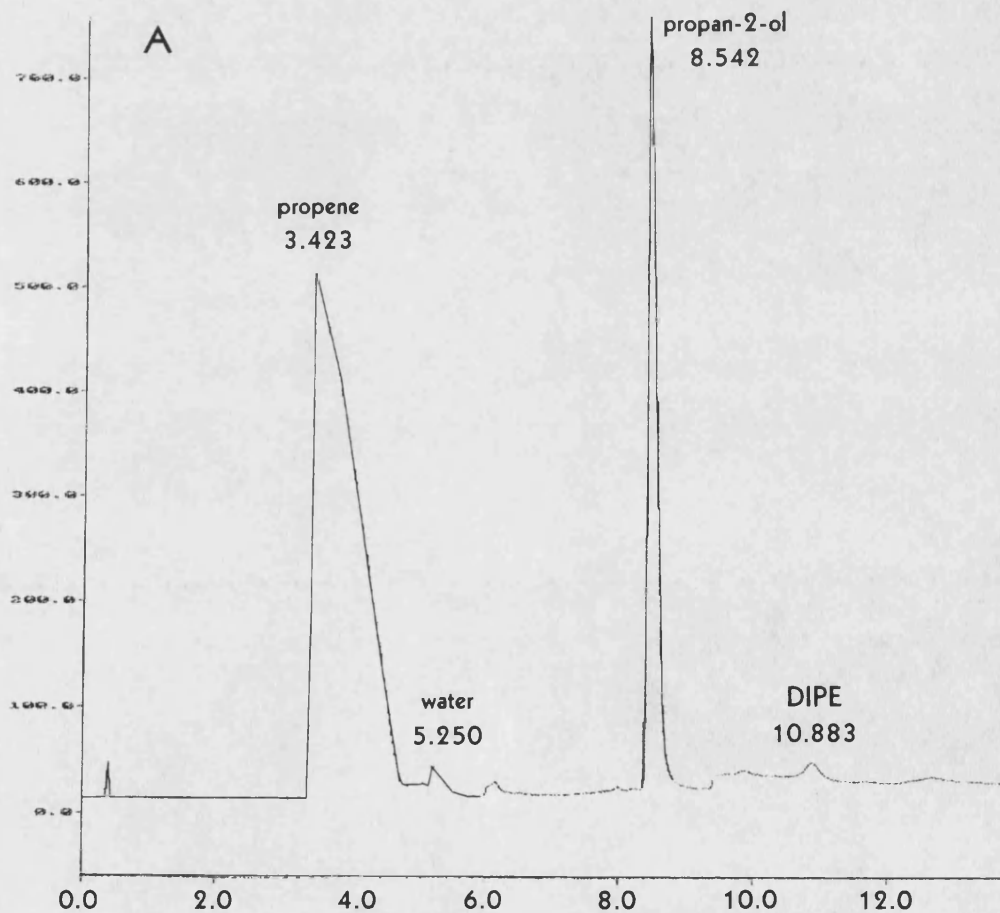
Figure III-25. GC chromatographs recorded in batch and membrane reactor experiments.
Experimental conditions: (A) 55wt% acid, 120⁰C, 100rpm, 1.9MPa initial pressure
                             (B) 85wt% acid, 126⁰C, 100rpm, 2.0MPa initial pressure
                             (C) 85wt% acid + surfactant Triton K-60

(benzyldimethyldodecyl ammonium bromide) 120°C,
100rpm, 1.8MPa initial pressure
(D) 95% acid at 120°C, 100rpm, 1.9MPa initial pressure
(E) MEMBRANE REACTOR, 85wt% acid, 130°C, 2.7MPa,
35 sec contact time

C

propene
3.381

propan-2-ol
8.488

8.202

DIPE
10.858

water
5.222

9.605

9.865

D

9.550

7.955

propene
3.423

9.763

12.465

6.150

11.600

propan-2-ol
8.542

10.020

water
5.250

8.270

377
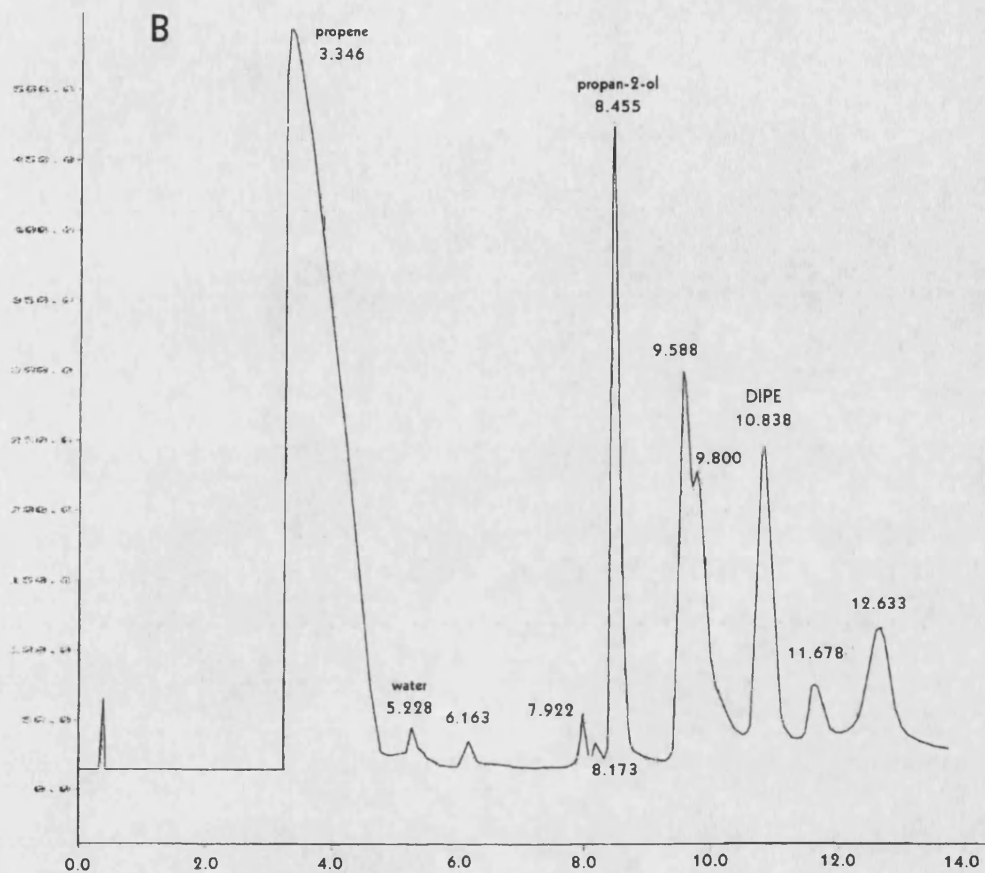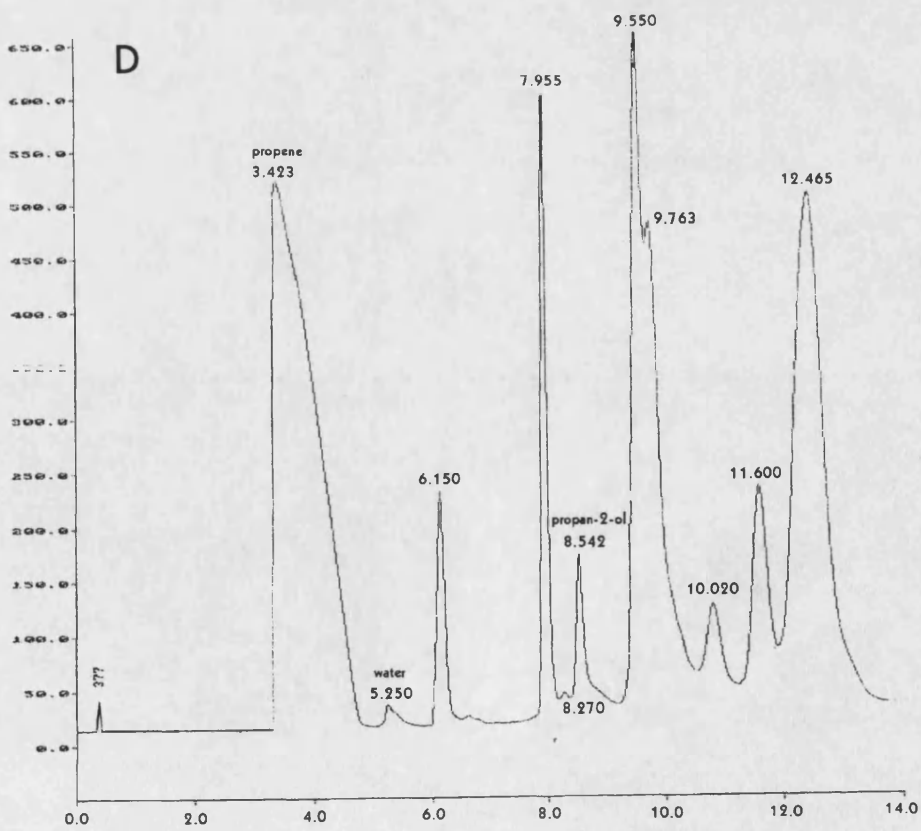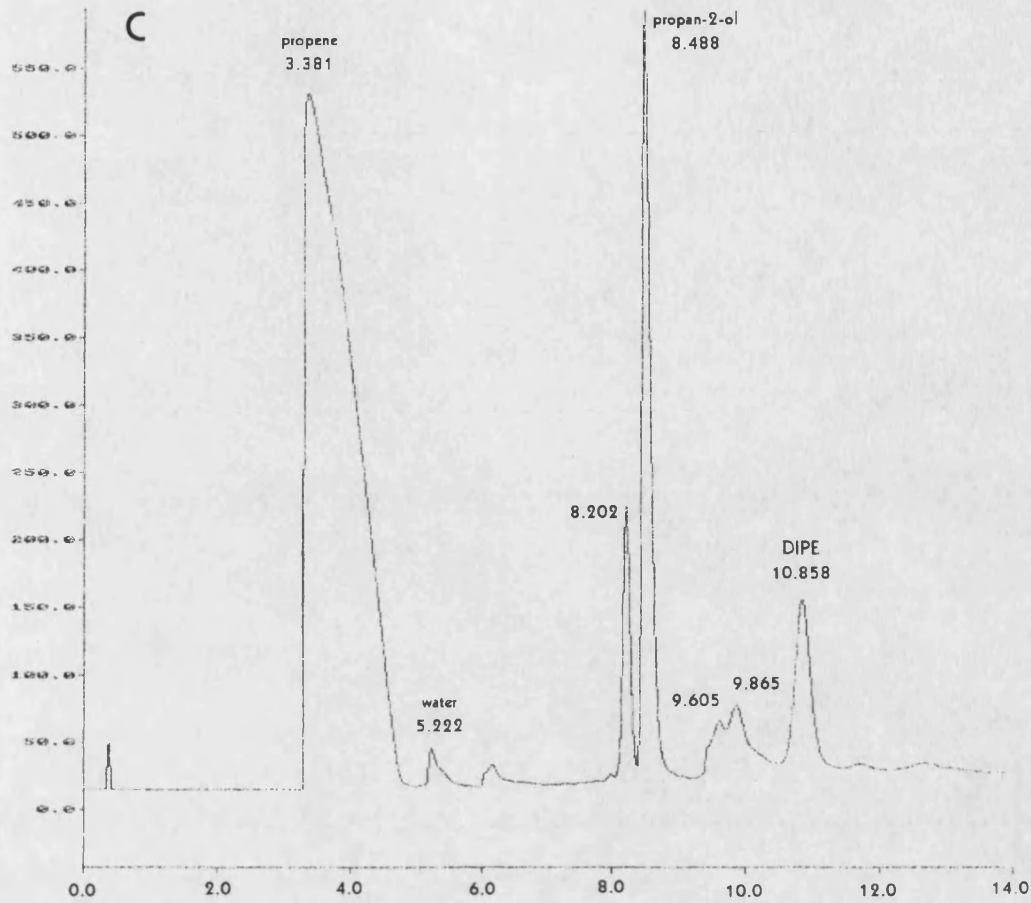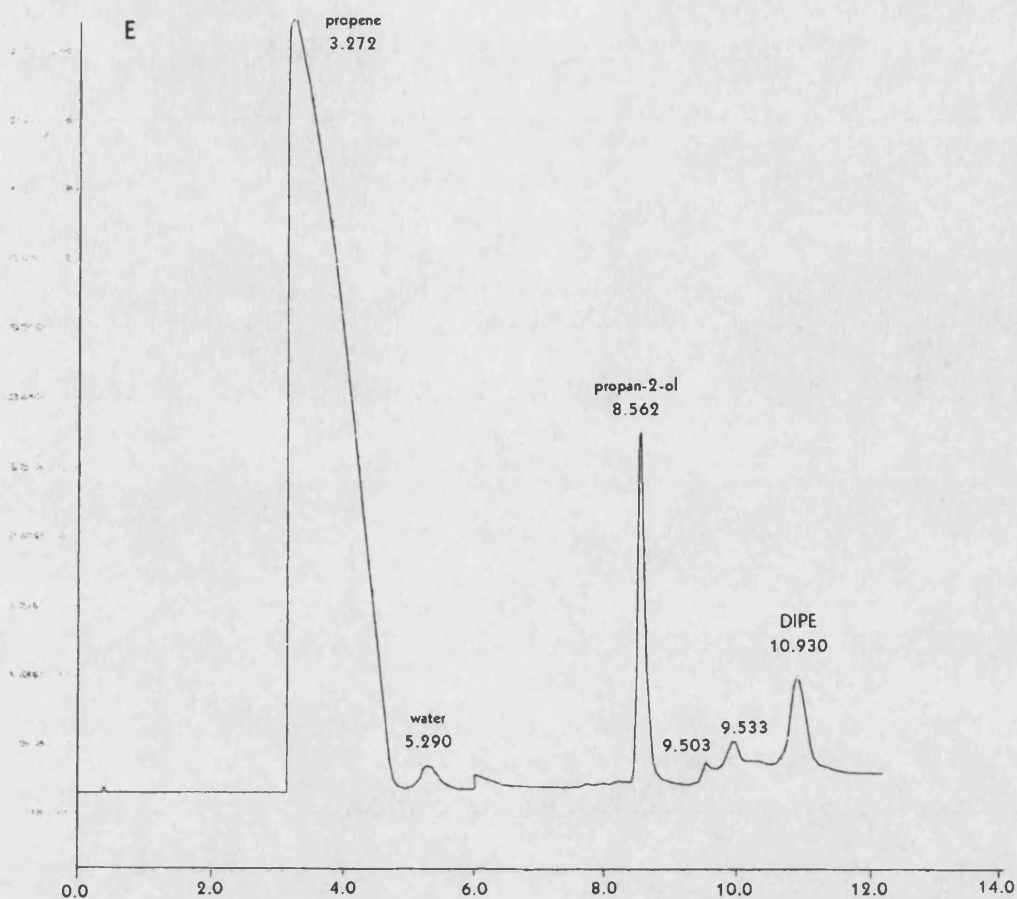
III.7.2. GC-MS determination of by-products

In a special experiment, the batch reaction with 95wt% phosphoric acid at 120°C was terminated after ca. 3 hours and the gaseous products were purged through methanol. The condensed products accumulated inside the reactor (between the glass lining and the steel body of the reactor) were also collected. Both solutions were analysed using the Perkin Elmer GC-MS system, consisting of an Autosystem GC equipped with a polar BP20 capillary column, and Q-MASS 910 mass spectrometer. The results of these experiments are shown in Figure III-26 and Figure III-27. The list of components identified by the instrument's database is given after each figure. In some cases a number of components fit the same mass spectra. These components are listed in the same table cell. The components that appear in both spectrums are given in bold.
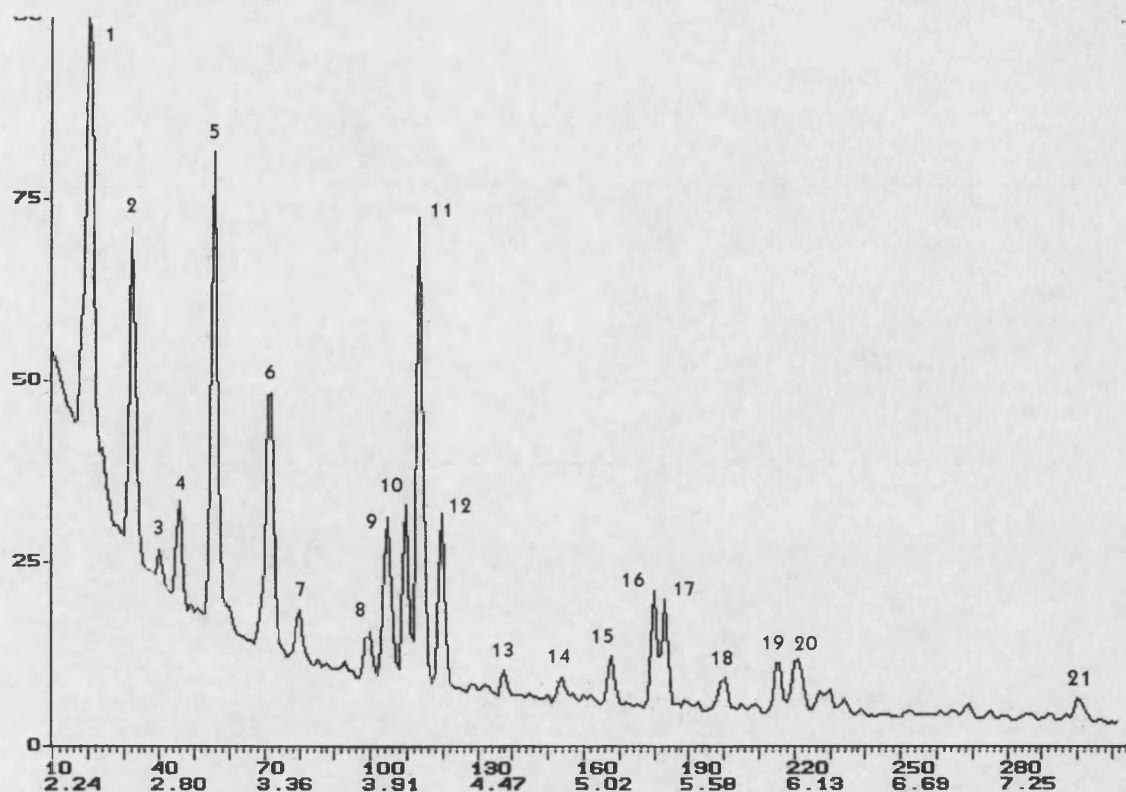
Figure III-26. GC-MS analysis of gaseous products of hydration reaction absorbed in methanol.

No	Min	Name	No	Min	Name
1	2.45	**2-methyl pentane**	11	4.17	**2,3-dimethyl pentane**
2	2.65	**3-methyl pentane**	12	4.28	**3-methyl hexane**
3	2.79	2-methyl-1-pentene 3-methyl-1-pentene 3-methyl-2-pentene	13	4.62	**4,4-dimethyl-2-pentene** **3,4-dimethyl-2-pentene**
4	2.88	hexane	14	4.92	**2-methyl-2-hexene**
5	3.10	4-methyl-2-pentanol	15	5.17	**4,4-dimethyl-2-pentene** **3,4-dimethyl-2-pentene**
6	3.36	**2,2-dimethyl pentane** **2,4-dimethyl pentane**	16	5.39	**2,5-dimethyl hexane**
7	3.55	3,4,5-trimethyl pentane 2,3,3-trimethyl hexane	17	5.44	**2,4-dimethyl hexane**
8	3.91	**2,4-dimethyl-2-pentene** **3,4-dimethyl-2-pentene** **4,4-dimethyl-2-pentene**	18	5.77	4,4-dimethyl-2-hexene 3,4-dimethyl-2-hexene **2,3-dimethyl-2-hexene**
9	3.98		19	6.05	2,3,4-trimethyl pentane
10	4.10	**2-methyl hexane**	20	6.13	**diisooctyl ester of diphosphoric acid**
			21	7.62	**2-ethyl-4-methyl-1-pentanol**
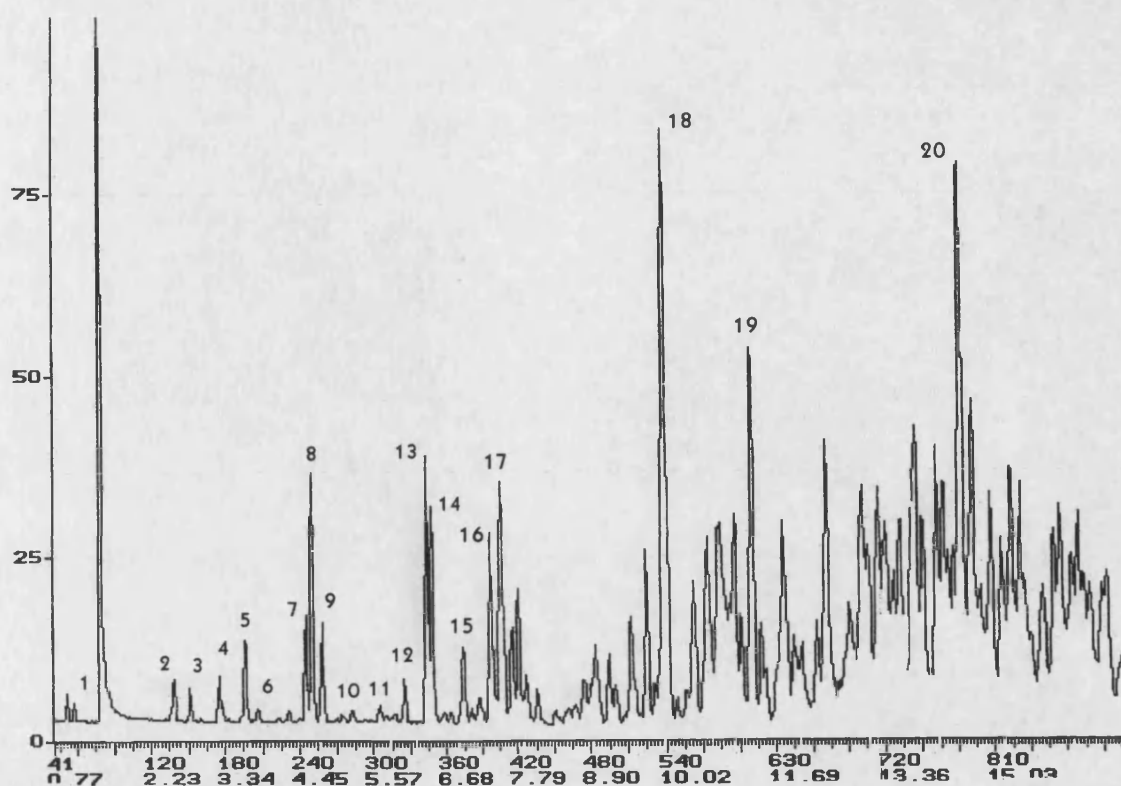
Figure III-27. GC-MS analysis of condensed vapour phase products.

No	Min	Name	No	Min	Name
1	1.04	propene	11	5.72	**2-methyl-2-hexene**
					3-methyl-2-hexene
2	2.60	**2-methyl pentane**	12	6.11	**4,4-dimethyl-2-pentene**
3	2.86	**3-methyl pentane**	13	6.37	2-methyl heptane
					2,5-dimethyl hexane
4	3.25	DIPE	14	6.50	**2,4-dimethyl hexane**
5	3.64	**2,4-dimethyl pentane**	15	6.96	3,4-dimethyl-3-hexene
		2,2-dimethyl pentane			2,3,-dimethyl-3-hexene
					2,3-dimethyl-2-hexene
6	3.77		16	7.35	**2,3-dimethyl hexane**
7	4.55	**2-methyl hexane**	17	7.54	**diisooctyl ester of diphosphoric acid**
8	4.68	**2,3-dimethyl pentane**	18	10.00	**2-ethyl-4-methyl-1-pentanol**
9	4.81	**3-methyl hexane**	19	11.30	3,5,5-trimethyl-2-hexene
					2,5,5-trimethyl-1-hexene
10	5.07	2,3-dimethyl-2-pentene	20	14.55	2,6-dimethyl-3-octene
		2,4-dimethyl-2-pentene			2,6-dimethyl-2-octene
		3,4-dimethyl-2-pentene			
		4,4-dimethyl-2-pentene			

It should be noted that both solutions appear to have 2-methyl and 3-methyl pentane as well as all possible isomers of dimethyl pentane. It is also interesting that in both spectrums the C_8 ester of phosphoric acid was registered. On the basis of the mechanisms of reactions involving carbenium ions [138] the following reaction scheme may be drawn (see Figure III-28).

$C_6H_{14}O$

H_2O $\nearrow$ H_3O^+ VII

$CH_3\text{-}CH\text{-}CH_3$
OH^+
$CH_3\text{-}CH\text{-}CH_3$

$\uparrow$ H_2O VI

CH_3CHCH_3
OH

H_3O^+ H_2O H_2O

$CH_2{=}CH\text{-}CH_3$ $\xrightarrow{\text{I}}$ $CH_3\text{-}CH^+CH_3$ $\xrightarrow{\text{II}}$ $CH_3\text{-}CH\text{-}CH_3$ $\xrightarrow{\text{III}}$ $CH_3\text{-}CH\text{-}CH_3$

H_2O OH_2^+ H_3O^+ OH

$CH_2{=}CH\text{-}CH_3$ IV

VIII $\downarrow -H_2$

$CH_3\text{-}CH\text{-}CH_2\text{-}CH^+CH_3$ $\xrightarrow{\text{IX}}$ $CH_3CH_2\overset{+}{C}\text{-}CH_2CH_3$

CH_3 CH_3

$CH_3\text{-}C\text{-}CH_3$
O

H_2O V H_3O^+

$CH_3\text{-}CH\text{-}CH_2CH{=}CH_2$ $CH_3\text{-}CH\text{-}CH{=}CH\text{-}CH_3$

CH_3 CH_3

$\downarrow +H_2$ $+H_2$

$CH_3\text{-}CH\text{-}CH_2CH_2\text{-}CH_3$ $CH_3CH_2CH\text{-}CH_2CH_3$

CH_3 CH_3
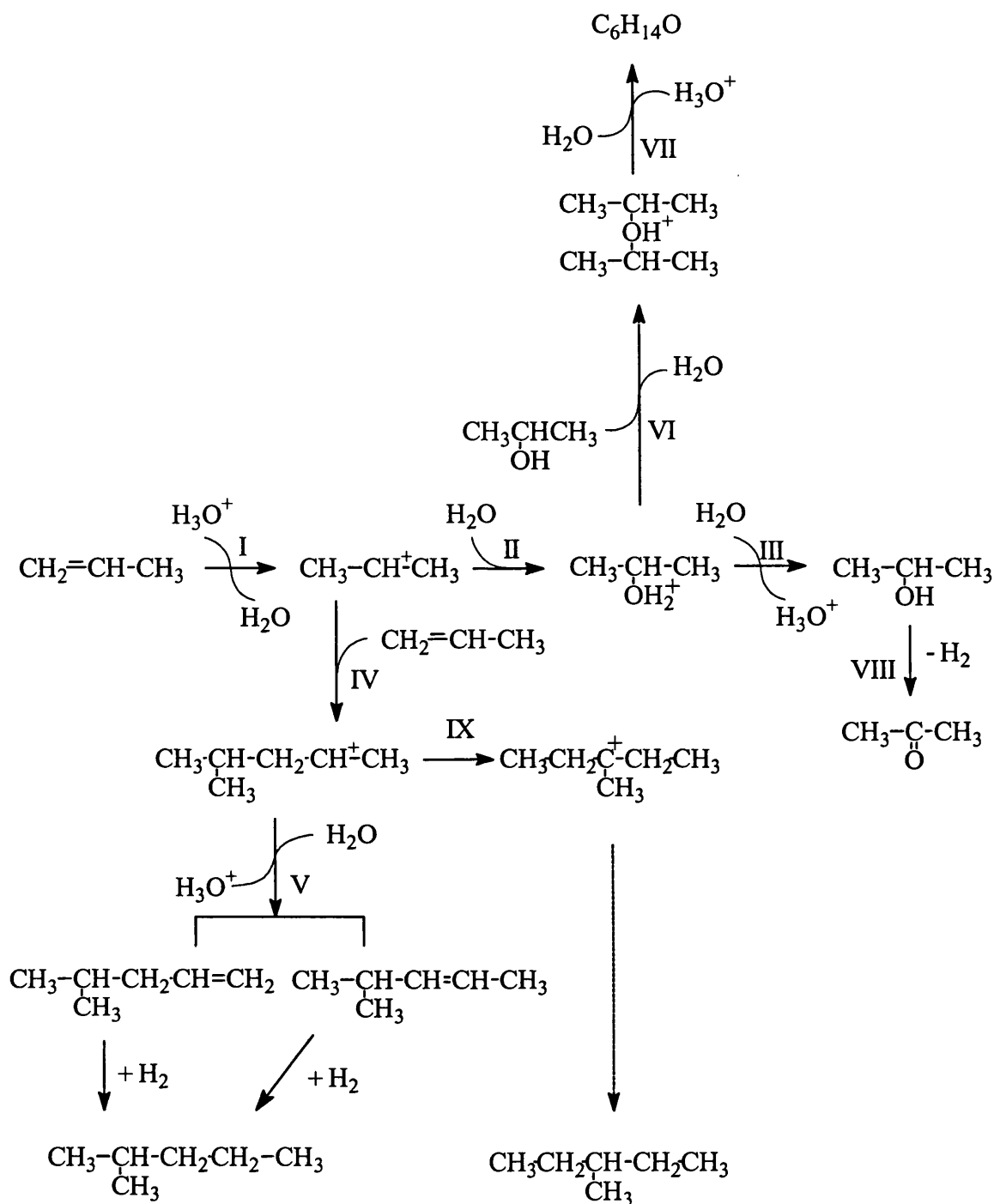
Figure III-28. Direct hydration of propene reaction pathways.

Reaction (IX) shows the pathway to the formation of 3-methyl pentane via skeletal isomerisation of the carbenium ion towards a more stable tertiary structure. Formation of dimethyl pentane is possible if ethylene were present as an impurity in the propene feed or via C-C bond cleavage reaction. Formation of phosphoric acid esters is a known reaction and is described in [138] for the case of propene.

A number of components that have been identified from the reaction mechanism (Figure III-28) and GC-MS analysis were obtained from Aldrich (analytical grades) and

their retention times were recorded using the same method as used for all kinetic and membrane reactor studies. The results of these experiments are shown in Table III-5. In all the experiments the components were dissolved in propane-2-ol or methanol in the volumetric ratio of ca. 1:1000.

Table III-5. Comparison of retention times of the unknown components and pure substances.

No	Retention time, t_r	Name	t_r of unknown compound
1	6.1	methanol	6.15
2	7.76	ethanol	7.95
3	8.27	acetone	8.27
4	9.37-9.49	4-methyl-1-pentene cis-4-methyl-2-pentene	
5	9.54-9.63	2-methylpentane	9.55-9.60
6	9.72	3-methylpentane	9.76-9.86
7			10.02
8			11.60
9	12.62	2,3-dimethylpentane	12.46

The retention times for all pentane-ols was longer than the normal analysis time for this mixture, therefore none of the pentanols could have been registered in the reaction runs.

III.7.3. Liquid phase analysis

The liquid phase reaction mixture contains a concentrated aqueous solution of phosphoric acid with dissolved propene, isopropyl alcohol, diisopropyl ether and other possible by-products. Direct analysis of this mixture presents considerable difficulties and to the best knowledge of the author such direct analysis has never been achieved.

The water content in the samples was analysed by Karl-Fisher titration using a Toledo Mettler instrument (TL6). It was found that high concentrations of metal ions leached from the stainless steel reactor parts strongly affected the Karl-Fisher analyser. Hence not all the samples could be analysed.

High concentration of phosphoric acid in the samples made any direct analysis of other components impossible. The only feasible method for direct quantitative analysis of such mixtures was found to be FTIR spectrometry. It was found that CaBr windows of FTIR cells could withstand prolonged contact with concentrated phosphoric acid. The optimum path-length was found to be less than 12μm. A shorter path-length would

diminish the masking effect of phosphoric acid and water. The shortest path length may be achieved in a total reflection IR cell. Such a cell provides a ca. 3μm path-length. A "Golden Gate" ATR cell with the diamond window was available for a brief period and was successfully tested. This cell is a high-pressure thermostated cell that could allow on-line zero dead-volume analysis of the reaction mixture. Such analysis allows the study of intrinsic kinetics of the direct hydration reaction in strongly acidic media. Unfortunately this equipment was not accessible for routine use during this study.

The possibility of using UV spectrometry was explored. It was found that a model sample containing pure isopropyl alcohol and diisopropyl ether could be successfully analysed: the maximum absorbance of alcohol is at 210 nm wavelength, followed by a sharp decrease, while the maximum ether absorbance was found at 280 nm. Unfortunately, the samples containing phosphoric acid and unknown concentration of metal ions masked both peaks. In order to separate the sample components an HPLC system was tested. A reverse phase column was used with ultra-pure water being the elluent. No separation of alcohol, ether and acetone (a possible by-product) was found. Furthermore, strong interaction between the column and ether was observed resulting in a considerable increase in pressure. It was concluded that HPLC analysis of this mixture was not feasible.

The possibility of evaporating liquid samples with consecutive GC analysis was rejected on the grounds of increasing volatility of phosphoric acid at high temperatures and the high cost of modifying the GC sampling system required to accommodate such a module.

There are several indirect methods of analysis of alcohol that were used in the earlier studies of this process and based on organic reactions of alcohols. Two methods provide a good quantitative analysis of isopropyl alcohol. In [139] a method described according to which the alcohol containing mixture is reacted with sodium dichromate solution in dilute sulphuric acid, followed by reaction with KI and titration with sodium thiosulphate. All procedures are timed and temperature is kept below 25°C. Another method [140] involves transformation of alcohol into nitrite by reacting with sodium nitrite in hidrochloric acid solution with consecutive extraction in n-heptane and measuring optical density of the organic phase. All procedures are timed.

The possibility of using an extraction method was investigated further. The problem of extracting alcohol from aqueous solutions exists in fermentation processes. In [141] an extractive system is described that was selected from 1330 potential solvents. The best

extraction system found contains 95%vol Adol 85 NL and 5%vol 4-heptanone with a very low distribution coefficient of 0.298 $(g/L)_{org}/(g/L)_{aq}$.

A number of other extracting agents is described in the literature, including tetrachlormethane [142], toluene, benzene and cyclohexane [143]. For all of these solvents the distribution coefficient was less than 2.6. Because solubility of solvents in water and distribution coefficients both depend on the alcohol concentration, the quantitative analysis based on solvent extraction would require knowledge of appropriate three-component phase diagrams. It should also be noted that simultaneous analysis of alcohol and ether in the liquid phase would be necessary to achieve a significant advance in the kinetic modelling of the hydration reaction.

The exact composition of the liquid phase would have provided useful information for deriving a detailed kinetic model for further use in this study. Although there are no measurements of the intrinsic (liquid phase) kinetics of this reaction, there is sufficient data available in the literature for comparison with the results obtained in this study and for deriving a reactor model. It was therefore concluded that all the information must necessarily be derived from the vapour phase composition data and literature data.

III.8. Error analysis

For evaluation of the accuracy of the experimental data obtained, the experimental errors were estimated using the standard error propagation equation [137]:

$$\text{for } F = f(A,B,C), \quad F = F_0 + \Delta A \left(\frac{\partial A}{\partial f}\right)_{B,C} + \Delta B \left(\frac{\partial B}{\partial f}\right)_{A,C} + \Delta C \left(\frac{\partial C}{\partial f}\right)_{A,B} \qquad \textbf{Eq. III-9}$$

where A,B,C are variables.

The deviations from an exact value, which are shown in the equation above as deltas, are usually not known and have to be determined either from the statistical distribution of experimental trials or from the accuracy of experimental measurements.

The average errors of gas chromatographic analysis of the vapour phase concentrations are shown above (see page 59). The error of determination the vapour phase concentrations can be estimated as follows:

$$C_i [mole/L] = \frac{n[mole]}{V_s [L]} + \Delta n \frac{1}{V_s} - \Delta V_s \frac{n}{V_s^2} \qquad \textbf{Eq. III-10}$$

where n is the number of moles determined by the GC calibration and V_s is the volume of the GC sampling loop or a syringe.

A 250µl sampling loop was used throughout. Although the supplier (Perkin Elmer) did not indicate the accuracy of the sample loop volume measurement, it is reasonable to assume ΔV to be negligibly low. The same assumption is valid for the syringe injection (for a 1000µl sample and 50µl accuracy of the volume reading, the contribution towards the error in concentration is only 1.3%). Therefore, considering only the error of the GC calibration, the average error of the chromatographic concentration determination in the range of concentrations between 1.9×10^{-4} and 1.2×10^{-2} mole/L does not exceed 4.7%.

The yield of propan-2-ol from the membrane reactor was calculated using the following formulae:

$$Yield[kg \times m^{-3} \times hr^{-1}] = \frac{n[mole] \times Mw[kg/mole] \times v[m^3/hr]}{V_s[m^3] \times V_{acid}[m^3]} \qquad \textbf{Eq. III-11}$$

Expanding the above equation in a Taylor series produces the equation for the error. The individual contributions to this equation are considered in turn below.

The error originating from the chromatographic analysis has already been discussed. For a typical experiment at 2.1MPa pressure and 130°C, the contribution of this error to the overall error of yield being about 3.4% (calculated for the experiment at 35sec contact time). The error associated with the volume of the GC sampling loop can be ignored. The flow at the experimental pressure and temperature was calculated using the formulae:

$$v(P_2, T_2) = \frac{v(P_1, T_1) \times P_1 \times T_1 \times z_1}{P_2 \times T_2 \times z_2}, \qquad \textbf{Eq. III-12}$$

where z is the compressibility factor and subscripts refer to the two sets of the experimental conditions: P_1 refers to atmospheric pressure, T_1 to temperature at which the flow measurements were made; (P_2, T_2) are the experimental conditions in the membrane reactor.

The flow at atmospheric pressure was determined using precision Gillmont rotameters. Although the accuracy of flow reading from these rotameters is high, the devices are calibrated for air and 298K. Therefore, during each experiment the rotameter used was calibrated using a bubble flow-meter. The accuracy of the bubble flow-meter and time reading determine the accuracy of the flow and estimated to be about 1.7% for a flow of 92.3 ml/min.

The compressibility factor for propene was determined graphically from the literature data [127]. Assuming that the literature data are exact, the accuracy of determining the compressibility factors from the enlarged graph is about $z = z_0 \pm 0.01$. Combining this with

the error of pressure and temperature measurements given above (see the corresponding section on p.43), the overall error of calculating the flow at experimental conditions (on the basis of the flow measurements at atmospheric pressure outside the reactor) does not exceed 5%. Combining this error with the error of chromatographic analysis results in a maximum overall error of 10% (calculated for the experiment at 35sec contact time).

This error corresponds to the accuracy of experimental measurements and can be calculated for each experimental point. One more contribution to the error of determining the yield is the accuracy of calculating the volume of acid within the pores of a membrane. This value is calculated from the geometrical volume of each membrane and the average porosity determined by mercury porosimetry for a sample of membranes (see p.29). Because of the large deviation in the values of porosity between the samples, the accuracy of calculating the volume of acid within each membrane sample is very low. But this error would be the same for all the experiments.

The result of the low-pressure semi-batch experiments are presented in units of yield [mmol/hr/g(acid)] (see Chapter V). The error of these experiments is estimated to be 11%.

The kinetics of propene hydration was studied experimentally in order to evaluate the parameters of the reaction model to be used for simulation of the membrane contactor system. The major limitation in the kinetic study was the absence of any data on the composition of the liquid phase. This was due to experimental difficulties in measuring composition of the concentrated acidic medium (see Section III.7.3). Only vapour phase data were recorded and correlated with the temperature and acidity variations. It was therefore not possible to evaluate the rates of elemental reaction steps.

Earlier experimental observations reported in [59] showed that the apparent rate of reaction is directly proportional to the Hammett acidity function h_0, i.e. a plot of $\log_{10} W$ vs. h_0 is linear with the slope close to 45 degrees. This linear dependence was recorded over the range of acidity between $h_0 = -3$ and -4.2, which corresponds to a phosphoric acid concentrations 75 and 93 wt% (the literature data on acidity vs. concentration of phosphoric acid is given in Figure IV-1). A similar dependence was observed in this work for the range of acid concentrations between 63 and 94wt% (see Figure IV-4). For these experiments the phosphoric acid concentration was calculated from measurements of water concentration by Karl Fisher titration. The corresponding values of Hammett acidity were calculated using the correlation given in Figure IV-1. At acid concentrations above 94wt%, the rate of alcohol production decreases due to an extremely low water concentration and an increase in the rate of polymerisation.

The acidity function for the reaction mixture containing phosphoric acid, propene, water and products of the hydration reaction is not of constant value. It was shown in a number of earlier papers (see [59] for a detailed discussion), that alcohol, being a weak base, decreases the acidity and, therefore, the rate of hydration. Propene also influences values of the acidity but such influence is only weak due to the low liquid-phase propene concentration. Arguably, the decrease in acidity due to formation of propan-2-ol is compensated for by a decrease in the water content [59]. The activation energy of propan-2-ol formation over a thin-film phosphoric acid catalyst remains constant with change of acid concentration within the range of linear dependence on h_0 [59]. For 84.3% acid concentration, the activation energies for the forward and backward reactions were

found to be 47.8 and 84.6 kJ/mole respectively [59]. In the work reported in this thesis the activation energies were evaluated by fitting the experimental data to a model.
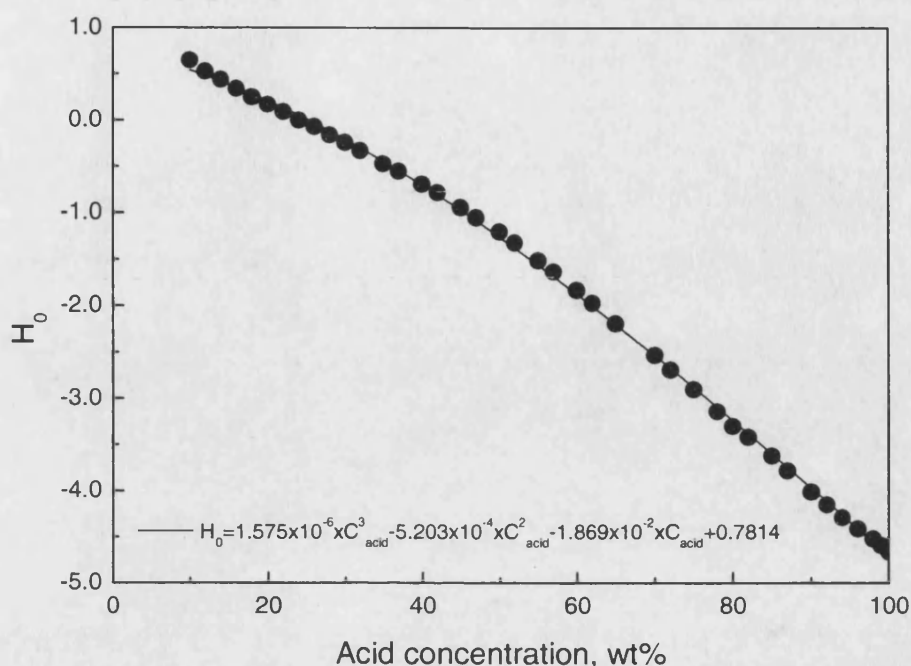
Figure IV-1. Hammett acidity function H_0 vs. acid concentration for phosphoric acid [144].

The model developed for propene hydration in a batch reactor is based on a number of assumptions. The main assumption is ideal behaviour in the vapour phase. Using this assumption, propene concentration in the liquid phase was calculated from Henry's law and vapour pressures of propan-2-ol and DIPE were calculated using Raoult law. The necessary data (Henry constants and vapour pressures of pure compounds) were obtained by fitting available experimental data in the literature.

The data on propene solubility in water is shown in Figure IV-2. This figure also illustrates the range of pressures where Henry's law is applicable at each temperature. Henry constant is a strong function of temperature. In the case of propene-water binary VLE the temperature dependence of Henry coefficient is shown in Figure IV-3.
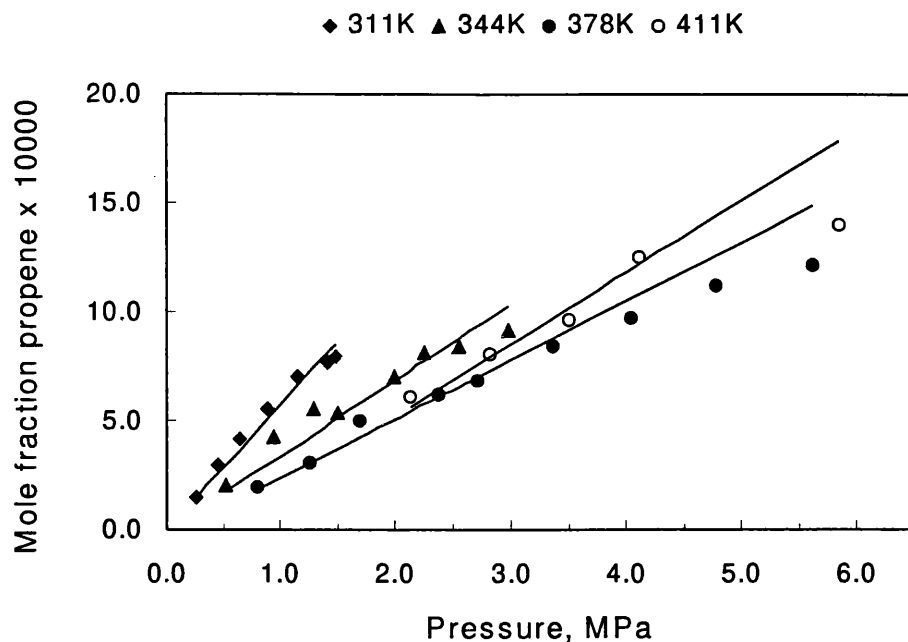
Figure IV-2. Mole fraction of propene in the liquid phase vs. total pressure [145]. Solid lines fitted by Henry's law.
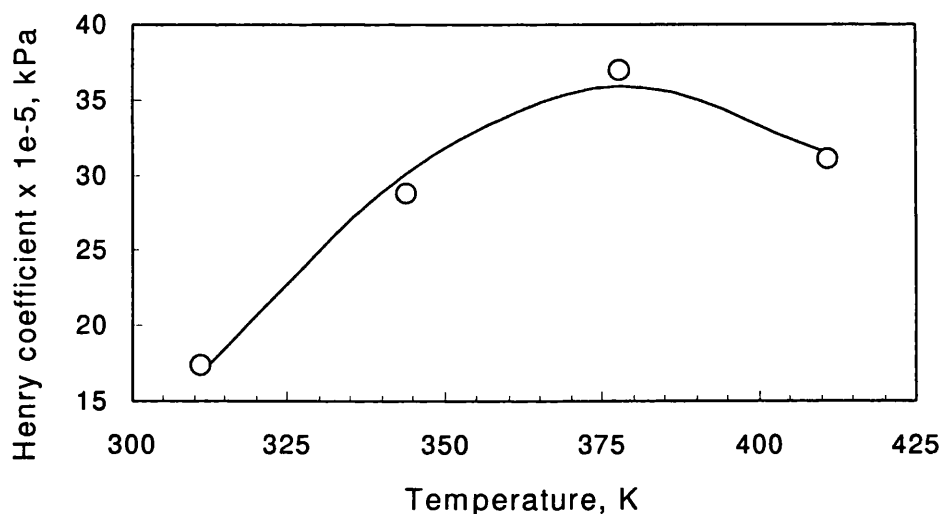
Figure IV-3. Temperature dependence of Henry coefficient for propene solubility in water.

The vapour pressure of water above phosphoric acid solutions has been reported in a number of publications. The dataset shown in Figure IV-5 was used to approximate the vapour pressure of water above phosphoric acid solutions. The linear interpolation routine of the solver was used to obtain the value of the water pressure at given acid concentration and temperature.
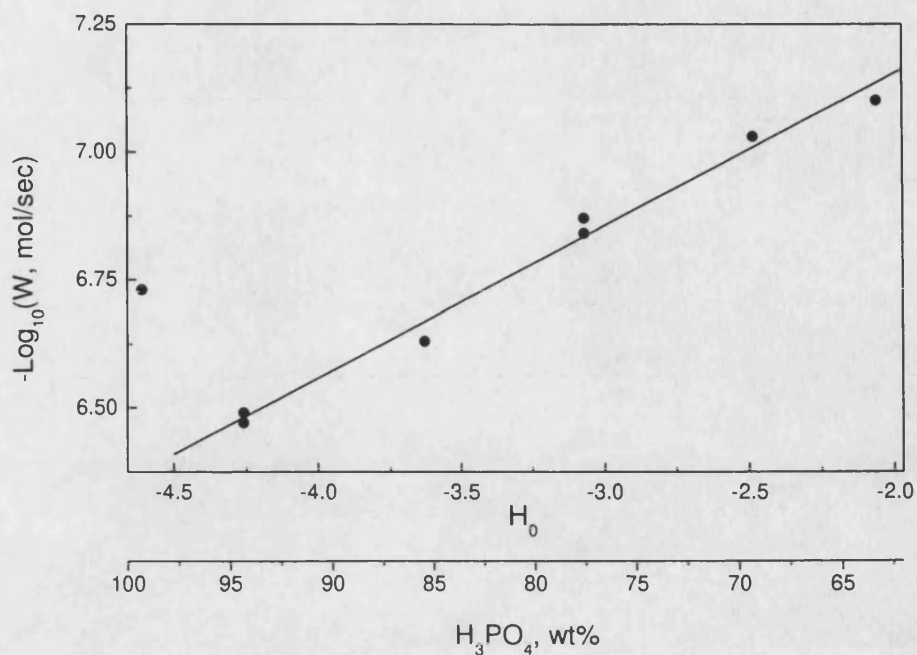
Figure IV-4. Rate of propan-2-ol production vs. Hammett acidity.
Concentration range 64.3-99.3 wt% phosphoric acid. All experiments performed at 118°C with ca. 130g acid and 2.1 MPa initial pressure.
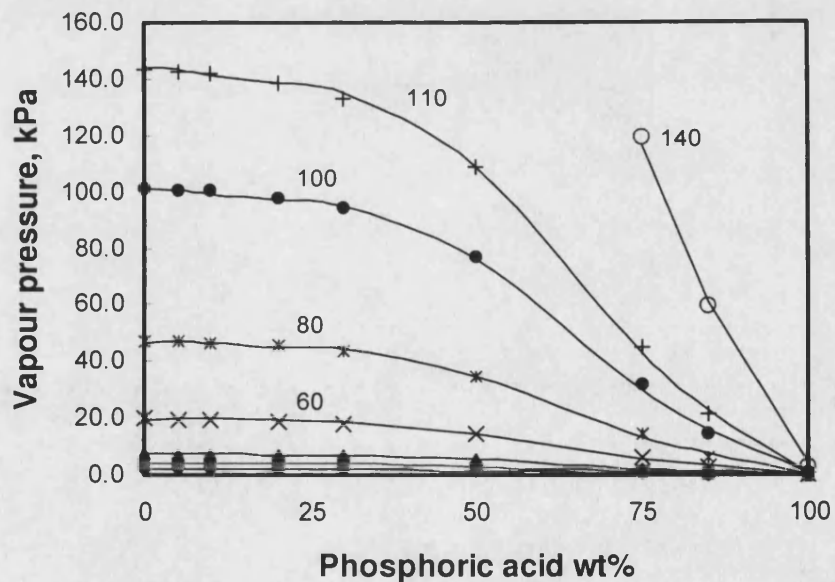
Figure IV-5. Vapour pressure of water in phosphoric acid solutions [146].
Temperature in Celsius is shown next to corresponding graphs.

Coefficients for estimating the vapour pressure of propan-2-ol were obtained by fitting the Wagner equation [147] (see Eq. IV-1) to the experimental data [148] (see Figure IV-6).

$$\log_{10} P_{vpr} = \frac{1}{Tr}\left(\alpha\tau + \beta\tau^{1.5} + \gamma\tau^3 + \delta\tau^6\right)$$

where $P_{vpr} = P_{vp}/P_c$, P_c – critical pressure; T_r – reduced temperature; and $\alpha,\beta,\gamma,\delta$ are fitting parameters.

For many pure components the coefficients of the Wagner equation are given in [147]. Such tabulated data was used to estimate the vapour pressure of pure diisopropyl ether. This source also lists the coefficients for water and propan-2-ol, but the coefficients found in this work give a better fit to the set of experimental data available.
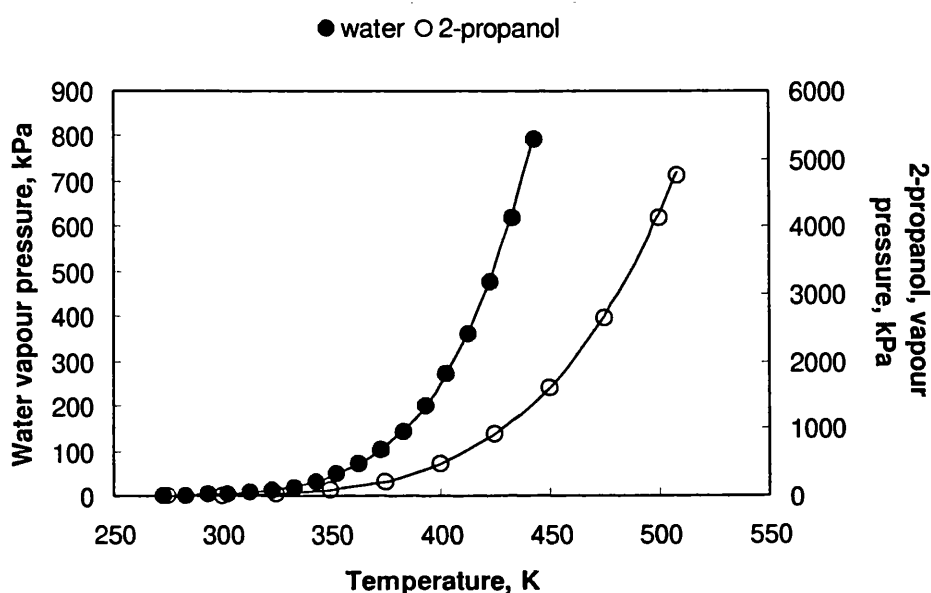
Figure IV-6. Vapour pressure of pure water and pure 2-propanol.
Solid lines were fitted by equation Eq. IV-1.

In order to calculate vapour-liquid equilibrium, a relaxation technique was used. The two-film model for interfacial mass transfer was implemented with values of mass transfer coefficients sufficiently high to ensure that the system is not mass transfer limited. Equations describing gas-liquid mass transfer are given in Chapter VII.1.

The rate expressions to be used in the model were derived from the following reaction steps:

1	$C_3H_6 + H^+ \leftrightarrow C_3^+$	fast
2	$C_3^+ + H_2O \leftrightarrow [C_3 \cdots H_2O]^+$	slow
3	$[C_3 \cdots H_2O]^+ \leftrightarrow C_3H_7OH + H^+$	fast
4	$[C_3 \cdots H_2O]^+ + C_3H_6 \leftrightarrow [C_3 \cdots HO \cdots C_3]^+$	slow
5	$[C_3 \cdots HO \cdots C_3]^+ \leftrightarrow C_6H_{14}O + H^+$	fast
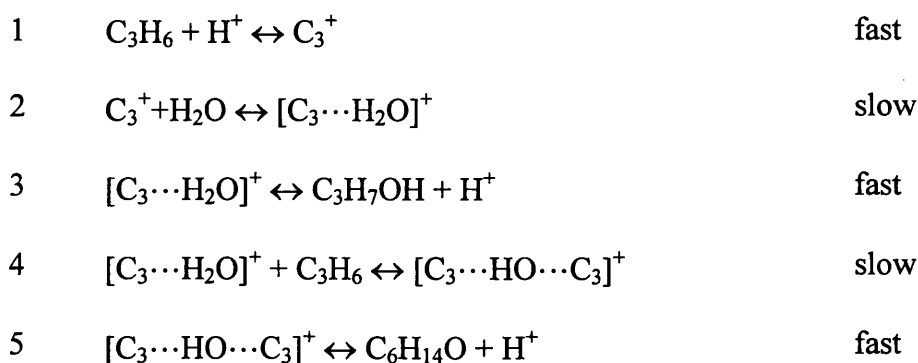
A similar reaction scheme was used in [59]. Reactions 1, 3 and 5 are considered to be fast and in equilibrium. Using the steady state assumption for concentrations of all carbenium ion components, the following kinetic expressions were obtained:

$$\left[C_3^+\right] = \frac{k_{1+}}{k_{1-}}[C_3H_6]a_{H^+} \quad \frac{f_{C_3H_6}}{f_{C_3^+}} = \frac{k_{1+}}{k_{1-}}h_0[C_3H_6]$$

Eq. IV-2

$$\frac{d[C_3H_7OH]}{dt} = k_{2+}\frac{k_{1+}}{k_{1-}}h_0[C_3H_6][H_2O] - k_{2-}\frac{k_{3-}}{k_{3+}}h_0[C_3H_7OH]$$

Eq. IV-3

$$\left[C_3\cdots H_2O\right]^+ = \frac{k_{3-}}{k_{3+}}[C_3H_7OH]a_{H^+} \quad \frac{f_{C_3H_7OH}}{f_{C_3H_2O^+}} = \frac{k_{3-}}{k_{3+}}h_0[C_3H_7OH]$$

Eq. IV-4

$$\frac{d[C_6H_{14}O]}{dt} = k_{4+}\frac{k_{3-}}{k_{3+}}h_0[C_3H_6][C_3H_7OH] - k_{4-}\frac{k_{5-}}{k_{5+}}h_0[C_6H_{14}O]$$

Eq. IV-5

$$\left[C_3\cdots HO\cdots C_3\right]^+ = \frac{k_{5-}}{k_{5+}}[C_6H_{14}O]a_{H^+} \quad \frac{f_{C_6H_{14}O}}{f_{C_3HOC_3^+}} = \frac{k_{5-}}{k_{5+}}h_0[C_6H_{14}O]$$

Eq. IV-6

It is clear, that this mechanism corresponds to the two main reactions:

6    $C_3H_6 + H_2O \leftrightarrow C_3H_7OH$

7    $C_3H_6 + C_3H_7OH \leftrightarrow C_6H_{14}O$
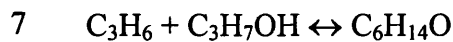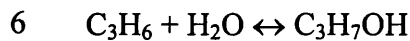
In some earlier publications the two reactions of DIPE formation were considered, i.e. formation of ether in the reaction between alcohol and propene (7), and formation of ether in the dehydration of alcohol (8):

8    $2C_3H_7OH \leftrightarrow C_6H_{14}O + H_2O$
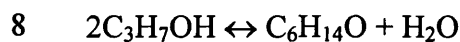
However, if described by elementary steps, these two reactions yield the same equation given above for the elementary reaction 4 (see Eq. IV-5). The following expressions for equilibrium constants were used to calculate the backward reaction kinetic constants:

$$K_{ca} = \frac{[C_3H_7OH]}{[C_3H_6][H_2O]} = \frac{k_{a+}}{k_{a-}}$$

Eq. IV-7

$$K_{ce} = \frac{[C_6H_{14}O]}{[C_3H_7OH][C_3H_6]} = \frac{k_{e+}}{k_{e-}}$$

Eq. IV-8

Using equations IV-7 and IV-8, the kinetic expressions given by equations (IV-3) and (IV-5) result in the following:

$$\frac{d[C_3H_7OH]}{dt} = h_0 k_{a+}\left([H_2O][C_3H_6] - \frac{[C_3H_7OH]}{K_{ca}}\right)$$ Eq. IV-9

$$\frac{d[C_6H_{14}O]}{dt} = h_0 k_{e+}\left([C_3H_6][C_3H_7OH] - \frac{[C_6H_{14}O]}{K_{ce}}\right)$$ Eq. IV-10

This model was implemented in the ODE solver Madonna developed at the University of California at Berkeley. The curve fitting routine of the solver was used to fit the experimental data to the model and obtain kinetic and equilibrium constants.

Typical experimental kinetics of the hydration reaction are shown in Figure IV-7. A complete list of batch experiments is shown in Table IV-1. Here the vapour phase concentrations were represented as mole fractions. Only four main components were taken into account. All measurements were performed at the same stirrer speed of 100rpm. No significant changes in the initial reaction rates were observed upon increase of stirrer speed from 100 to 200rpm. Low stirrer speed have been used in order to prevent acid foaming and entrapment in the gas sampling line, which can result in damage of gas chromatograph.
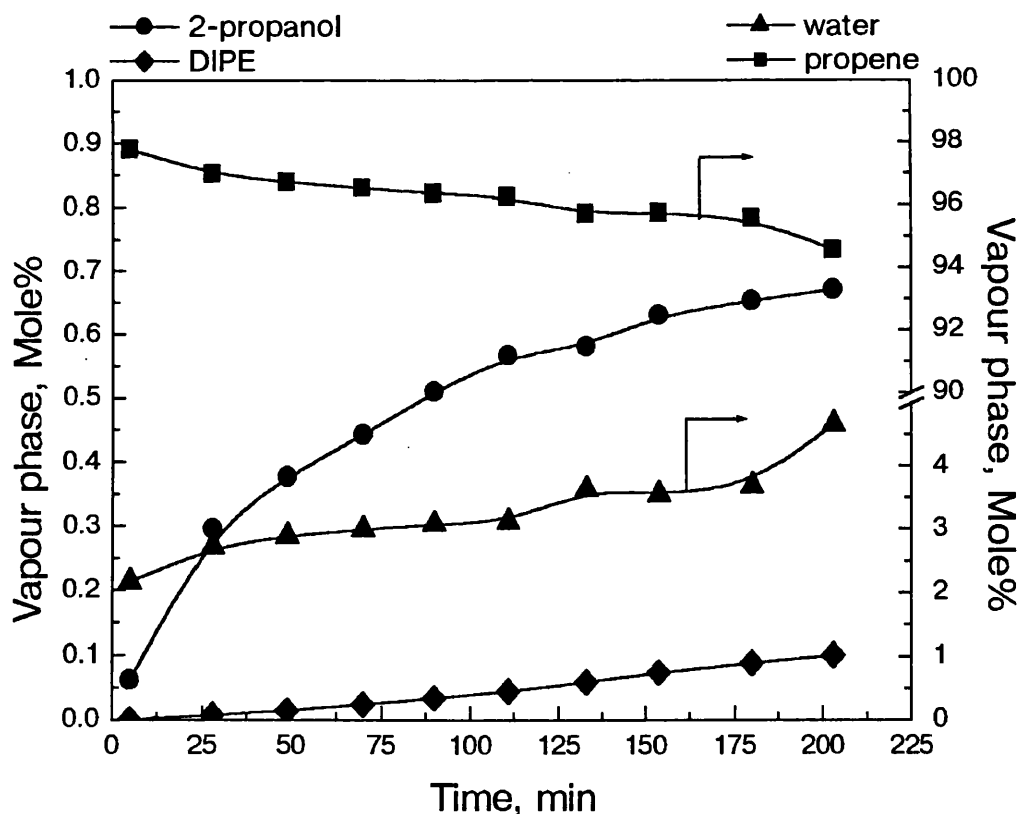
Figure IV-7. Kinetics of propene hydration.
Reaction conditions: 391K, 2.1MPa, acid 85%wt.

The induction period in the kinetics of ether formation is an indication of a consecutive reaction. Vapour phase concentration of water appear to increase despite the fact that water is consumed in the reaction. Peculiarities of the vapour-liquid equilibrium in the system are most likely to be responsible for the increase in the vapour phase concentration of water. In order to calculate the activation energies of formation of propan-2-ol and DIPE, experiments were performed over the temperature range between 80-158°C. Results were fitted with the computer model described above.

Temperature dependencies of the forward reaction rate constants, i.e. k_{a+} and k_{e+} are shown in Figure IV-8. The apparent activation energies derived from an Arrhenius plot are 35kJ/mol for the formation of propan-2-ol and 51.7kJ/mol for the formation of DIPE. The latent heat of dissolution of propene should be added to the value of apparent activation energy of propan-2-ol formation [59], giving a value of 54 kJ/mol. This value of the activation energy of formation of propan-2-ol is slightly higher than the value reported in [59]. It should be pointed out that the values of kinetic and equilibrium constants found in this thesis are only considered as fitting parameters. The real activation energy of the liquid-phase reaction is masked by latent heats of vaporisation and condensation, mixing effects in strongly nonideal mixtures as well as the presence of by-product formation, discussed in detail in the Experimental section (see page 63). The intrinsic kinetics of the olefin hydration reaction catalysed by strong mineral acids is yet to be investigated. Similarly, analysis of liquid phase composition would be necessary in order to evaluate the equilibrium constants. Comparison of the predictions of this simplified model and experimental data is given in Figure IV-9 and Figure IV-8. Figure IV-11 shows model prediction of propane-2-ol formation kinetics at different acid concentrations.

Reaction rate data can be used to estimate the dimensionless parameter β, which is a useful indicator of predominantly bulk or surface reaction [149].

$$\beta = \frac{\sqrt{k_2 C_w D_p}}{k_l}$$

Eq. IV-11

where C_w is concentration of water [mol/L]; D_p is the liquid phase diffusion coefficient of propene [m^2/sec]; k_2 is the second order rate constant for reaction of formation of propan-2-ol [L/mol/sec] and k_l is the mass transfer coefficient [m/sec].

Estimation of parameters for Equation IV-11:

Diffusion coefficient of propene in water at 298K is given in [147]	$D_p = 1.44 \times 10^{-9}$ m^2/sec
Concentration of water in 85wt% phosphoric acid solution	$C_w \approx 14$ kmol/m^3
Mass transfer coefficients used in the model	$k_l = 4e^{-3}$ m/sec
Forward reaction rate constant at 130°C	$k_{a+} = 1.1 \times 10^{-10}$ m^3/mol/sec

$$\beta \approx 1 \times 10^{-5}$$

Slow reactions with $\beta < 0.01$ occur predominantly in the bulk of the liquid phase.
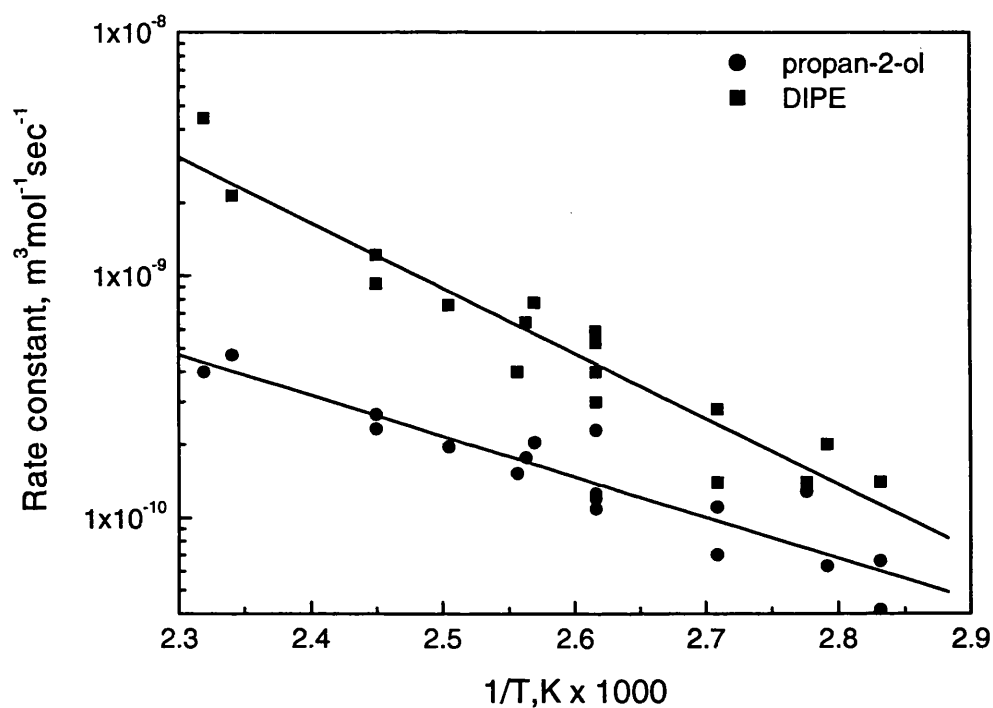
Figure IV-8. Arrhenius plots for forward reaction constants of propan-2-ol and DIPE formation.
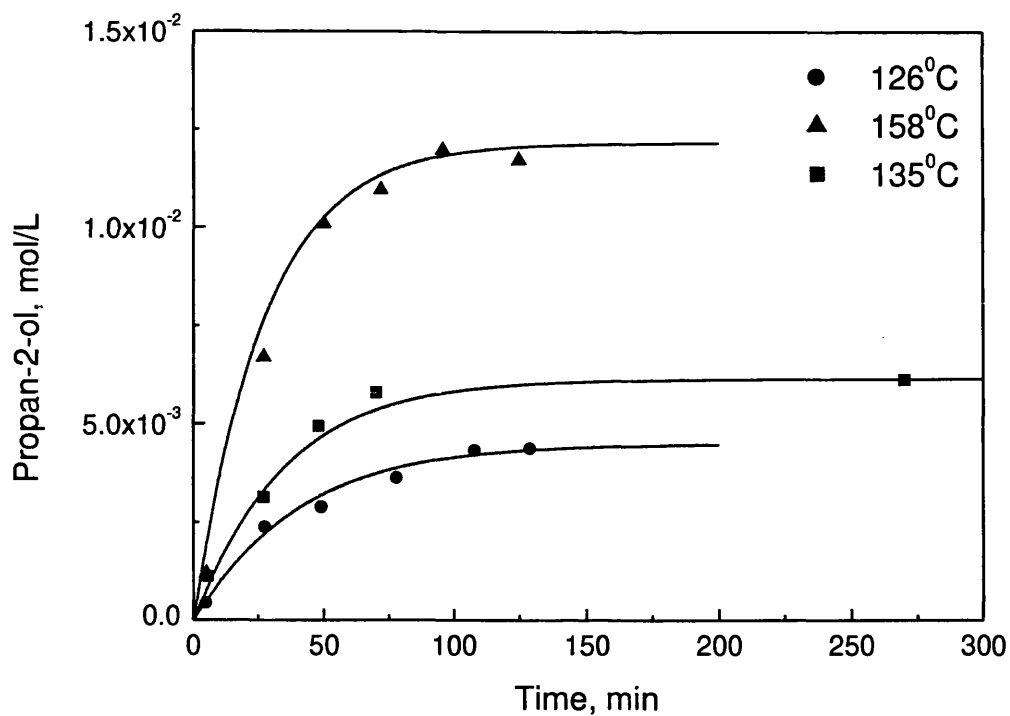
Figure IV-9. Kinetics of propan-2-ol formation in the batch reactor.
All experiments at 2.3 MPa initial pressure. Solid lines — model prediction.
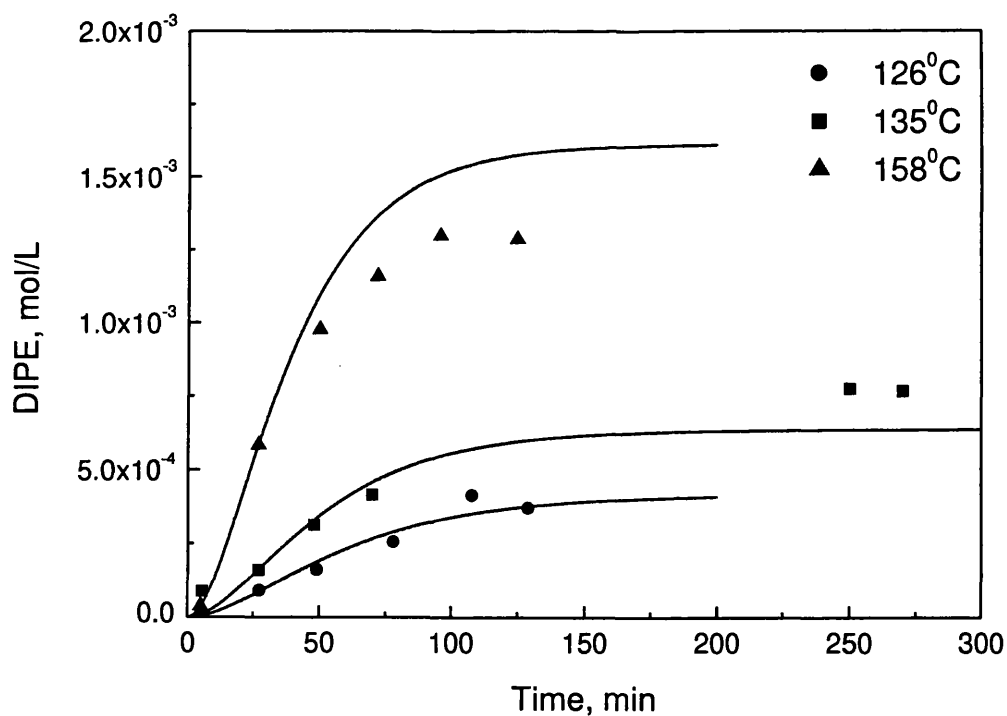
Figure IV-10. Kinetics of diisopropyl ether formation in the batch reactor.
All experiments at 2.3 MPa initial pressure. Solid lines — model prediction.
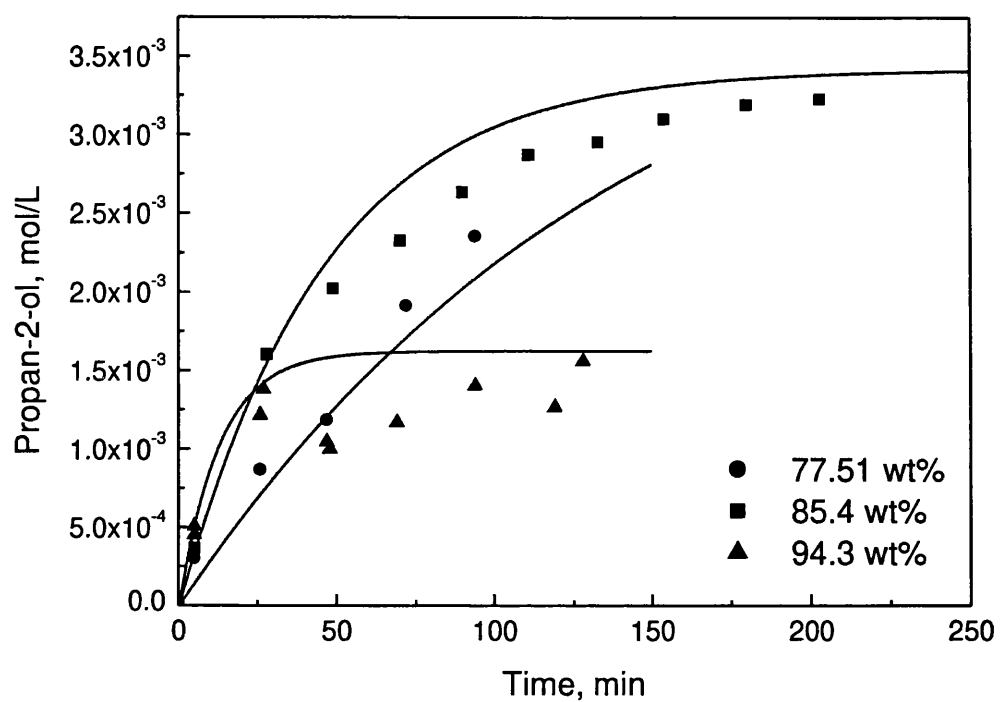
Figure IV-11. Model prediction of propane-2-ol formation catalysed by phosphoric acid of different strength.
Solid lines — model prediction. All experiments at 120°C and 2.1 MPa initial pressure.

Table IV-1. Experimental conditions and rate constants of propene hydration in batch reactor

No	T, K	P^0, MPa	Stirrer, rpm	$[H_3PO_4]$, wt%	$m_{H_3PO_4}$, g	$W^0_{C_3H_7OH} \times 10^{-7}$ mol/s	$W^0_{C_6H_{14}O} \times 10^{-7}$ mol/s	Comments
1	353	2.5	100	85.4	141.4	0.816	0.016	W^0 – initial rates of reaction calculated from the vapour phase data, i.e. the initial rates of increase in vapour phase concentrations of propan-2-ol and diisopropyl ether.
2	353	2.6	100	85.4	158.7	0.226	0.008	
3	358	2.1	100	85.4	146.3	0.345	0.007	
4	360	2.4	100	85.4	128.2	0.821	0.020	
5	369	2.4	100	85.4	132.0	1.10	0.025	
6	369	2.0	100	85.4	132.0	0.91	0.016	
7	382	2.3	100	85.4	124.0	1.61	0.144	
8	382	2.4	100	85.4	136.0	2.23	0.169	
9	382	2.4	100	85.4	145.8	1.28	0.078	
10	382	2.3	100	85.4	131.8	3.12	0.194	
11	382	2.2	100	85.4	132.0	3.04	0.214	
12	389	2.3	200	85.4	137.0	3.28	0.273	
13	390	2.0	100	85.4	127.0	2.32	0.095	
14	391	2.1	100	85.4	127.4	2.32	0.133	
15	399	2.2	100	85.4	129.0	3.72	0.195	
16	408	2.2	100	85.4	141.7	4.36	0.398	
17	408	2.2	100	85.4	151.8	6.06	0.332	
18	427	2.2	100	85.4	130.6	15.0	0.872	

Table IV-1. Experimental conditions and rate constants of propene hydration in batch reactor (continuation)

No	T, K	P^0, MPa	Stirrer, rpm	$[H_3PO_4]$, wt%	$m_{H_3PO_4}$, g	$W^0_{C_3H_7OH} \times 10^{-7}$ mole/s	$W^0_{C_6H_{14}O} \times 10^{-7}$ mole/s
19	431	2.2	100	85.4	130.0	12.5	1.16
20	393	1.9	100	63.54	138.7	0.790	
21	389	2.2	100	69.25	136.0	0.812	
22	397	2.0	100	69.25	144.0	0.913	
23	391	2.0	100	69.25	134.0	1.10	
24	391	2.1	100	77.51	130.0	1.44	
25	391	2.0	100	77.51	129.2	1.36	
26	393	2.1	100	94.3	130.0	3.38	
27	393	2.1	100	94.3	132.2	3.21	
28	390	2.0	100	99.3	133.6	1.83	

V.   Can surfactants improve yield of alcohol?

Data presented in [127] show that some surfactants considerably increase the solubility of propene in water. An increase in the liquid phase concentration of propene would have a positive effect on the yield of propan-2-ol. To the best knowledge of the author, there is no literature on the application of surfactants to increase the solubility of olefins in liquid phase hydration reactions. Application of surfactants to improve the solid-liquid interaction between heteropoly acid based catalysts and organic solvents is described in [90]. The latter example suggests that there are surfactants stable in strong acidic media.

To investigate whether surfactants would have any effect on the reaction of the direct hydration of propene catalysed by phosphoric acid solutions, a series of experiments was performed in a low-pressure semi-batch reactor and a high-pressure batch reactor. Both reactors are described in the Experimental chapter (page 42). A list of all experiments performed with surfactants and surfactant-organic solvent mixtures is given in Table V-1 and Table V-2.

The choice of surfactants was largely determined by the literature data. It was shown in [127] that the surfactant Triton K-60 increases the solubility of propene in water by a factor of 10. The chemical structure of this surfactant is described in [150]. It is a chlorinated quarternary ammonium salt, i.e. a cationic surfactant. A similar surfactant with a bromine anion was also tested. The experiments performed in the low pressure semi-batch reactor revealed two unknown by-products (see Figure V-1. The concentration of by-products was estimated assuming the same sensitivity coefficient as that of propan-2-ol). Both by-products appear during the reaction and slowly disappear. It is most likely that the by-products originate from reactions with the halogen anion present in the solution from the dissociated surfactant. The observed decrease in the vapour phase concentration of by-products could be associated with the decline in the halogen concentration and continuous removal of the halogenated compound by the flow of propene. A similar effect was observed with the chlorine containing surfactant. A single by-product peak was registered at 8.2min retention time.

Application of non-ionic surfactants for solubilisation of gases is described in [151]. It was shown for the case of polyethoxylated lauryl alcohol surfactants (which have the

common brand name Brij) that the ethylene oxide groups are ineffective in gas solubilisation and only hydrophobic lauryl alcohol groups within each micelle provides sites for gas solubilisation. Considerable increases in the solubility of propane in aqueous solutions of Brij-35 and Brij-30 surfactants were demonstrated.

A number of Brij surfactants were tested in the work described in this thesis (see Table V-1). No by-products originating from decomposition of the surfactant molecules were registered in the low-pressure experiments, although the initially discoloured transparent solutions slowly attained a dark yellow colouration. A two-phase system containing an aqueous solution of phosphoric acid and Brij-58 surfactant and n-decane was also tested. The two-phase system formed a large-droplet emulsion of light yellow colour.
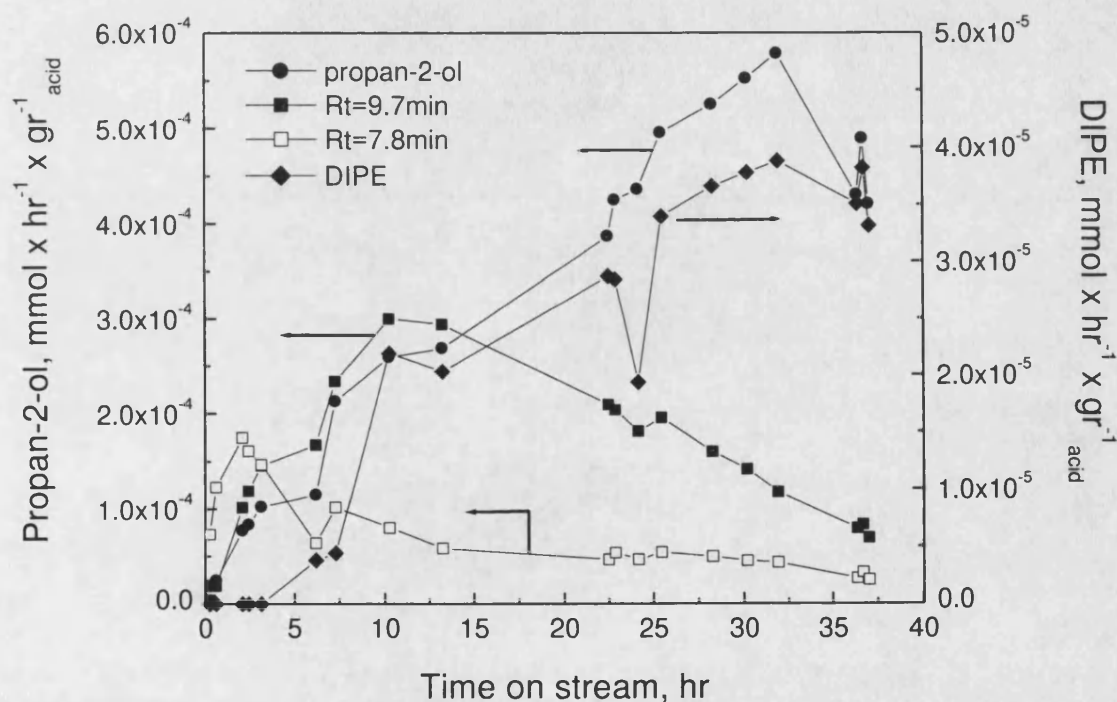
Figure V-1. Vapour phase yield of propan-2-ol, DIPE and two unknown components in low-pressure semi-batch experiment with benzyldimethyldodecyl-ammonium bromide.
Reaction conditions are given in Table V-1 Exp#2.

A number of representative experiments performed in the low-pressure semi-batch experimental rig described earlier (see p.42) is shown in Figure V-2. A "blank" experiment performed without any surface active agents is shown in Figure V-2 as dark circles with error bars. The error at each point corresponds to the estimated average error of these experiments calculated as described in the Experimental Chapter (see p.69). All

other results shown in Figure V-2 have similar errors; the corresponding error bars were omitted from the figure for visual clarity.

It can be seen from Figure V-2 that the effect of surfactants is very small if not absent. Four experiments seem to demonstrate a marginal increase in the yield of propan-2-ol. Notably, the two quarternary ammonium salt surfactants show an increased yield of propan-2-ol in comparison to the pure acid solution despite the high concentration of by-products formed in both reactions (see above). A significant difference in the effect of the pure Brij-58 and an emulsion containing Brij-58 and decane can be seen in Figure V-2. An addition of 2 ml of decane to the aqueous solution of phosphoric acid and Brij-58 surfactant increases the yield of propan-2-ol in comparison to the pure phosphoric acid solution and the acid with Brij-58 solution. Also an increase in concentration of Brij-35 surfactant seem to have an adverse effect on the yield of propan-2-ol.
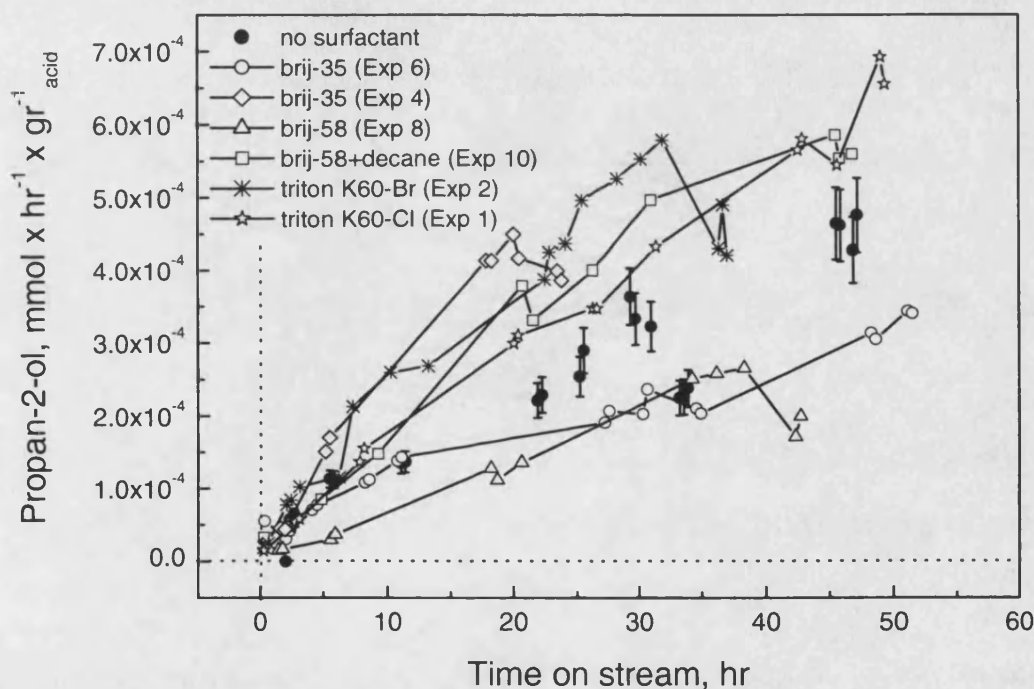
Figure V-2. Yield of propan-2-ol in low pressure semi-batch reactor in the absence and presence of surfactants.

It should be pointed out that the reaction in the semi-batch reactor at atmospheric pressure is strongly mass transfer limited: simulation of a kinetic model at the same temperature and atmospheric pressure predict that the equilibrium conversion should be reached after 6.5 hours. Hence, it is impossible to deduce whether the addition of surfactants to the reaction mixture at low pressure had any effect at all on the solubility of propene or only had an effect on the rate of mass transfer.

A number of experiments with Brij-58 and Triton K-60 surfactants were performed in a high pressure batch reactor (see Table V-2). In all experiments with surfactants at high pressure, high concentrations of by-products were observed. Figure V-3 is a comparison of the batch experiments with and without surfactants. The solid line represents the best fit to the experimental data on the batch hydration of propene at 382K. It was calculated using the model described in the previous chapter. Considering the very large deviation between experimental curves, it is difficult to make a definite conclusion from these experiments. It seems that the molecules of surfactants take part in the reaction with the formation of new by-products. An in-situ analysis of the liquid phase composition is necessary to provide a more definitive answer.
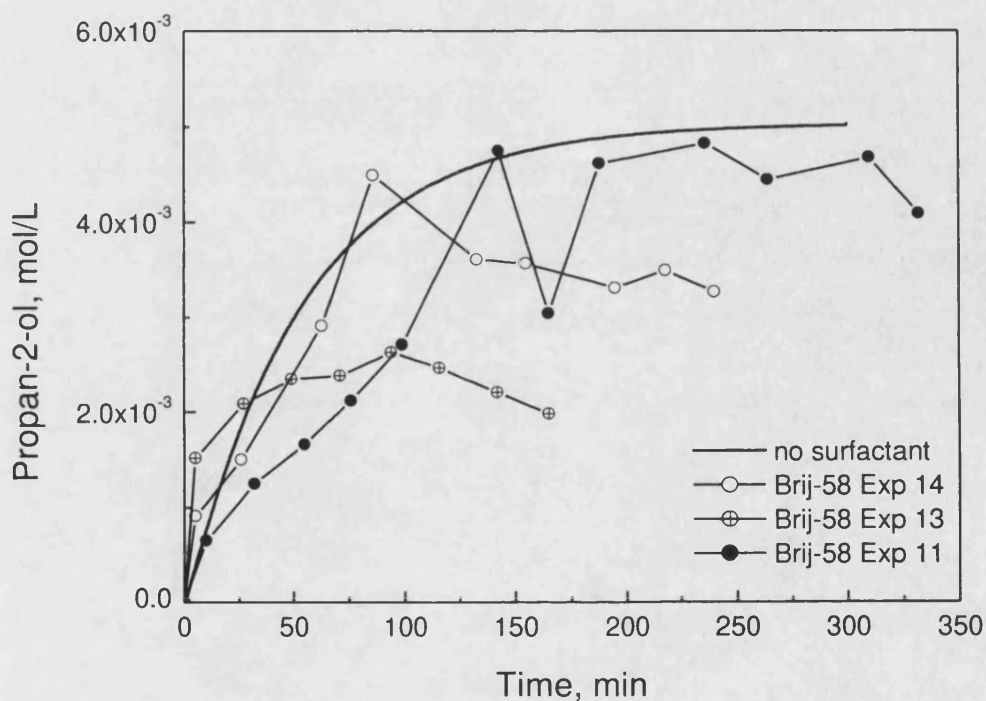
Figure V-3. Vapour phase concentration of propan-2-ol in the batch reaction with surfactants.

Table V-1. Low pressure semi-batch experiments with surfactants and surfactant-organic solvent mixture.

No	T, K	Acid weight, gr	Surfactant brand name	$C_{surfactant}$, mmol/L	Surfactant chemical name/formula	Type	Effect
1	376	299	Triton K-60	152.3	benzyldimethyldodecylammonium chloride	cationic	+
2	376	291	-	62.8	benzyldimethyldodecylammonium bromide	cationic	+
3	376	302	Brij-35 + Brij-30	129.1	polyoxoethylene 4 lauril ether $C_{12}H_{25}(OCH_2CH_2)_4OH$	nonionic	0
4	376	297	Brij-35	1.43	polyoxoethylene 23 lauril ether	nonionic	+
5	376	284	Brij-35	8.0	$C_{12}H_{25}(OCH_2CH_2)_{23}OH$	nonionic	+
6	376	294	Brij-35	15.3		nonionic	0/-
7	376	291	Igepal CO-720	57.3	4-(C_9H_{19})-$C_6H_4O(OCH_2CH_2)_{11}CH_2CH_2OH$	nonionic	-
8	377	295	Brij-58	35.5	$C_{16}H_{33}(OCH_2CH_2)_{20}OH$ polyoxoethylene 20 cetyl ether	nonionic	-
9	380	298	Brij-58 + decane	27.5 + 1.5ml		nonionic	0
10	378	293	Brij-58 + decane	31.8 + 2ml		nonionic	+

Table V-2. High pressure batch experiments with surfactants.

No	T, K	P, MPa	Acid weight, gr	Stirrer, rpm	Surfactant brand name	$C_{surfactant}$, mmol/L
11	382	2.4	128.7	100	Brij-58	35.3
12	382	2.5	127.8	150	Brij-58	35.3
13	382	2.18	135.0	150	Brij-58	32.7
14	380	2.25	134.2	100	Brij-58	32.7
15	387	2.35	128.7	150	Brij-58	32.7
16	393	2.1	132.3	100	Triton K-60	58.6

VI.   Performance of the carbon membrane contactor

The performance of the carbon membrane contactor for the direct hydration of propene was tested using the reactor described in detail in the Experimental Section (page 43). The primary objective of the membrane contactor experiments was to demonstrate the feasibility of a high pressure membrane contactor system. Preliminary studies showed that flat carbon disks, (NOVOCARB™) with a mean pore diameter of ca. 0.5 µm and 2 mm thickness, withstand a transmembrane pressure of up to 0.3MPa. The entering pressure of the concentrated solution of phosphoric acid exceeds this threshold at ambient temperature. It was thus necessary to evaluate the entering pressure of the phosphoric acid solution at the normal operating temperatures. It was also necessary to evaluate the performance of the control system and the influence of the vapour phase contact time and transmembrane pressure on the yield of propan-2-ol. The latter data would enable a comparison of the performance of a conventional SLP hydration catalyst with the catalytic membrane contactor.

Most experiments were performed at 130°C and ca. 2.1MPa pressure. All experiments were performed with an initial acid concentration of 85.4wt%. The choice of the operating temperature was dictated by a compromise between the rate of corrosion of the stainless steel reactor/tubing and the rate of propene hydration. Almost no coloration of the acid solution was noted at 100°C, but the reaction rate was very slow. An increase in temperature by 30°C resulted in a considerable increase in the reaction rate although the acid solution was found to be notably coloured (light green colour characteristic of nickel salts) after the first 3 hours of reaction. Previous batch experiments performed both in the stainless steel and the glass lined reactor showed no influence of metal ions on the rate of propene hydration. At 130°C the rate of reaction provided reasonable conditions for the dynamic measurements (considering 20 minutes to be a minimum time between consecutive measurements of the gas phase composition). It was therefore concluded that the membrane contactor system should be tested at this temperature. Several stainless steel tube connections were replaced following 3 months of reactor operation because of significant wall thinning.

Experiments were performed with membranes of ca. 2 mm and 4mm thickness prepared from the same batch of the precursor resin particles with an average particle

diameter 4.89μm (Table III-2, Batch 2). A summary of the membrane reactor experiments is given in Table VI-1.

The experimental results of representative catalytic runs are shown in Figures VI-1 to VI-3. The graphs show the yield of propan-2-ol recalculated with the assumption of a fully wetted membrane i.e. the yield of propan-2-ol is calculated in relation to the volume of the acid within the porous structure of each membrane of given porosity and dimensions. Figures VI-1 to VI-3 also show the molar selectivity between the reactions of formation of propan-2-ol and DIPE, the concentration of propan-2-ol in the gaseous condensate, operating transmembrane pressure and those instances when water or the 85wt% acid solution were added to the reaction mixture. The concentration of the propan-2-ol solutions was calculated on the basis of a vapour-phase composition analysis, assuming that only propan-2-ol, DIPE and water were present. Several attempts were made to measure the composition of the vapour phase condensate at the end of reaction but the small amount of condensate did not allow any reasonable accuracy of measurement.

Experiments were performed at several propene flow rates for a broad range of vapour phase contact times. The general trend in the dynamic behaviour of the reactor is similar at all contact times: an initial sharp increase in the yield of propan-2-ol is followed by a maximum and subsequent rapid decrease to a plateau with a considerably lower yield compared with the maximum value. The trend is more evident at longer contact times. The maximum of the propan-2-ol yield coincides with the maximum of the vapour phase alcohol concentration (recalculated to the weight per cent of propan-2-ol in the corresponding hypothetical condensate solution).

In general, at longer contact times the yield of isopropanol is lower than that at shorter contact time, although the results are not very consistent (see Table VI-1). The highest values of the propan-2-ol yield are comparable with the best values reported for the packed-bed SLP catalyst (207 kghr^{-1}m^{-3} [77]). Similarly, the concentration of alcohol in the output stream is comparable with commercial hydration processes (see Prior Art section). Another important result of these membrane reactor experiments is the viability of the high pressure contactor reactor based on porous inorganic membranes.

All contactor systems described in the open literature (see Chapter II) operate at pressures close to ambient. Operation at high pressures requires good control of the total and transmembrane pressure throughout the reaction cycle: start-up, normal operation and shut-down. This is achieved via a combination of accurate measurement, an online control system and tuning the porous structure of the membrane contactor i.e. pore size,

pore size distribution and surface chemistry. Preparation and characterisation of the carbon membranes used in this study was described in the Experimental Section. Performance of the designed control system during the start-up and shut-down of the reactor was also demonstrated in the Experimental Section. Stability of the control system during continuous operation and influence of the transmembrane pressure on the position of the gas-liquid interphase was observed during experiments performed in the experimental membrane system.

The lower part of Figures VI-1 to VI-3 shows the transmembrane pressure logged during each experiment. These values were calculated (by the control and acquisition software) as the difference between the measured pressure in the liquid and gaseous chambers of the membrane cell. Frequency of data logging was set manually and could be adjusted during experiment. Typical frequencies of data logging used were 1, 120, 180 and 300 seconds and it is clear from the plots (Figures VI-1 to VI-3) when a higher logging frequency was used. A positive transmembrane pressure corresponds to a higher pressure in the liquid phase. Most of the experiments were started at a transmembrane pressure set to $\Delta P=0.7$atm. The "flood" indicator – a conductivity sensor installed in the gas-chamber of the membrane cell – was used to indicate complete wetting of a membrane. The sensor was installed just above the surface of a membrane. The exact distance between the sensor tip and the membrane surface could not be determined due to the variation in the compression of the Viton™ O-rings from one experiment to another. Hence, it is most likely that the indication of contact with the liquid phase occurred when a continuous film of phosphoric acid had already been formed above the membrane surface. The value of $\Delta P=0.7$atm was found experimentally: an increase in ΔP to 0.85atm resulted in liquid contact. The consecutive decrease in ΔP to 0.7atm resulted in loss of the contact. Such a methodology was used in all experiments to adjust the maximum transmembrane pressure.

The experiments shown in Figures VI-1 to VI-3 were performed at different initial maximum transmembrane pressures. These differences arouse because of deviations in the membrane pore diameter and porosity from sample to sample. The results of membrane characterisation described in the Experimental Section clearly show such a possibility (page 29).

The data-logging of the transmembrane pressure shown in Figures VI-1 and VI-3 show that the transmembrane pressure gradually increased in the course of an experiment. This general trend was observed during most of the experiments: the maximum transmembrane pressure increases with the duration of an experiment. This

effect was observed when the transmembrane pressure was increased in order to try to compensate for the apparent decrease in the propan-2-ol yield.
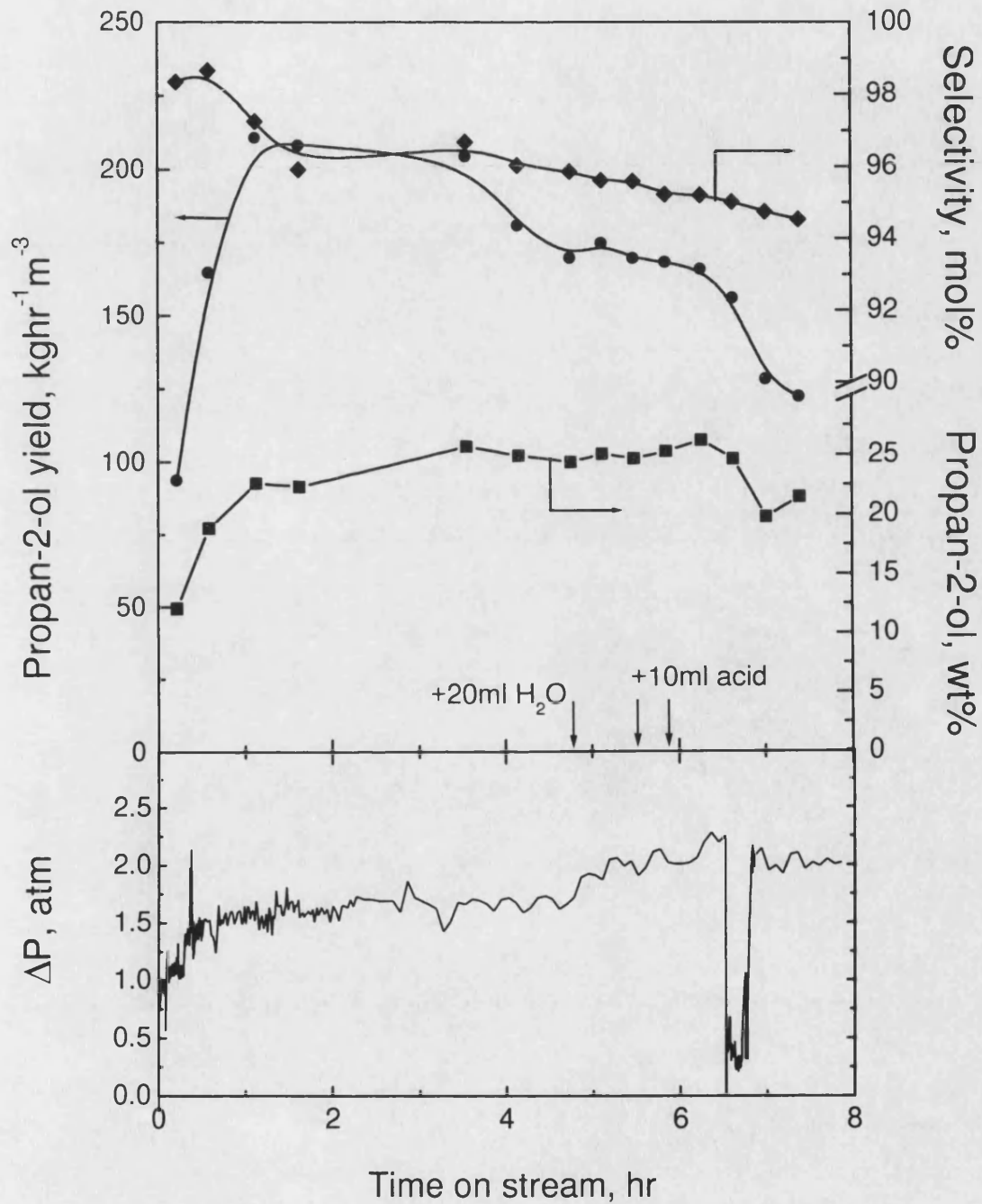
Figure VI-1. Hydration of propene in the porous carbon contactor reactor.
Reaction conditions: P_{gas}=20.7atm; T=130°C; τ=35sec; membrane thickness 2.0mm; initial acid concentration 85.4wt%

94
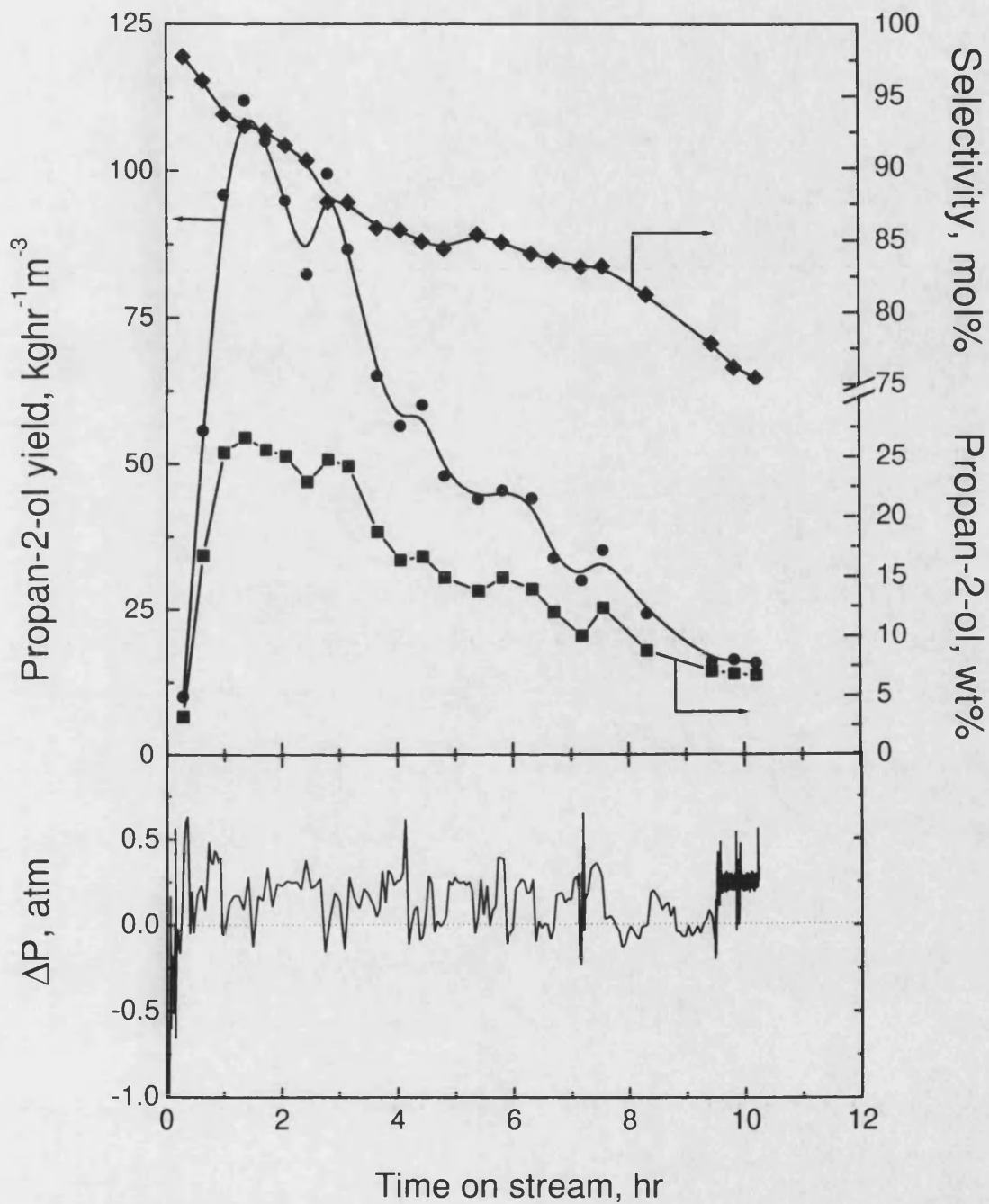
Figure VI-2. Hydration of propene in the porous carbon contactor reactor.
Reaction conditions: P_{gas}=20.9atm; T=130°C; τ=48sec; membrane thickness 2.1mm; initial acid concentration 85.4wt%
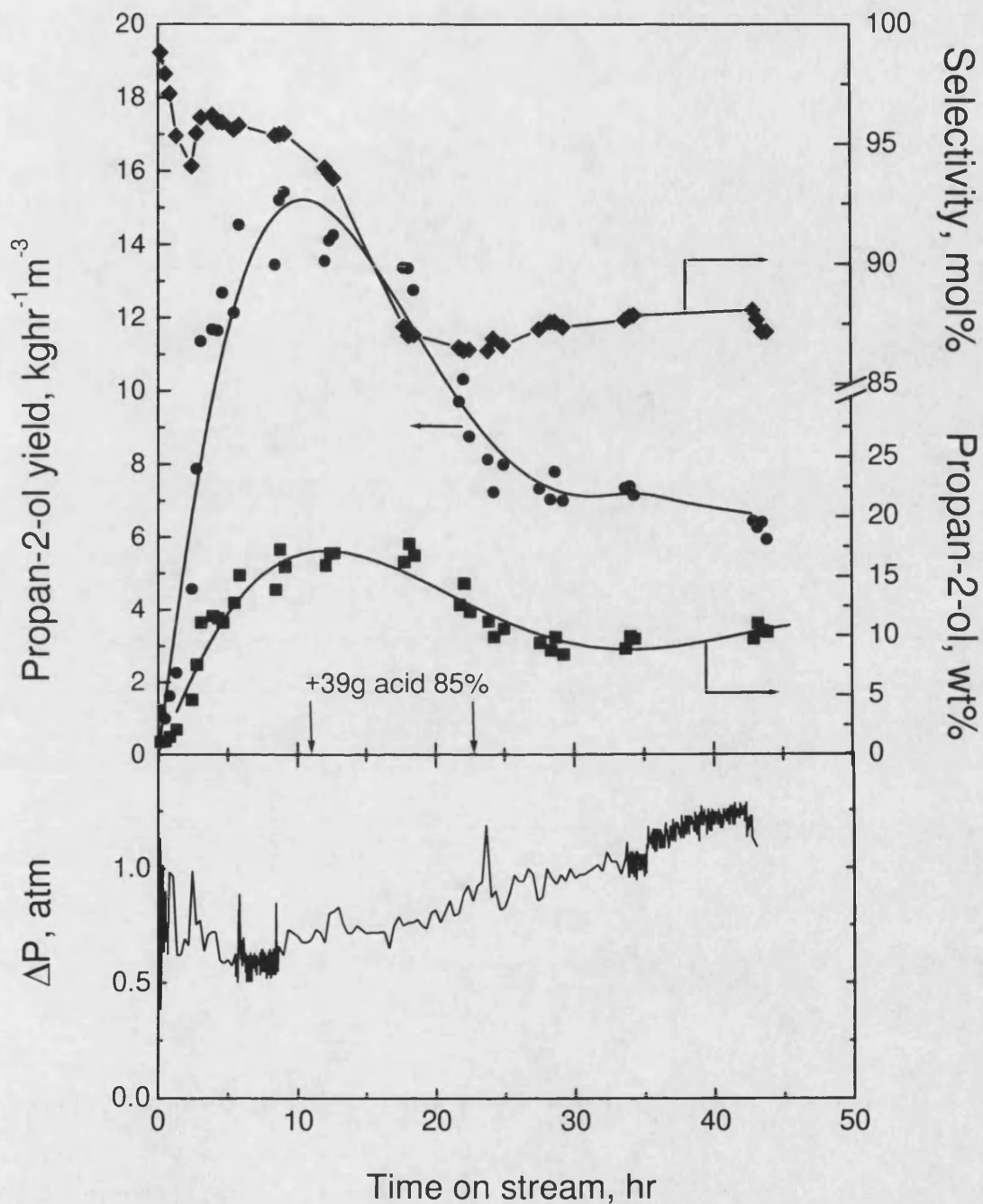
Figure VI-3. Hydration of propene in the porous carbon contactor reactor.
Reaction conditions: P_{gas}=21.4atm; T=130°C; τ=163sec; membrane thickness 4.3mm; initial acid concentration 85.4wt%

As can be seen from Figures VI-1 to VI-3, an increase in transmembrane pressure had no apparent effect on the yield of isopropanol. There are several possible causes for a decrease in the yield of isopropanol. Because reaction is performed in a semi-batch

mode, i.e. continuous operation in the gaseous phase and batch operation in the liquid phase, it is possible that the observed decrease in yield of alcohol is the result of the exhaustion of water in the bulk of the liquid phase. It is also possible that the thin layer of acid within the membrane is exhausted and transport of water in the liquid phase is limiting the reaction. A localised decrease in water concentration will result in an increase in acid concentration and, consecutively, in the rate of formation of long-chain by-products. This was demonstrated in the Experimental Section (page 59). Accumulation of long-chain by-products within the porous structure of a membrane is potentially detrimental because of decrease in the acid volume and change in the wetting angle. The latter will most likely result in retrieval of the acid phase from the membrane at a constant transmembrane pressure.

In order to check some of these hypotheses experimentally, step-changes of the transmembrane pressure were performed in addition to experiments when fresh acid solution and sometimes pure water or diluted acid solution were added to the bulk of the liquid phase during experiments. There was also a need for a periodic increase in the volume of the liquid phase due to a small leak in the circulating pump. Figures VI-4 and VI-5 show the effect of changes in the transmembrane pressure and occasional addition of fresh acid or water to the liquid phase on the partial pressure of water in the gaseous phase. These figures correspond to the experiments represented in figures VI-1 and VI-3.

The absolute values of the partial pressure of water are slightly higher than would be expected from [146] at such temperature and acid concentration (see Figure IV-5). The concentration of water measured in the batch experiments is similar to that obtained in the membrane experiments (85.4wt% acid and 126°C – ca. 70kPa; 85.4wt% acid and 135°C – ca. 125kPa). Figure VI-5 suggests that addition of fresh acid solution has an effect on the vapour pressure of water. Results in Figure VI-4 however, are inconclusive. A slight increase in the vapour pressure of water at the end of the experiment may have resulted from a step-change in the transmembrane pressure. The step-change was performed in order to push the acid solution from the membrane pores into the bulk to renew the solution at the gas-liquid interface. This resulted in a slight increase in the vapour pressure of water but did not have any positive effect on decrease in the yield of isopropanol (Figure VI-1).
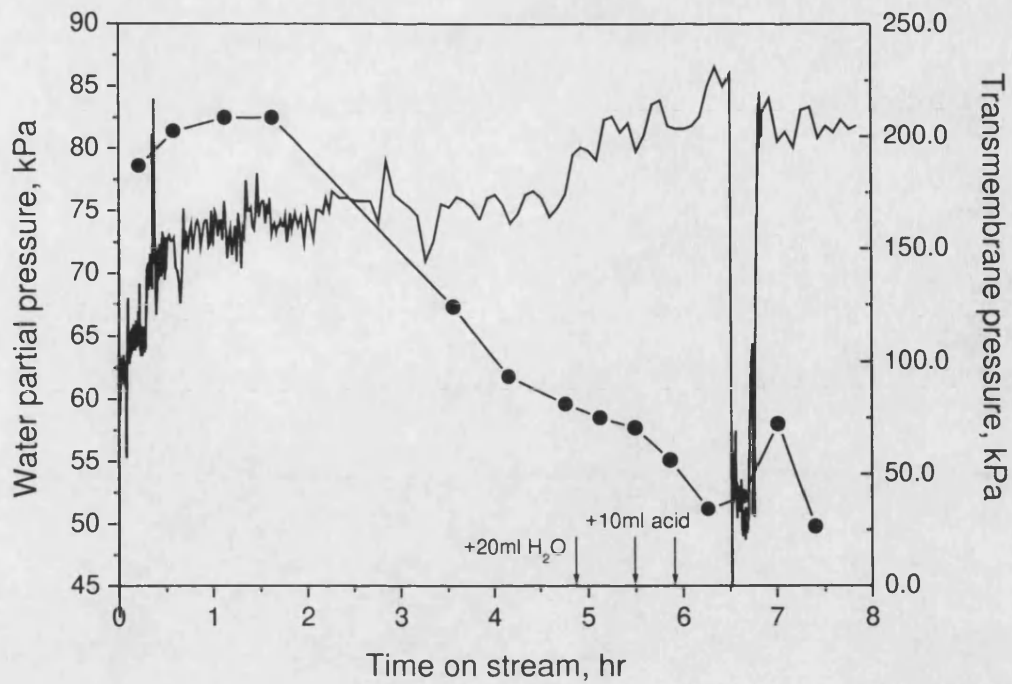
Figure VI-4. Evolution of water during membrane experiment.
Reaction conditions: P_{gas}=20.7atm; T=130°C; τ=35sec; membrane thickness 2.0mm; initial acid concentration 85.4wt%
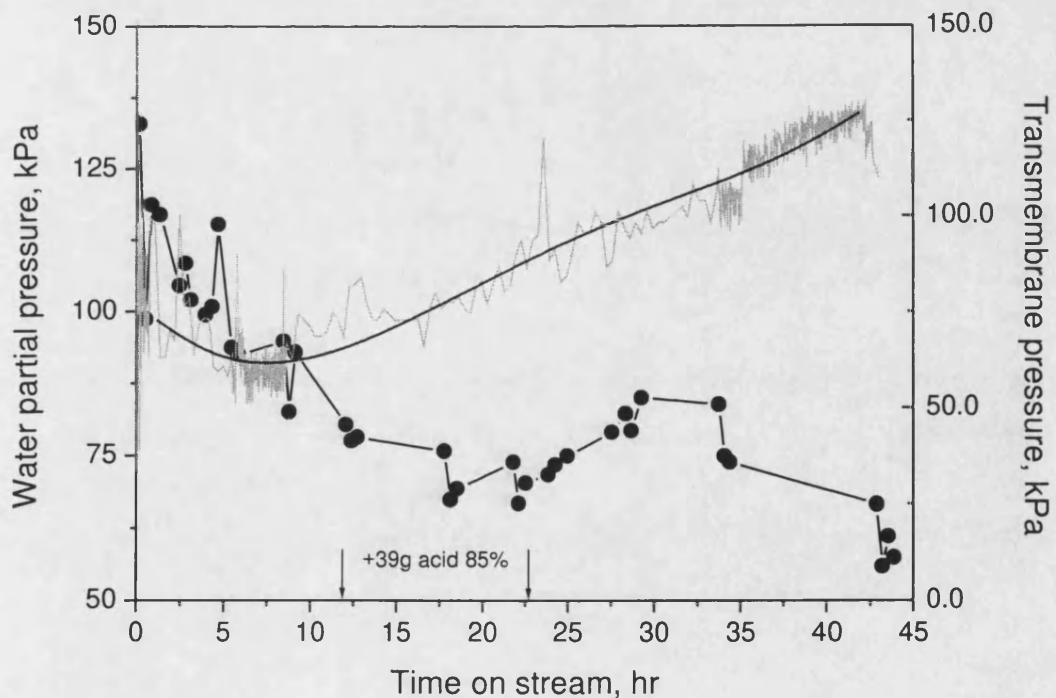
Figure VI-5. Evolution of water during membrane experiment.
Reaction conditions: P_{gas}=21.4atm; T=130°C; τ=163sec; membrane thickness 4.3mm; initial acid concentration 85.4wt%. Solid line is a polynomial approximation of the transmembrane pressure.

As it was noted earlier in this chapter, there is a significant effect of the contact time on the yield of propan-2-ol. The values of maximum yield vs. contact time are summarised in Table VI-1. The table also shows the approach to the equilibrium vapour concentration of isopropanol. These values were calculated as $100 \times \dfrac{C_{C_3H_7OH}}{C^{eq}_{C_3H_7OH}}$, where $C^{eq}_{C_3H_7OH}$ is the equilibrium vapour phase concentration of propan-2-ol at a given temperature and initial propene pressure calculated using the model described in Chapter IV.

It can be expected that, at high contact times, the concentration of alcohol in the vapour phase would be close to that at the equilibrium. It is shown in Table VI-1 and Figure VI-6 that the maximum value attained in the membrane reactor is 70% of the equilibrium concentration at 263s contact time. The values of alcohol concentration recorded in the experiment with 119s contact time are higher than that at equilibrium. This result contradicts to all other experiments and is therefore discarded from consideration as erroneous.
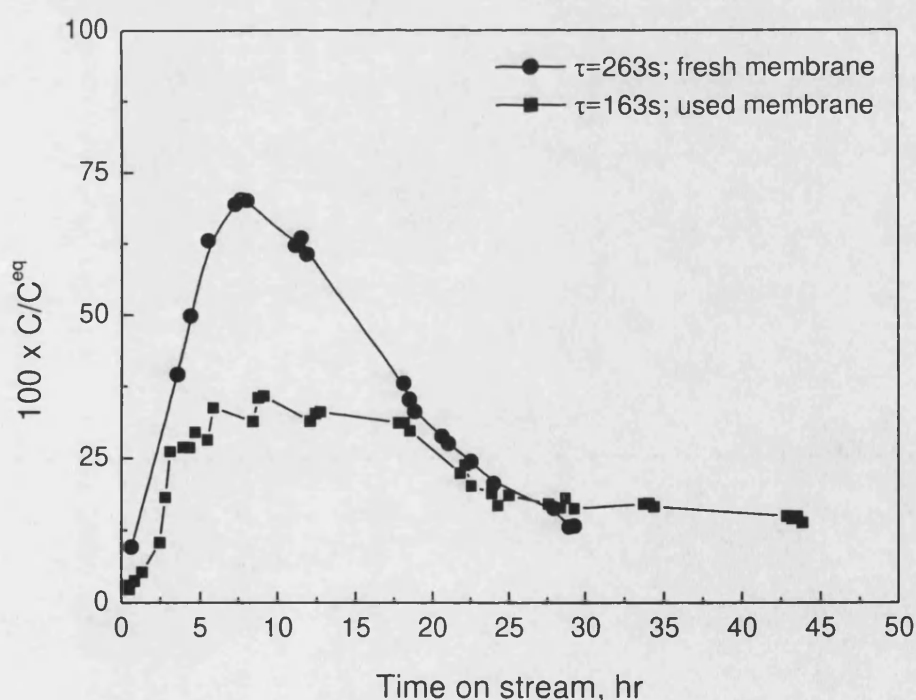
Figure VI-6. Approach to equilibrium conversion in membrane experiments.
Membrane thickness 4.3 and 4.2 mm; initial acid concentration 85.4wt%.

It is not clear why the maximum alcohol concentration at the same contact time (263s) differs significantly for thick (4.2mm) and thin (2.0mm) membranes (compare

experiments 4 and 5 in Table V-1). Further comparison of these results seem to indicate that higher alcohol concentrations are recorded in the experiments performed with membranes that have not been previously used in the hydration experiments.

Table VI-1. Experimental conditions and summary of results of membrane experiments.

No	Duration of experiment, hr	Membrane thickness, mm	ΔP, kPa	Used or fresh membrane	Contact time τ, sec	Max yield, $kghr^{-1}m^{-3}$	Selectivity at max yield, mol%	Max propan-2-ol concentration, wt%	Approach to equilibrium, per cent
1	9	4.3	60	used	65	10.9	95	4.6	11
2	53	4.3	60	used	159	4.6	94	5.9	11
3	44	4.3	70	used	163	17.2	94	16	36
4	29	4.2	70	fresh	263	19.2	96	25	70
5	8	2.0	70	fresh	262	6.8	97	6.4	12
6	*57*	*2.0*	*140*	*fresh*	*119*	*228.5*	*81*	*30.2*	*>100*
7	7	2.0	150	fresh	35.5	210.8	97	25.7	51
8	4	2.1	200	fresh	18.9	144.1	94	12	20
9	7	2.1	210	fresh	18.1	243.3	98	14.8	32
10	9	2.1	200	used	14.6	84.6	98	8.7	9
11	10	2.1	30	fresh	48.6	112.0	93	27	38

Other conditions:

Vapour phase pressure P_g=2.2 ÷ 2.5MPa; temperature T=403K; initial acid concentration 85.4wt%; liquid flow rate 101 ml/min.

VII. Membrane phase contactor model

VII.1. Model development

A number of hypotheses about the effects of liquid phase mass transfer, gas phase contact time and thickness of a membrane on performance of membrane contactor reactors were expressed in the previous chapter. These may be validated by mathematical modelling. The model described below is based on the kinetic model described in detail in Chapter IV and theoretical equations of mass conservation. To simplify the model it was assumed that the reactor is isothermal, the gas phase is ideal, mixing is ideal, the bulk gas and liquid phases are well mixed and the liquid phase is non-ionic. With such simplifications the model should describe the general trends observed experimentally, but it would be wrong to expect that the simulations of the reactor with a simplified model would describe the experimental data exactly.

Design of the gas distributor and collector in the chamber above the membrane (see membrane cell design in Appendix A) should ensure a well-mixed regime, thus satisfying the assumption of ideal mixing. Similarly, the assumption of ideal bulk liquid mixing is supported by fast recirculation of the bulk liquid phase. Recirculation was performed at a flow rate of about 100ml/min with the total volume of the liquid phase ca. 150ml and fast mixing in the liquid reservoir (see Chapter III.5).

The reactor is assumed to be isothermal. The three main reactions are shown in equations Eq. VII-1 to VII-3. Only the first and third reactions are taken into account in the kinetic model (see Chapter IV). Although the reactions are exothermic, the small size of the test reactor and other parameters of the experimental rig (i.e. large surface area of gas and liquid metal lines, large thermal mass of the cell, isothermal condition in the reactor enclosure) allows one to ignore any temperature variations due to the reactions, mixing or evaporation-condensation.

$$C_3H_6 + H_2O \rightarrow C_3H_7OH \qquad \Delta H = -52 \; kJ \, / \, mole \qquad \textbf{Eq. VII-1}$$

$$2C_3H_7OH \rightarrow C_6H_{14}OH + H_2O \qquad \Delta H = -7.4 \; kJ \, / \, mole \qquad \textbf{Eq. VII-2}$$

$$C_3H_6 + C_3H_7OH \rightarrow C_6H_{14}OH \qquad \Delta H = -66.8 \; kJ \, / \, mole \qquad \textbf{Eq. VII-3}$$

The two most prominent assumptions are that gas phase is ideal and the liquid is non-ionic. At typical reaction conditions (130°C, 2MPa and the gas phase composed of propene, steam, propan-2-ol, diisopropyl ether) the mixture is strongly non-ideal. At these conditions gas phase behaviour is usually described either via the introduction of activity coefficients or by a suitable cubic equations of state. In the case when either temperature or pressure for a given gas exceeds its corresponding critical value, it is generally not possible to identify the standard state for calculating the corresponding activity coefficient and equations of state should be used [152]. It has been shown in [68] that the Peng-Robinson equation of state satisfactory describes physical equilibrium of the mixture containing water, propene, propan-2-ol and diisopropyl ether.

A similar approach was adopted in this work during the initial stage of model development. The strength of this approach is not only in a more accurate simulation of physical equilibrium, but also in the potential incorporation of the description of electrolyte solutions [153]. Were the data on the composition of the liquid phase available, it would have been possible to pursue this more complex modelling route further. Without the data and having a reasonable simplified model for description of the batch reactor (Chapter IV) it was decided to limit work to the simplified model. Because the methodology applied to obtain the necessary coefficients for the equation of state and the data itself could be of potential interest, these results are presented in Appendix D.

The reactor model comprises four volumes separated by three boundaries (see Figure VII-1). The first volume represents the gaseous phase above the membrane. The first boundary in the model is the surface of a membrane. It is assumed that the flux across the surface of the membrane is the same as the diffusional flux in the gas-filled membrane pores. The boundary condition is therefore given by:

$$\frac{\partial C_i^{I}}{\partial z} = \frac{\partial C_i^{II}}{\partial z}$$

Eq. VII-4

where z is the axis perpendicular to the membrane surface; subscript i corresponds to i-th mixture component and superscripts I and II correspond to the bulk of the gas phase and the gas phase in membrane respectively (see Figure VII-1). Diffusional flux in the gas-filled membrane pores is approximated by:

$$J_{I-II} = A\frac{D_i^{g}}{d_{II}}\left(C_i^{I} - C_i^{III,g}\right)$$

Eq. VII-5

where J_{I-II} is the flux perpendicular to the membrane surface; D_i^{g} is the diffusion coefficient of the gaseous species i; C_i^{I} and $C_i^{III,g}$ are the concentrations of species i in the space above membrane and at gas-liquid interface correspondingly, d_{II} is the distance

103

from the surface of a membrane to the gas-liquid interface and A is the total surface area of pores.

Considering the flow in the gaseous space above the membrane and the flux perpendicular to the surface of the membrane (given by equation VII-2), the mass conservation in the gaseous space above the membrane is given by:

$$V_g \frac{dC_i^I}{dt} = \upsilon\left(C_i^{in} - C_i^I\right) + A\frac{D_i^g}{d_{II}}\left(C_i^I - C_i^{III,g}\right)$$

Eq. VII-6

where C_i^{in} is the concentration of i-th component in the inlet stream; υ is the volumetric gas flow rate and V_g is volume of gas above membrane.
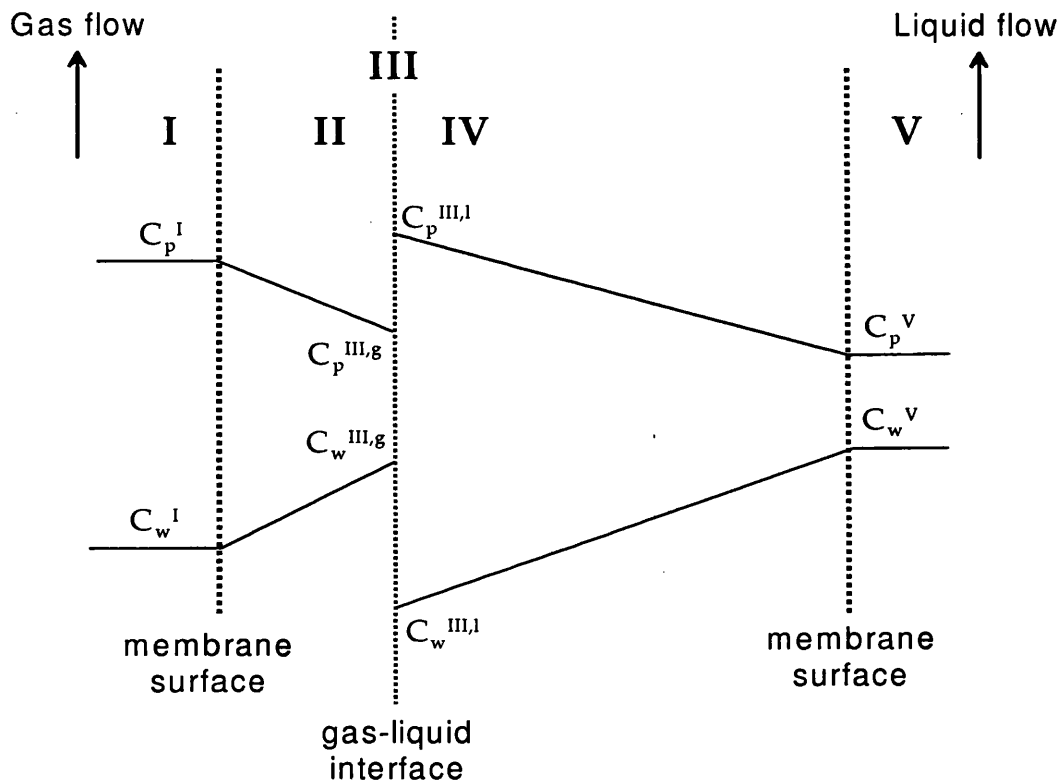
Figure VII-1. Schematic diagram of the reactor model.
Superscripts I,III and V refer to the zone in the model, superscripts g and l refer to gaseous and liquid phase correspondingly and subscripts p and w refer to propene and water correspondingly.

In order to estimate the gaseous diffusion coefficients the following assumptions were made. According to the experimental data the propene concentration in the gaseous phase is about 96 mole per cent. At such a high concentration of propene the influence of other components of the gaseous mixture on its diffusivity may be neglected. A reasonable assumption for the diffusion coefficient of propene would be the self-diffusion coefficient. The self-diffusion coefficient for propene was calculated following [154]:

$$\frac{D\delta}{T_r} = \frac{0.77 \cdot 10^{-5}}{\rho_r}, \quad \delta = \frac{M_w^{1/2}}{P_c^{1/2} V_c^{5/6}}$$

where D is self diffusion coefficient in cm^2/s; T_r is reduced temperature; ρ_r – reduced density; P_c is critical pressure; V_c is critical molar volume.

This relationship is valid for reduced gas densities less than unity. Density of propene at a given temperature and pressure was calculated using the literature data on compressibility factors [127]. The reaction conditions of interest are well within the range of applicability of the above equation.

A typical value of the self diffusion coefficient of propene estimated using Equation VII-7 is $D_{propene} = 0.005$ cm^2/sec at 2.1MPa and 403K.

The gaseous diffusion coefficients for other components were estimated as the binary diffusion coefficients in the corresponding mixtures with propene. Mutual influences of water, propan-2-ol and diisopropylether on each other were ignored. The Chapman-Enskog equation for binary diffusivity [147] was used:

$$D_{ik} = \frac{0.00266 T^{3/2}}{P\sqrt{M_{ik}}\,\sigma_{ik}^2 \Omega_d}$$

$$M_{ik} = 2\left(\frac{1}{M_i} + \frac{1}{M_k}\right)^{-1}$$

$$\sigma_{ik} = \frac{1}{2}(\sigma_i + \sigma_k)$$

$$\Omega_d = \frac{1.06036}{\left(T^*\right)^{0.15610}} + \frac{0.19300}{\exp\!\left(T^*0.47630\right)} + \frac{1.03587}{\exp\!\left(T^*1.52996\right)} + \frac{1.76474}{\exp\!\left(T^*3.89411\right)}$$

$$T^* = \frac{kT}{\varepsilon_{ik}}; \quad \varepsilon_{ik} = \sqrt{\varepsilon_i \varepsilon_k}$$

where σ_i and ε_i – Lennard-Jones parameters.

Typical values of diffusion coefficients estimated using Equations VII-8 are: $D_{water\,/\,propene} = 0.01$ cm^2/sec; $D_{propan-2-ol\,/\,propene} = 0.004$ cm^2/sec at 2.1MPa and 403K.

The interfacial area A was estimated from data on the average pore diameter and porosity obtained in Chapter III.2, and assuming the geometry of straight cylindrical pores. The distance between the gas-liquid interface and the membrane surface d_{ll} was assumed arbitrarily. In principle, the balance of forces between gas and liquid (i.e. gas and liquid pressure and the entering pressure of liquid into the pores) should enable the position of the gas-liquid interface within the membrane to be calculated. But this would

require an exact knowledge of the pore geometry and contact angle inside pores. Therefore, for the purpose of modelling, the position of the interface was assumed arbitrarily.

An assumption of instantaneous gas-liquid equilibrium was made to obtain the boundary condition for the gas-liquid interface (III in Figure VII-1). The equilibrium concentrations in both phases were estimated by assuming ideal behaviour. The corresponding coefficients for Henry's and Raoult's laws equations were estimated from the literature data (see Chapter IV).

A two-film model was applied to describe the mass transfer across the gas-liquid interface (see Figure VII-2). In order to satisfy the condition of instantaneous equilibrium, the mass transfer coefficients were assumed to be large. The same technique (dynamic relaxation) for calculating equilibrium was applied to solve the equilibrium batch model in Chapter IV. '
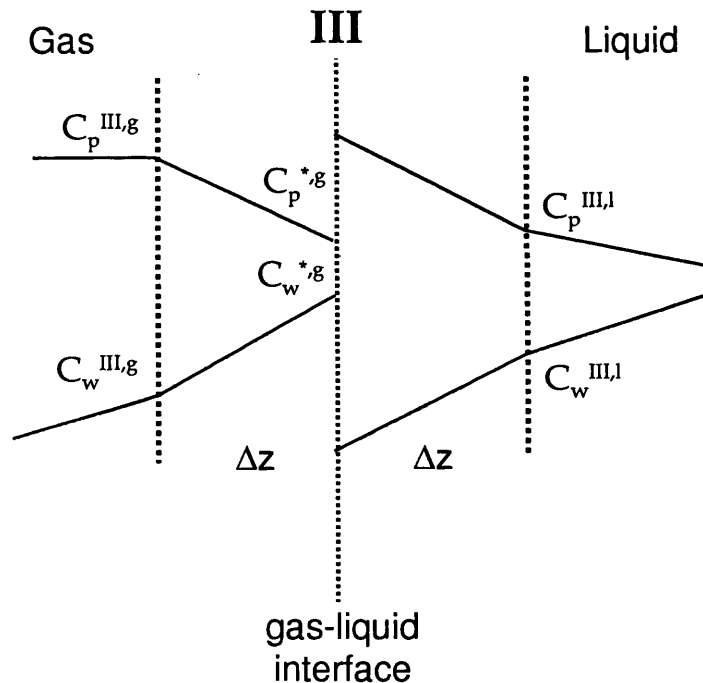
Figure VII-2. Two-film model describing mass transfer at gas-liquid interface. Subscripts m, g and l refer to membrane, gas phase and liquid phase correspondingly; asterisk refers to the equilibrium concentrations.

The thickness of the films (Δz) on each side of the interface was taken as equal to the grid length used for the solution of the diffusion equation in the liquid phase inside a membrane. Thus, thickness of the film has no physical meaning. The mass conservation equations for the gas-phase volume near the interface is therefore given by:

$$\mathrm{d}V\frac{dC_i^{III,g}}{dt} = -A\frac{D_i^g}{d_{II}}\left(C_i^I - C_i^{III}\right) + k_{ga}\mathrm{d}V\left(C_i^{*,g} - C_i^{III,g}\right)$$

Eq. VII-9

The mass conservation equation in the liquid filled pores takes into account the film model at the gas-liquid interface, diffusion, reaction and contact with the bulk of the liquid phase. Thus, the mass conservation equation for the volume adjacent to the gas-liquid interface is given by:

$$dV \frac{\partial C_i^{III,l}}{\partial t} = k_{la} dV \left(C_i^{*,l} - C_i^{III,l} \right) + D_i^l \frac{\partial^2 C_i^{IV}}{\partial z^2} + r_i dV \qquad \text{Eq. VII-10}$$

where D_i^l is the diffusion coefficient for species i in the liquid mixture; z is the co-ordinate perpendicular to the surface of membrane; r_i is reaction rate, described in Chapter IV and dV is the volume element.

The method of lines [155] was used in order to convert the second order differential equation into a corresponding difference equation. For the grid spaces 2 to N a central difference equation was used:

$$D_i^l \frac{\partial^2 C_i^{IV}}{\partial z^2} = D_i^l \times \frac{C_{i,z-1}^{IV} - 2C_{i,z}^{IV} + C_{i,z+1}^{IV}}{(\Delta z)^2} \qquad \text{Eq. VII-11}$$

where C_N^{IV} correspond to the liquid bulk concentration of i_{th} species and subscript z refers to the grid position.

For grid 1 the mass conservation equation is given by:

$$dV \frac{\partial C_i^{III,l}}{\partial t} = k_{la} dV \left(C_i^{*,l} - C_i^{III,l} \right) + D_i^l A \frac{\left(C_{i,2}^{IV} - C_{i,1}^{IV} \right)}{\Delta z} + r_i dV \qquad \text{Eq. VII-12}$$

Diffusion coefficients in the liquid phase were estimated using the modified Wilke-Chang equation for mixed solvents:

$$D_{im}^0 = 7.4 \cdot 10^{-8} \frac{\sqrt{\phi M} \cdot T}{\eta_m \cdot V_i^{0.6}} \ [\text{cm}^2 / \text{sec}], \quad \phi M = \sum_{\substack{j=1 \\ j \neq i}}^{n} x_j \phi_j M_j \qquad \text{Eq. VII-13}$$

where ϕ_i is the association factor; η_m is the kinematic viscosity of the mixture [cP]; V_i is molar volume [L/mol]; x_i is the molar fraction of compnent i in the mixture [147]. This equation is valid for non-ionic liquids in the approximation of diluted solution.

Viscosity of mixtures, η_m, was approximated by the value of viscosity of the corresponding phosphoric acid solution. Viscosity of phosphoric acid at high temperatures was extrapolated using Eq. VII-14 which was obtained by fitting the available literature data on viscosity of phosphoric acid solutions at three different temperatures [146] to the correlation for viscosity suggested in [147].

$$\eta = 3.508396 - 0.00875 \cdot T + \left(-0.07744 + 0.00028 \cdot T \right) e^{C_{H3PO4}/-18.0807 + 0.094873 \cdot T} \qquad \text{Eq. VII-14}$$

where $C_{H_3PO_4}$ - concentration of the phosphoric acid solution in weight per cent; T - absolute temperature, K.
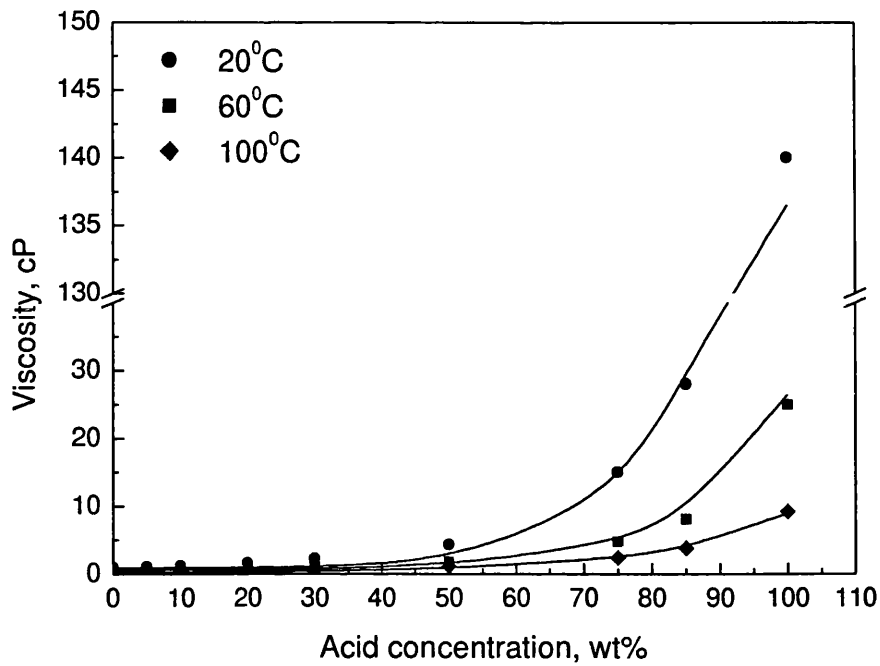
Figure VII-3. Interpolation of experimental data on viscosity of phosphoric acid solutions.
Solid lines calculated using Eq. VII-14.

Typical values of binary diffusion coefficients estimated using Equation VII-13 are:

$$D^l_{water} = 1 \times 10^{-7} \, cm^2 \, / \sec; \quad D^l_{propene} = 1 \times 10^{-7} \, cm^2 \, / \sec; \quad D^l_{propan-2-ol} = 1 \times 10^{-7} \, cm^2 \, / \sec$$

Finally, the mass conservation equation for the bulk liquid phase is governed by diffusional mass transfer across the membrane surface and chemical reaction:

$$V_l \frac{\partial C_i^V}{\partial t} = AD_i^l \frac{\partial C_{i,N}^{IV}}{\partial z} + r_i V_l \qquad \textbf{Eq. VII-15}$$

where V_l is the volume of the bulk liquid phase. It is assumed that mixing in the liquid phase is fast and the concentration distribution in the bulk liquid phase is uniform. The complete set of ordinary differential equations was solved using the commercial ODE solver Berkeley Madonna (v.8.2) loaded on a Pentium III-800Mhz workstation.

VII.2. Simulation of membrane phase contactor behaviour

All kinetic and equilibrium constants were found by fitting the experimental batch data to the kinetic model developed on the basis of the known mechanism of the hydration reaction catalysed by mineral acids (see Chapter IV). The model described above contains two unknown parameters: (1) position of the gas-liquid interface and (2) gas-liquid interfacial area. In all the models presented below position of transmembrane pressure is fixed arbitrary. In the first model the gas-liquid interface is fixed near the gas side of the membrane, i.e. the membrane is fully wetted. Gas-liquid interfacial area is in most cases approximated by the total crossectional pore area, assuming a certain pore geometry. In the second model two adjustable parameters are introduced: (1) the volume of a well-mixed liquid in contact with the gas phase and (2) the length of a stagnant liquid film. The former parameter is required to fit the predicted values for the gas-phase concentrations to experiment, whereas the latter parameter is required to account for diffusional resistance in the liquid-filled pores.

VII.2.1. Fully wetted membrane. Interfacial area=pore area

Assuming that the membrane is fully wetted and liquid in the pores is stagnant the physical model is similar to that of absorption of a gas into a reactive liquid displaying reversible second order kinetics, with an additional mass transfer resistance introduced by the membrane. The mass transfer area between bulk gas phase and the gas film is taken to be equal to the geometrical area of membrane. The gas-liquid interface can be approximated by the total area of pores, assuming a specific pore model. The simplest pore model is that of cylindrical straight-through pores of medium diameter (the latter found by mercury porosimetry measurements: Chapter III.2). The total interfacial area approximated in such a way is likely to underestimate the actual value. It is therefore natural to expect that the simulation would predict lower vapour phase concentrations of the reaction product and therefore a lower yield from the reactor. However, the predicted values of the vapour phase concentration of propan-2-ol at two gas phase contact times (see Figure VII-4) are much too low compared to the values obtained in the membrane reactor experiments (see Figure VI-6 and Table VI-1). Furthermore, the profile of the vapour phase concentration of propan-2-ol vs. time-on-stream is significantly different in the simulated experiments compared to the experimental data.

It should be noted that this simulation was performed with liquid phase diffusion coefficients estimated using Equation VII-13, disregarding the tortuosity of membranes. It is indicated in [124] that in the case of liquid phase diffusion in porous media, the effect of porous structure is minimal, although in some cases tortuosity factors as high as 10 were required to adequately describe the experimental data.
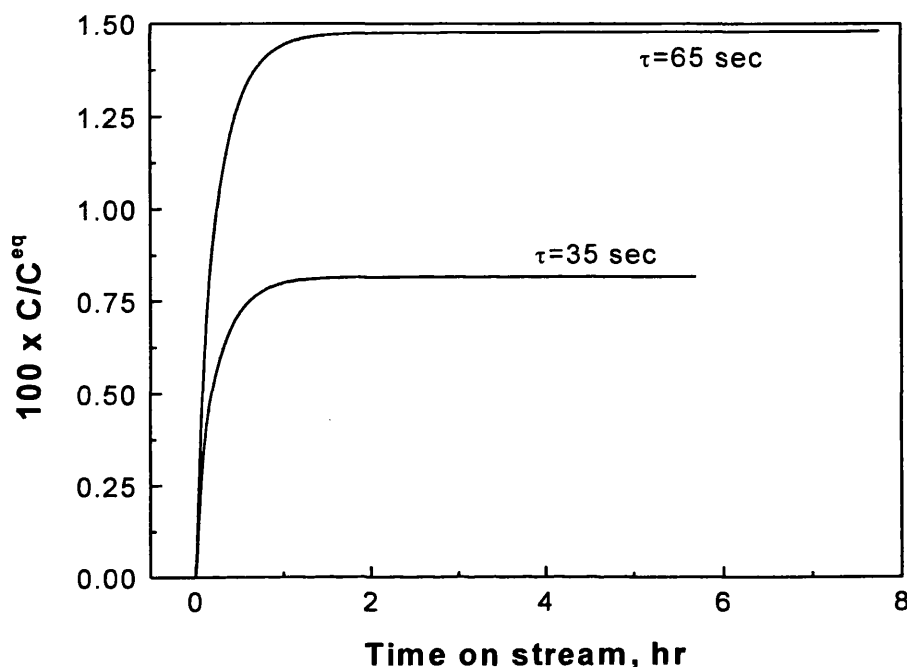

Figure VII-4. Simulation of membrane phase contactor: vapour phase concentration of propan-2-ol vs. time-on-stream.
Reaction conditions: 2.1MPa, 130°C. Membrane porosity 13%. Pore diameter 0.75μm. Gas phase contact time shown.

In this work the tortuosity factor was estimated using gaseous diffusion measurements (see Chapter III.2). The tortuosity factor was found to be ca. 12. The effect of tortuosity was tested in a series of simulations shown in Figure VII-5 and Figure VII-6. It is apparent that an increase in the liquid phase mass transfer resistance (decrease in effective diffusivity invoked by increase in tortuosity factor) results in a decrease in the maximum vapour phase concentration of propan-2-ol and changes the profile of the vapour phase concentration vs. time-on-stream. The profile of propan-2-ol vapour phase concentration shown in Figure VII-6 is similar to that obtained experimentally in the membrane reactor: the initial rapid increase in concentration, followed by maximum and consequent decrease to a plateau (Figure VII-4). In other words, an increase in the liquid phase mass transfer resistance increases the time required for the reactor to reach a steady state.

Figure VII-5. Simulation of membrane phase contactor: vapour phase concentration of propan-2-ol vs. time-on-stream.

Reaction conditions: 2.1MPa, 130°C. Membrane porosity 13%. Pore diameter 0.75μm. Gas phase contact time 35sec. Tortuosity shown in bold.
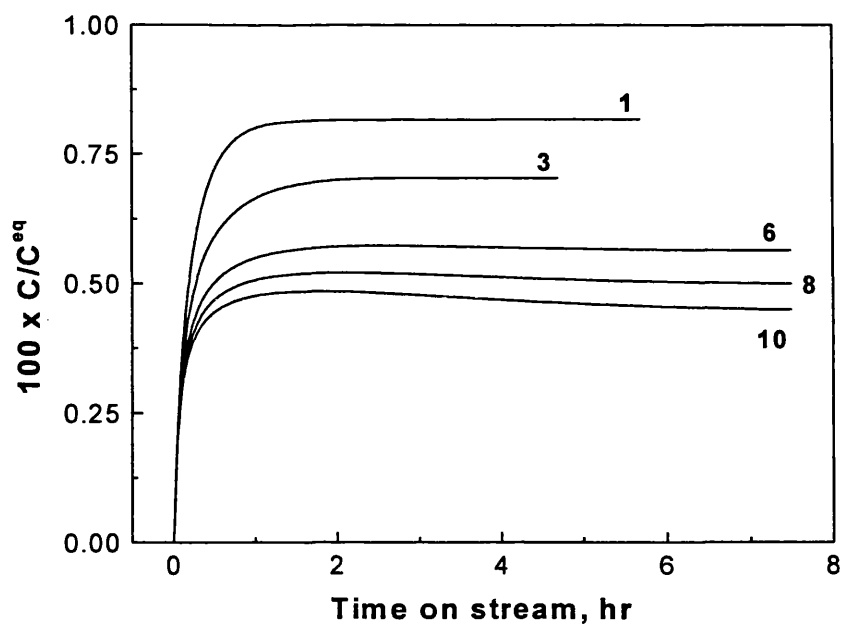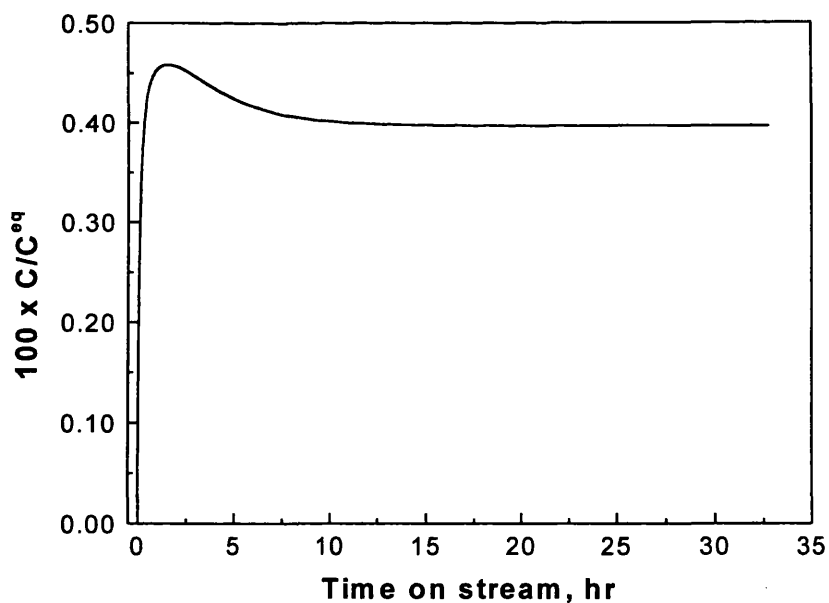

Figure VII-6. Simulation of membrane phase contactor: vapour phase concentration of propan-2-ol vs. time-on-stream.

Reaction conditions: 2.1MPa, 130°C. Membrane porosity 13%. Pore diameter 0.75μm. Gas phase contact time 35sec. Tortuosity = 12.

The concentration profiles of propan-2-ol, diisopropyl ether and water across the membrane thickness at the steady state is shown in Figure VII-7. The shape of the concentration profiles of propan-2-ol and diisopropyl ether (Figure VII-7) at the steady state can easily be attributed to the local concentration of water. The concentration of water is lower near the gas-side of the membrane, thus favouring the formation of diisopropyl ether. Closer to the liquid side of the membrane, the water concentration increases due to diffusion from the liquid bulk and a slower reaction (lower concentration of dissolved propene). Therefore the formation of alcohol is favoured which is reflected by the convex shape of the concentration profile of propan-2-ol.
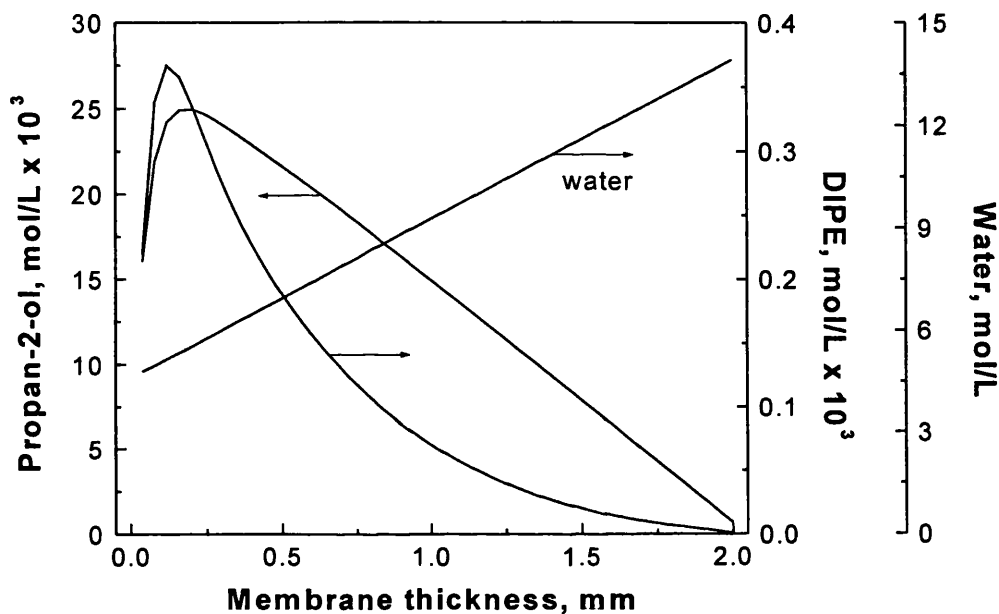
Figure VII-7. Simulation of membrane phase contactor: concentration profiles across membrane at time-on-stream = 33hr.
Reaction conditions: 2.1MPa, 130°C. Membrane porosity 13%. Pore diameter 0.75μm. Gas phase contact time 35sec. Tortuosity = 12.

Figure VII-8 shows that the concentration profile of propan-2-ol across the membrane is decreasing with a decrease in the gas-phase residence time until it reaches a minimum at a contact time of ca. 20sec. A decrease in contact time to 11 seconds has little apparent effect on the liquid phase concentration profile, thus indicating that at these contact times reaction is diffusion limited.
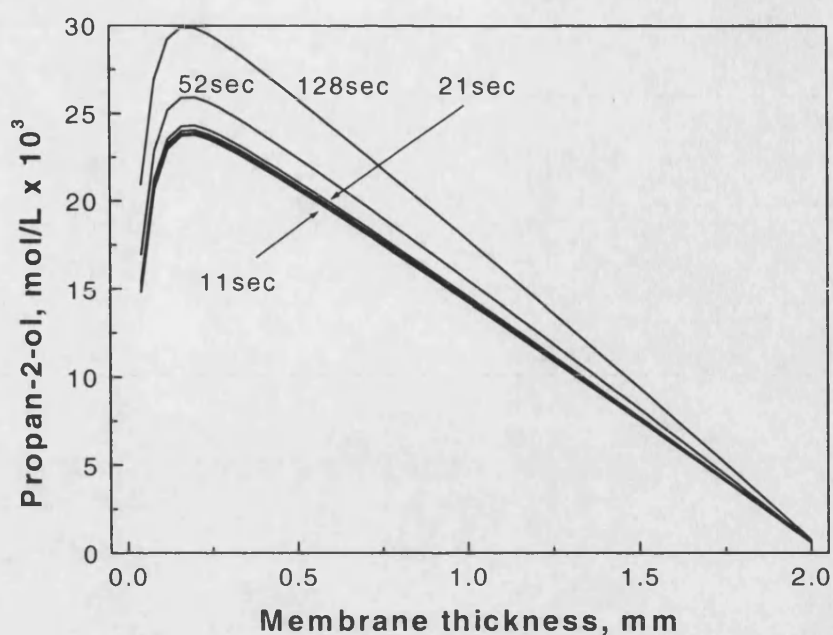
Figure VII-8. Simulation of membrane phase contactor.
Concentration profile of propan-2-ol across membrane at time-on-stream=15hr. Gas phase contact times shown.

The vapour phase concentrations predicted by this model are considerably lower than those observed experimentally. This is likely to be due to a very low volume of acid within the pores of the membrane. As it was shown in Chapter IV, the reaction is slow and occurs in the bulk of liquid phase. This is also illustrated by the concentration profiles within the liquid-filled pores shown in Figure VII-7. Thus high experimental values for the vapour-phase concentrations indicate that the volume of acid actively participating in the reaction is larger than the volume of pores, the latter being taken in the model as the volume of liquid in the membrane.

Assuming that the volume of acid contained within the membrane pores can potentially be increased by an increase in the membrane porosity (see Chapter III.2 for membrane characterisation), the effect of porosity on the gas-phase propan-2-ol concentration is shown in Figure VII-9. This result was obtained assuming a tortuosity factor 1 and assuming that liquid within the pores is stagnant. It is apparent that an increase in porosity can not explain the experimental values of alcohol conversion.

The assumption of diffusional mass transfer limitation within the liquid-filled membrane, i.e. stagnant liquid layer within the membrane pores, disregards fluctuations in the transmembrane pressure observed experimentally. Results shown in Figure VI-1 to

VI-3 indicate a considerable fluctuation of the transmembrane pressure, which undoubtedly induces a certain degree of convective mass transfer within the membrane. This process could potentially increase the volume of acid in contact with the gas phase and decrease the diffusional mass transfer resistance.
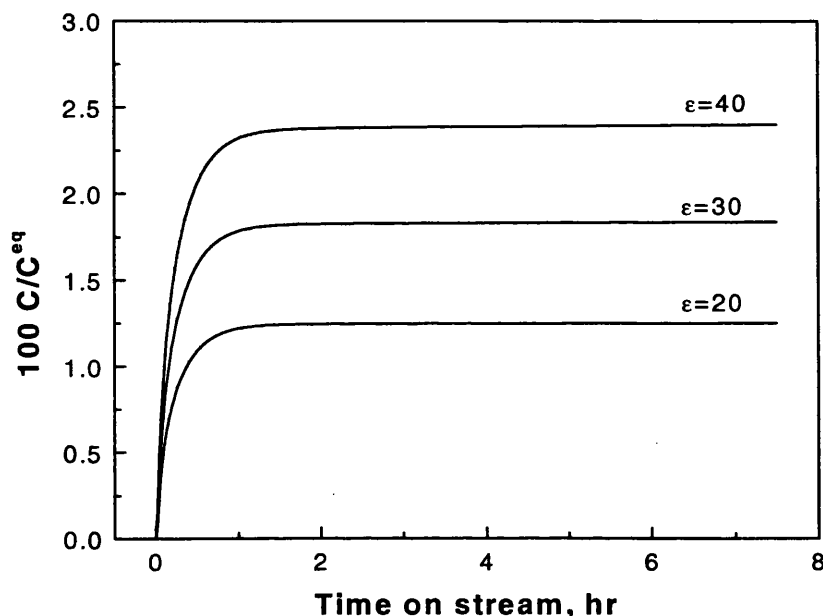

Figure VII-9. Simulation of membrane phase contactor: effect of membrane porosity.
Reaction conditions: 2.1MPa, 130°C. Pore diameter 0.75μm. Gas phase contact time 35sec. Tortuosity = 1. Porosity values shown.

VII.2.2. Concept of "effective" membrane thickness

Fluctuations of the transmembrane pressure invoke convective mass transfer in the liquid-filled membrane pores, which decreases the mass-transfer resistances in the liquid phase. The fluctuations of transmembrane pressure are periodical, with the period of ca. 10sec, which is lower than the experimental gas-phase contact times (>18sec) and the period between sampling the gas phase composition (ca. 20min). A physical model of the periodic pressure fluctuations could be represented by the concept of an "effective" liquid film and an "effective" membrane thickness.

The amplitude of the pressure pulse defines two extreme situations: (1) at higher transmembrane pressure liquid is pushed into the membrane and the gas-liquid interface is then near the surface of the membrane; (2) at lower transmembrane pressure the gas-liquid interface is within the membrane. In the former situation the area of gas-liquid

mass transfer can be taken to be equal to the geometrical membrane area, rather than the total pore area. In the latter case the interface is formed by the liquid film and droplets trapped within the irregular and highly tortuous porous matrix of the membrane. This area can potentially be very high.

Perhaps the more important effect of the convective mass transfer within the liquid-filled porous membrane is that the volume of acid "in contact" with the gas phase is potentially larger than the total pore volume due to the continuous renewal of the liquid phase within the pores. It was shown in Chapter IV that the direct hydration of propene is a slow reaction which occurs predominantly in the bulk of the liquid acid. Therefore, for this reaction the "effective" volume of acid which is involved in the reaction due to the forced convection within the pores is of more importance than the "effective" area, which might be generated by the same process. In this model the area of gas-liquid mass transfer was varied over two orders of magnitude with no significant effect. Similarly, mass transfer coefficients were varied over an order of magnitude, without any effect.

Two fitting parameters were introduced in this model: (1) the volume of "well-mixed" liquid in contact with the gas phase and (2) the "effective" thickness of membrane filled with the stagnant liquid. The second parameter represents the residual diffusional mass transfer resistance in the membrane. Gas-phase resistance was ignored in the model. The schematic diagram of this model is shown in Figure VII-10. The liquid-liquid interface shown in the figure represents the interface between the well-mixed volume of acid and the film of stagnant liquid. It is assumed that the liquid film (II) is well mixed, thus avoiding the introduction of a diffusion equation. Liquid within the pores is assumed stagnant and the "effective" thickness of membrane is an adjustable parameter.

The two adjustable parameters were varied until a reasonable fit was found between the experimental results at the gas-phase contact time of 35 seconds and the model prediction. These parameters were then used to calculate the predicted reactor performance at contact times between 14 and 266 seconds as shown in Figure VII-11. It was found that the volume of the "well-mixed" liquid influences the maximum concentration of alcohol in the gas phase, whereas the "effective" membrane thickness controls the decline of concentration in time. By comparing the experimental and simulation results it is clear that the results at the contact times of 18 and 35 seconds are in reasonable agreement. At a contact time of 48 seconds the predicted values are slightly higher than the experimental values, falling on the predicted line for 22 seconds contact time. The experimental results obtained at the contact time of 262 seconds are too low.

Values of the volume of "well-mixed" liquid and the "effective" membrane thickness that were found to fit at least the short contact time experiments are $1.27 \times 10^{-6} m^3$ and 0.06mm. The total pore volume of the membranes used in this study is ca. $1.9 \times 10^{-7} m^3$, which means that the model requires the volume of liquid involved in the reaction to be almost an order of magnitude higher.
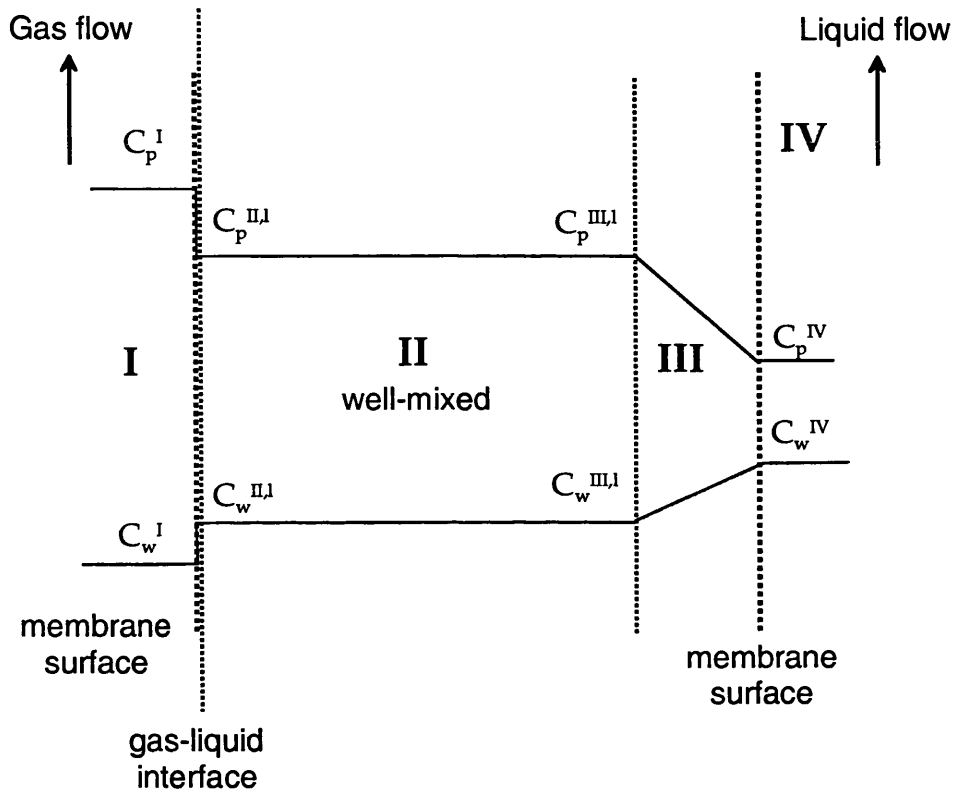

Figure VII-10. Schematic diagram of the reactor model.
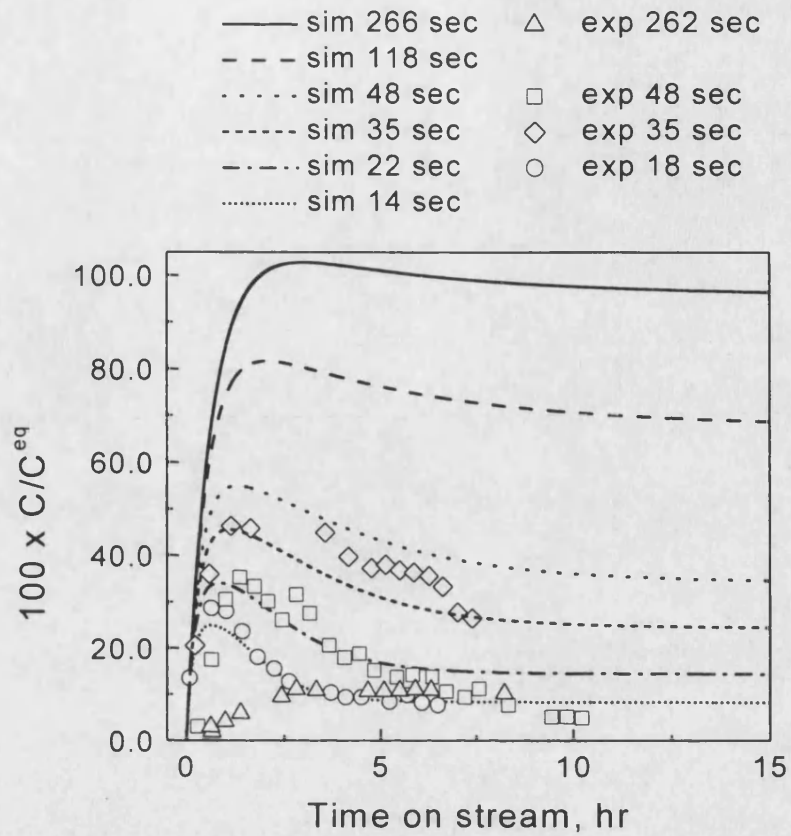No gas-phase resistance. Gas-liquid interface is an adjustable parameter.

Figure VII-11. Comparison of experimental results and simulation of the membrane reactor: vapour phase concentration of propan-2-ol vs. time-on-stream.
Reaction conditions: 2.1MPa, 130°C. Membrane porosity 13%. Pore diameter 0.75μm.

VIII.1. Membrane material and preparation

The only membrane material used in this study is synthetic porous carbon. Conventional packed-bed supported liquid phase (SLP) catalysts of hydration reactions are based on a phosphoric acid supported on either a natural inorganic high silica content material such as kieselgur or a synthetic aluminosilicate. These materials have a suitable pore structure and liquid loading characteristics. In the case of SLP catalysts, an appropriate support whould be wetted by acid and thus have weak chemical interaction between the support and acid because the active catalyst is free phosphoric acid. The liquid loading plays a very important role as it not only controls the amount of acid available for reaction but also the amount of free gas space available for diffusive and convective transport of reactants and products (see Figure VIII-1).

C_3H_6
C_3H_7OH
$C_6H_{14}O$
H_2O

diffusion   reaction

VLE ⇄

vapour phase   liquid phase

C_3H_6
H_2O
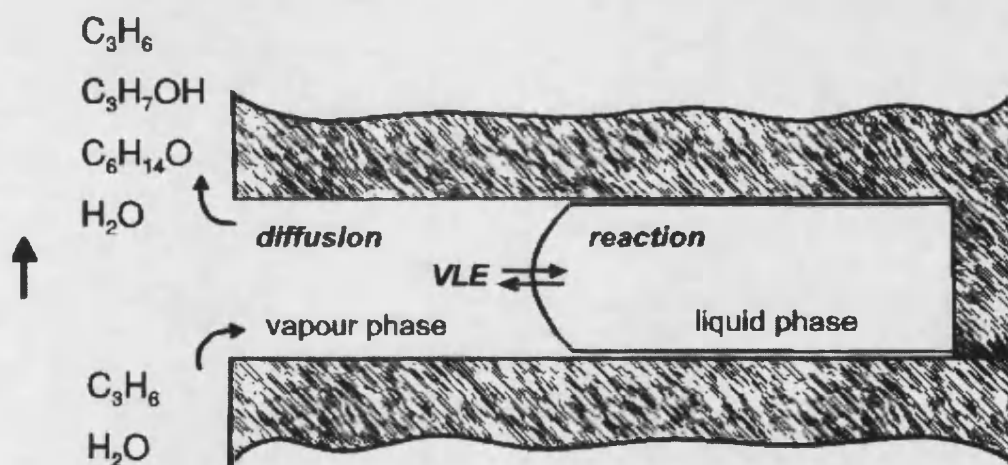
Figure VIII-1. Schematic representation of a single pore of an SLP hydration catalyst

In the case of a membrane phase contactor reactor, the amount of acid within pores is dictated by the transmembrane pressure applied and the physicochemical characteristics of the system, i.e. liquid-solid contact angle and gas-liquid interfacial tension. Thus, such reactors will have a greater potential for fine-tuning the position of the interface and therefore the amount of acid available for reaction and the amount of free gas space available for mass transfer.

Earlier works on gas-liquid membrane contactors have been concerned with atmospheric pressure applications or test reactions (see Chapter I), whereas in this study the typical reactor operating conditions are 2.0MPa pressure and 130°C temperature. One of the differences between atmospheric pressure experiments and elevated pressure experiments is that in the former, the position of the gas-liquid interface within a membrane is controlled chemically (i.e. in order to operate with the "dry" membrane, the membrane material should be non-wetted by the liquid phase) whereas in the latter (this work) the position of the interface is controlled primarily by the transmembrane pressure. Hence, it makes little difference if the membrane is hydrophilic or hydrophobic. Other important factors are the mechanical strength, porosity and the chemical stability of membranes.

Porous inorganic membranes can be available in many materials, alumina and silica being the most popular but zirconia, titania, porous steel, porous glass and carbon have also being reported in the open literature (see Chapter II). Among these materials synthetic porous carbon seems the most suitable. Carbon is stable in phosphoric acid solutions [84]. The particular synthetic carbon which has been used in this study is characterised by relatively high porosity (ca. 40%) bi-porous structure consisting of micro- and macropores and high chemical purity [121].

The results of membrane preparation and characterisation showed that (1) the membranes prepared using phenolic resin precursor particles with diameters less than 5μm, have very low porosity (ca. 12%), (2) the external surface of the membranes is hydrophilic, whereas the internal surface is hydrophobic and (3) the membranes have a bi-porous structure: a macropore structure of interstices, with mean pore diameter of ca. 0.5μm and pore volume of ca. $0.081cm^3/g$, and a developed micropore structure with a micropore volume of ca. $0.2cm^3/g$ and BET surface area of $492m^2/g$ (see Figure III-10).

The relatively low porosity of the prepared membranes may be explained by the deformation of resin particles during the hot pressing procedure. This hypothesis is supported by estimation of the carbonised particle sizes from measurements of the gas flux through the membranes and by SEM imaging.

As it was mentioned above, in the case of high operating pressure the surface chemistry of the phase contactor is of no significance as long as it does not interfere with the reaction. The membranes studied in this work exhibited the behaviour of a hydrophobic material, although the clean surface of the membranes was hydrophilic. It is reasonable to assume that due to the small pore sizes some residual organic material is left within the pores after carbonisation, which makes the internal surface of such

membranes hydrophobic. In practical terms it means that a higher liquid phase pressure would be required to push the gas-liquid interface into the membrane and closer to the gas-phase side of membrane.

This particular carbon material is by no means ideal for the fundamental study of a novel reactor. The pore size distribution and porosity varied significantly from one sample to another because each membrane was prepared individually. This makes any comparison between the individual catalytic experiments difficult. It is also difficult to assess the total gas-liquid interfacial area. Some idea about the gas-liquid interfacial area could have been obtained experimentally by measuring the rate and equilibrium of absorption of gases into liquids through a carbon membrane. However, the aim of this particular study was to evaluate the performance of the phase contactor in a high pressure homogeneous catalytic reaction and prove its feasibility. Detailed theoretical investigation of the coupling of reaction and mass transfer in the pores of an inorganic membrane was beyond the scope of this study.

VIII.2. An "ideal" membrane phase contactor behaviour

The two main differences between the contactor type reactor and the commercial reactor based on an SLP type catalyst are: (1) the gas and liquid phase reagents can be supplied to the reaction zone from the opposite sides of a membrane and (2) the position of the gas-liquid interface is controlled by transmembrane pressure (see Figure VIII-2).
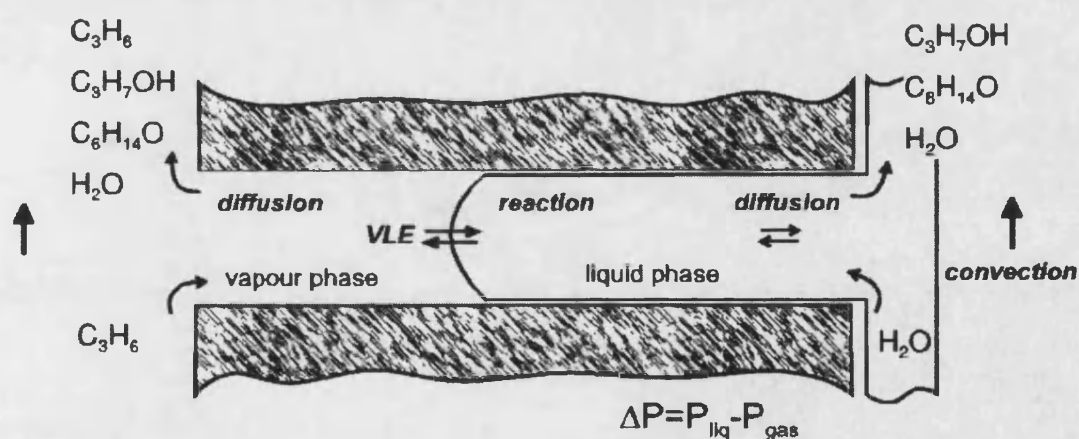

Figure VIII-2. Schematic representation of a single pore of a membrane contactor hydration catalyst

The two potential advantages of the membrane phase contactor, apart from its main function i.e. retention of the liquid phase catalyst, are an increase in the equilibrium conversion and an increase in the vapour phase concentration of the main product (with respect to water).

The former effect i.e. an increase in the equilibrium conversion follows simply from continuous removal of the main product of an equilibrium reaction. Using the model of an "ideal" membrane phase contactor (which ignores mass transfer resistance invoked by the membrane itself (see Figure VIII-3)) it is easy to show that there is an optimum gas phase residence time at which a considerable increase in the equilibrium conversion could be obtained (see Figure VIII-4).
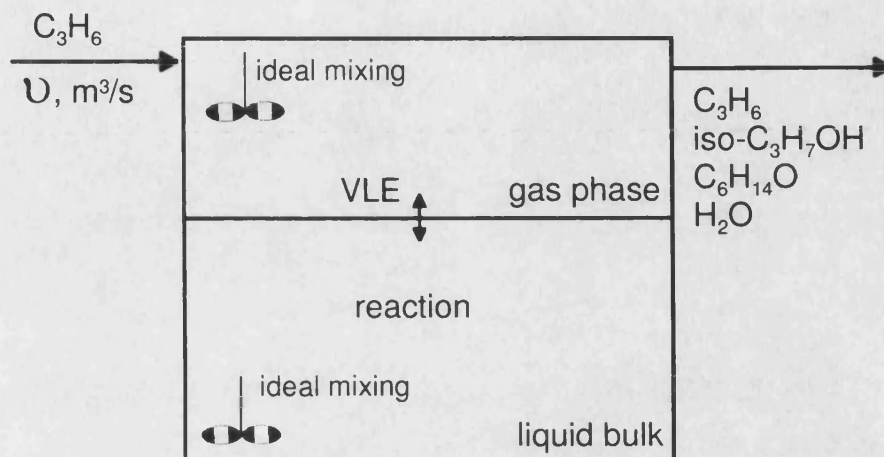

Figure VIII-3. Schematic diagram of the model of an "ideal" membrane reactor.
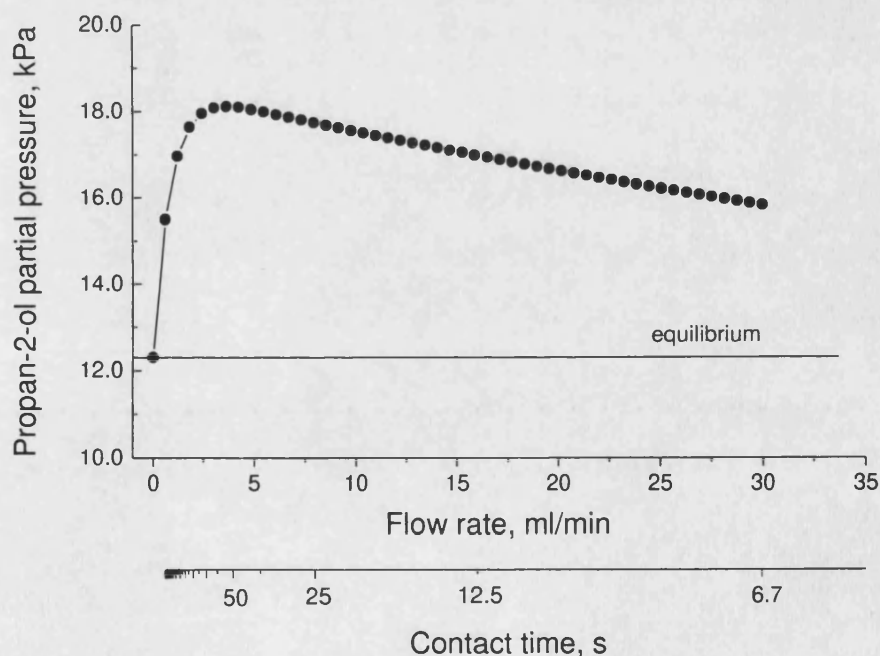

Figure VIII-4. Effect of the gas phase contact time on the partial pressure of propan-2-ol in the "ideal" membrane reactor.
Reaction conditions: reactor volume 350ml; liquid phase volume 200ml; temperature 126°C; propene pressure 2.1MPa; initial acid concentration 85.4wt%.

According to the simulation the behaviour of the propene "ideal" membrane reactor, a 47% increase in the equilibrium conversion can be achieved in comparison with batch operation at an optimum gas phase residence time (ca. 50sec). This is the sole effect of the removal of a product of reversible reaction. The exact value of the optimum flow rate/contact time depends upon the volume of the liquid phase.

The dynamic behaviour of an "ideal" phase contactor reactor is shown in Figure VIII-5. A slow decrease in the vapour phase concentration (solid lines) is due to a continuous decrease in the water content within the reactor by evaporation and reaction. Addition of water either to the vapour or liquid feed overcomes this decrease in the propan-2-ol yield (see dotted lines in Figure VIII-5).
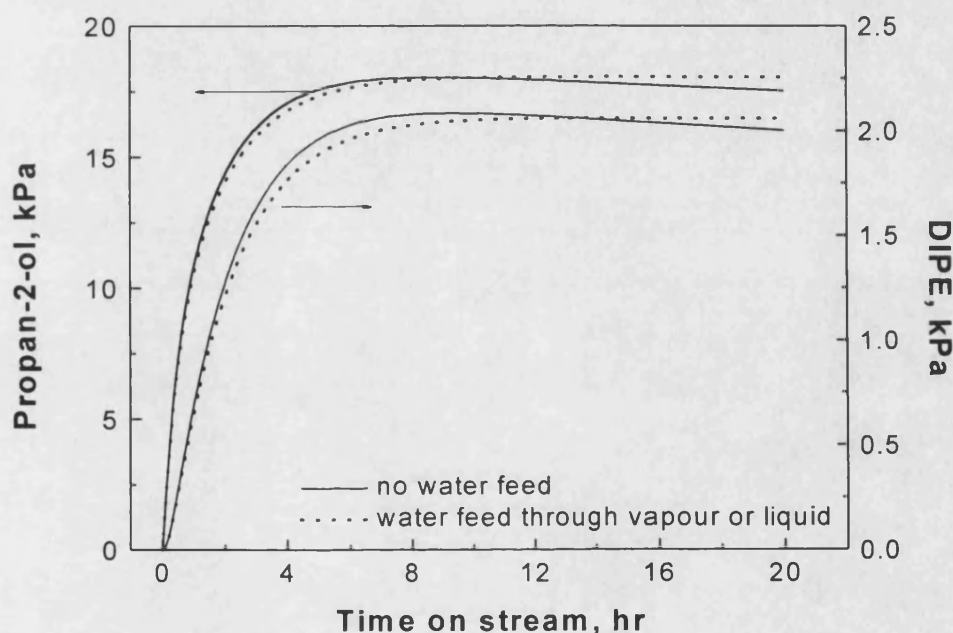
Figure VIII-5. Dynamic behaviour of an ideal phase contactor reactor.
Reaction conditions as described in caption to Figure IV-3. Gas phase flow rate 5ml/min. Dotted line: water in the vapour or liquid feed streams.

The advantage of a liquid phase water feed is that it does not affect the composition of the vapour phase and therefore does not require an increase in total pressure. This is illustrated in Figure VIII-6. At constant total pressure, an increase in the steam feed ratio results in a continuous decrease in the propene partial pressure and consequently propene concentration in the liquid phase and therefore the amount of alcohol produced. If the partial pressure of propene is kept constant as steam pressure is increased, then the corresponding curves for the vapour pressure of propan-2-ol for the cases of the liquid

water and steam feed coincide, whereas the concentration of alcohol in the vapour stream is higher in the case of the liquid phase water feed (Figure VIII-7).

Figure VIII-6. Effect of water feed on the propan-2-ol partial pressure and concentration in the vapour phase at constant pressure.
Reaction conditions: 2.1MPa, 126°C, 20ml/min vapour phase flow rate.

Thus, in the ideal case, when resistance to mass transfer is absent, the membrane phase contactor shows a higher performance than the packed-bed reactor due to an increase in the vapour phase concentration of the main product at the same partial pressure.
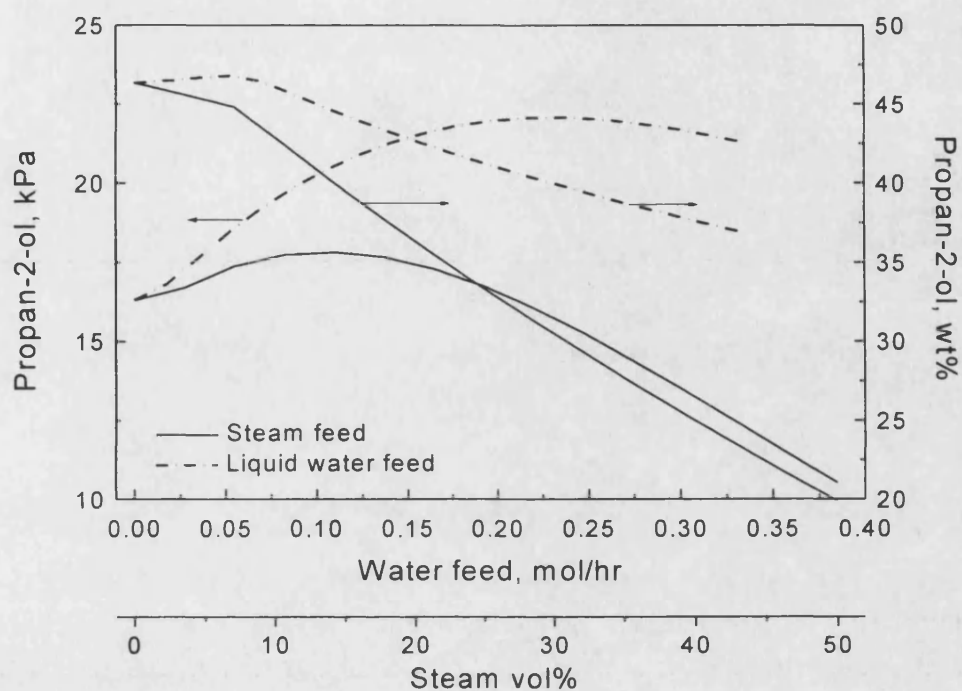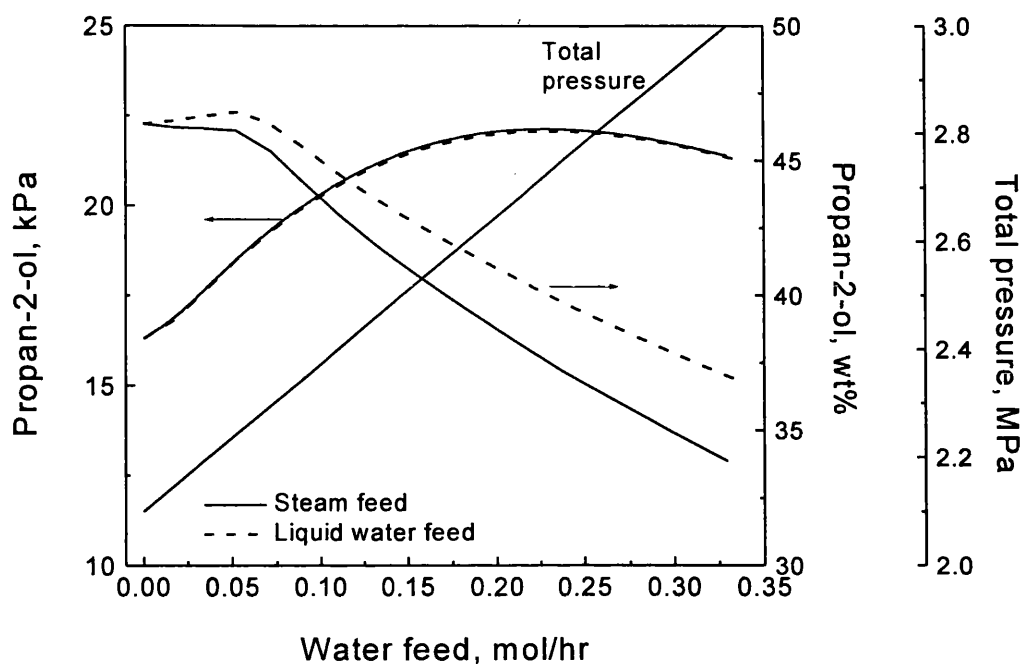
Figure VIII-7. Effect of water feed on the propan-2-ol partial pressure and concentration in the vapour phase at constant partial pressure of propene.

VIII.2.1. Performance of the membrane phase contactor

The experiments performed in the membrane contactor reactor using the prepared carbon membranes with an average macropore diameter of about 0.5μm and porosity of about 12% are described in Chapter VI. The most important result of this study is the fact that such a reactor can be operated at high pressure and temperature with reasonable stability and yield of the main product. This proves the practical feasibility of the reactor concept. The observed yield of propan-2-ol is comparable with that reported for competing technology – phosphoric acid based supported liquid phase (SLP) catalyst. The comparison was made between the yields expressed in terms of kg(alcohol) per m^3(acid) per hour and the volume of acid was taken to be equal to the total pore volume. The second important result is the high concentration of alcohol in the vapour stream. This result was predicted using the model of an "ideal" membrane reactor described in the previous section.

However, behaviour of the experimental membrane reactor is rather different from that predicted by the model of "ideal" membrane reactor. Concentration of alcohol in the vapour phase does not reach equilibrium values (apart from one experiment considered to

be erroneous), which indicates a considerable mass transfer resistance due to the membrane. Furthermore, the shape of the plots of the vapour phase concentration of propan-2-ol vs. time on stream predicted by model of the "ideal" membrane reactor (Figure VIII-5) and those obtained experimentally (Figure VI-1 to VI-3) differ significantly. In the case of the experimental membrane reactor the initial increase in the vapour phase concentration is followed by a maximum and subsequent rapid decrease leading to a slower decrease (almost plateau) in concentration of product. In the case of the "ideal" reactor the simulation does not predict a rapid decrease in concentration. Simulations of the membrane reactor using the mass transfer model showed that similar behaviour can be obtained, when significant diffusional mass transfer resistance is introduced (Figure VII-6). Furthermore, this could only be obtained if the tortuosity factor is introduced, thus increasing the diffusional resistance. It is therefore reasonable to assume that in the experimental reactor the observed decrease in the vapour phase concentration of propan-2-ol is due to the decrease in the water concentration in the liquid phase near the membrane. Mass transfer resistance in the liquid phase is responsible for the extremum behaviour of the vapour phase concentration of alcohol and slow establishment of the steady state.

Other factors that may affect the performance of the membrane contactor reactor: (1) curvature of gas-liquid interface influences the area of contact and vapour pressure; (2) formation of long-chain by-products may affect the surface wetting characteristics and decrease the pore volume. Evidence to support the effect of long-chain by-products was obtained experimentally: the yield of propan-2-ol was always lower for the second and further experiments performed with the same membrane sample. The extent of this effect was not possible to analyse accurately due to large discrepancies in the experimental data and the difference in the pore structure of the individual membrane samples.

Simulation of the membrane reactor was performed using the model based upon empirical kinetics and simplifying assumptions of ideal gas and liquid behaviour. This model fits the experiments at short contact times reasonably well, i.e. when the assumption of zero gas-phase resistance is justified by high gas flow rate. At longer contact times (low flow rates) the model overestimates the vapour phase composition in the reactor. This is attributed to a laminar gas film at the surface of the membrane.

A physical model, considering diffusion and reaction in the stagnant liquid within the membrane pores can not adequately describe the experimental data: the predicted values of the gas-phase concentration of propan-2-ol were considerably lower than those observed experimentally. At the same time the shape of the profile of concentration vs.

time-on-stream was similar to the experimental. This indicates that the volume of liquid involved in the reaction (which in this model was taken to be equal to the total pore volume) is underestimated. A new model was devised (Chapter VII.2.2) which included two adjustable parameters: the volume of "well-mixed" liquid in contact with the gas phase and the "effective" membrane thickness. Periodical fluctuations of the transmembrane pressure provide effective mixing of liquid within membrane pores and involve a larger volume of liquid than the total pore volume. There is a residual diffusional resistance which, for simplicity, is described as a thin layer of stagnant liquid. Such a model predicted a similar level of the gas-phase concentrations observed experimentally as wells as a characteristic decrease of the concentrations in time.

If the hypothesis described above is correct, this implies that the real performance of the membrane contactor reactor in the case of the direct hydration of propene, i.e. in the absence of periodic pressure fluctuations, is considerably lower and this reactor would not compete with any commercial reactor based on SLP catalysts. This is because of the high mass transfer resistance in the liquid phase and slow reaction kinetics.

One situation which has not yet been discussed is when the membrane is "dry", i.e. the gas-liquid interface is on the liquid side of the membrane. In this case the whole volume of liquid is involved in the reaction and mass transfer resistance is only due to gaseous transport in the porous membrane. The membranes used in this work are characterised by low porosity (ca. 13%) and high tortuosity. Tortuosity was estimated to be ca. 12 (Chapter III.2), which is likely to be an overestimation. Simulation of the membrane reactor performance in this case was done assuming that a thin (1mm) homogeneous membrane with 40% porosity was used. Simulation was performed assuming two gas-phase contact times. The result is shown in Figure VIII-8. The two top lines represent gas-phase concentration of propan-2-ol near the gas-liquid interface, whereas the two bottom curves represent the gas-phase concentration in the gaseous chamber above membrane (note that ideal mixing is assumed in the gas phase). In the case of a shorter contact time the reaction equilibrium is shifted towards the main product. The difference between the concentration of propan-2-ol above membrane and that near the gas-liquid interface is due to the diffusional mass transfer resistance within the membrane and the continuous removal of the product from the gaseous chamber. This result indicates that the gas-phase resistance in the membrane is significant. For the case of the contact time of 35sec the flux of propan-2-ol can be estimated as follows:

$$J_{propan-2-ol} = A \frac{D_{ap}}{\tau d} \left(C^i - C^g \right),$$ where A is the area of mass transfer (approximated

by the total crossectional pore area), D_{ap} is the diffusion coefficient of propan-2-ol in propene, τ is the tortuosity factor, d is membrane thickness, C^i is the concentration near the gas-liquid interface and C^g is the concentration in the gaseous chamber above membrane. Using the numerical data the flux of propan-2-ol across the membrane is

$$J_{propan-2-ol} \approx 6 \times 10^{-8} \frac{mol}{s} .$$

The reaction rate or yield of propan-2-ol may be estimated if the volume of acid is known. If the volume of acid is equal to the minimum volume estimated in the second reactor model (p.114), then the yield of propan-2-ol using the flux just calculated would be only ca. $10 \frac{kg}{m^3 hr}$. This is much lower than the yield of industrial hydration process and lower than the experimentally measured yield of fully wetted membrane reactor. This suggests that the way of improving the performance of the membrane contactor reactor is via reducing the gas-phase mass transfer resistance in the membrane by improving the membrane pore structure. A totally non-wetting membrane with an asymmetric porous structure would potentially give a much better overall performance.
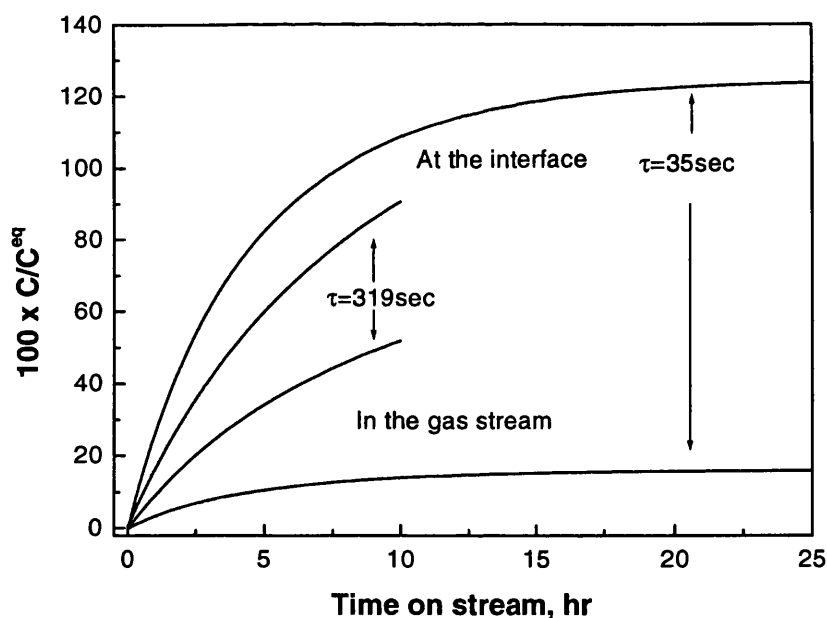

Figure VIII-8. Simulation of the membrane contactor reactor: gas-filled membrane. Vapour phase concentration of propan-2-ol vs. time-on-stream. Reaction conditions: 130°C, P=2.1MPa. Gas phase contact time=35sec. Membrane thickness 1mm. Membrane porosity 40%.

The aim of this work was to establish the feasibility of the application of a porous inorganic membrane contactor reactor for gas-liquid homogeneous catalytic reactions. Prior to this work it was suggested that the membrane contactor reactor should have three major benefits: (1) fixation of the gas-liquid interface (i.e. effective retention of the homogeneous liquid catalyst and prevention of acid leaching characteristic to the SLP catalysts), (2) a decrease in the vapour phase concentration of water (i.e. an increase in the concentration of the condensed alcohol) and (3) a shift in reaction equilibrium.

This study showed that stable operation of a membrane contactor reactor at elevated pressures can be achieved by (a) adjusting the pore structure of the membranes; (b) providing an accurate pressure measurement and control system. There is a direct link between the pore size, yield from the reactor and the required accuracy of pressure measurement and control. An increase in the pore size results in a decrease in the mass-transfer resistance in the membrane (and therefore an increase in the yield from the reactor), but requires more accurate control of pressure. Conversely, a decrease in the pore size results in an increase in the mass transfer resistance (and therefore a decrease in the yield from the reactor) but requires less accurate control of pressure. Thus, adjusting the pore structure of membranes allows one to optimise the yield from the reactor at an achievable controllability of pressure, and provides a complete retention of the homogeneous catalyst.

Decrease in the vapour concentration of water is a result of the introduction of the separate feed of reagents: olefin is fed as a gas, whilst water is fed via the liquid phase. This effect is only possible in the case of membrane reactors for gas-liquid reactions. This has been observed experimentally and was also predicted via mathematical modelling of the membrane reactor.

A shift in reaction equilibrium due to the continuous removal of reaction products was predicted by the model of the reactor disregarding resistances to mass-transfer invoked by the membrane. Experimental study and the results of mathematical modelling indicate that in the case of slow reactions (i.e. when reaction occurs predominantly in the bulk of the liquid phase), thin non-wetted membranes with an asymmetric pore structures

may potentially have a sufficiently low mass-transfer resistance to effect a shift in reaction equilibrium.

Recommendations for further study:

(1) Availability of inorganic membranes with the required pore structure is a common problem of many membrane processes. Further research in the development of membrane materials is required. In the case of NOVOCARB™ membranes, the membrane formation process should be improved in order to retain maximum porosity of the fabricated membranes. Research in formation of asymmetric pore structure has recently been started at MAST Carbons, but it requires more effort as the potential of asymmetric membranes is much greater than membranes with a homogeneous pore structure.

(2) NOVOCARB™ membranes possess a bi-porous structure, consisting of macro- and micropores. The effect of micropores on the reaction that occurs within a liquid filled membrane is an interesting scientific problem. Investigation of adsorption of reagents and products onto porous carbon and effective diffusivities of these molecules in the micropores is required, as well as more detailed modelling of the physical processes occurring in this system.

(3) In order to describe the physical processes occurring in a membrane contactor during reaction more accurately (e.g. effect of pore geometry, mass transfer effects, effect of position of the gas-liquid interface etc), a model system should be developed. Such a system should employ a simple reaction with the well-known kinetics and an analysis of composition in both phases. Membranes with a well-defined geometric porous structure would also be advantageous for such a model. Several materials could be used for such a study: anodised alumina membranes (Whatman), track-etched membranes and multichannel glass plates, normally used in optics. The latter material is of particular interest because it can be produced with a range of pore sizes and two distinctive pore geometries: straight channels and random packing of microspheres. Its only disadvantage is cost: up to £1000 per sample (Photonics, France).

(4) Application of surfactants to increase the solubility of gases in gas-liquid catalytic reactions also requires further investigation.

1. G.K.Boreskov, "Catalysis", Transactions of Institute of Catalysis, Nauka Pub., Novosibirsk, USSR, 1971 (Russian).

2. "Applied homogeneous catalysis with organometallic compounds", B.Cornils, W.A.Herrmann Ed., Wiley-VCH, 2000.

3. M.R.Cramarossa et al, Reactivity of transition-metal-modified, Keggin-type heteropolycomplexes in the homogeneous oxidation of cyclohexane and adamantane, *J.Mol.Cat. A: Chemical, 127 (1997) 85-94.*

4. J.N.Armor, Striving for catalytically green processes in the 21st century, *Appl.Cat.A:General, 189 (1999) 153-162.*

5. (a) Keurentjes J.T.F., Jansen G.H.R., Gorissen J., The esterification of tartaric acid with ethanol. Kinetics and shifting the equilibrium by means of pervaporation, *Chem.Eng.Sci., 49 (1994) 4681-4689.* (b) L.Bagnell et al, The use of catalytically active pervaporation membranes in esterification reaction to simultaneously increase product yield, membrane permselectivity and flux, *J.Membr.Sci., 85 (1993) 291-299.*

6. (a) W.Pronk et al, The hydrolysis of triglycerides by immobilised lipase in a hydrophilic membrane reactor, *Biotechn. Bioeng., 32 (1988) 512.* (b) M.Rucka, B.Turkewitcz, Hydrolysis of sunflower oil by means of hydrophobic membrane with lipolytic activity, *Biotechnol.Lett., 11 (1989) 167.*

7. Feldman J., Ovchin M., Membrane-supported rhodium hydroformylation catalysts, *J.Mol.Cat., 63 (1990) 213-221.*

8. (a) L.W.Gosser, W.H.Knoth, G.W.Parshall, Reverse osmosis in organometallic synthesis, *J.Am.Chem.Soc., 95 (1973) 3436-3437.* (b) L.W.Gosser, W.H.Knoth, G.W.Parshall, Reverse osmosis in homogeneous catalysis, *J.Mol.Cat., 2 (1977) 253-263.* (c) O.M.Ilinitch, Yu.S.Vetchinova, Membrane assisted liquid phase catalytic oxidation of sulfides, *J.Mol.Cat., 25 (1995) 423-428.*

9. K.Seelbach, U.Kragl, Nanofiltration membranes for cofactor retention in continuous enzymatic synthesis, *Enz.Microbial Techn., 20 (1997) 389-392.*

10. U.Kragl, Continuous asymmetric synthesis in a membrane reactor, *Angew.Chem.Int.,* *35 (1996) 642-644.*

11. D.E.Bergbreiter, Attach catalysts and reagents to polymers that dissolve... sometimes, *CHEMTECH (1987) 686-690.*

12. P.Plucinski, private communication

13. N.Yoshimura, M.Tamura, in "Successful design of catalyst", Y.Inui Ed., Elsevier, 1989, p.307-314.

14. B.Cornils, Exciting results from the field of homogenous two-phase catalysis, *Angew.Chem.Int.Ed.Engl., 34 (1995) 1575-1577.*

15. W.Leitner, "Homogeneous catalysis and catalysts recycling using supercritical carbon dioxide", presentation at the Conference on "Engineering Catalytic Chemistry", University of Duram, Stockton Campus, 17-19 July 2000.

16. A.Gabelman, S.-T. Hwang, Hollow fiber membrane contactors, *J.Membr.Sci., 159 (1999) 61-106.*

17. S.B.Iversen et al., Characterisation of microporous membranes for use in membrane contactors, *J.Membr.Sci., 130 (1997) 205-217.*

18. R.Prasad, K.K.Sirkar, Dispersion-free solvent extraction with microporous hollow-fiber modules, *AIChE J., 34 (1988) 177.*

19. R.-S.Juang, H.-C.Huang, Non-dispersive extraction separation of metals using hydrophilic microporous and cation exchange membranes, *J.Membr.Sci., 156 (1999) 179-186.*

20. S.Farrell, K.K.Sirkar, A reservoir-type controlled release device using aqueous-organic partitioning and a porous membrane, *J.Membr.Sci., 130 (1997) 265-274.*

21. E.L.Cussler, Hollow fibre contactors, in "Membrane processes in separation and purification", J.G.Crespo, K.W.Boddeker Eds., Kluwer Ac.Pub., Dordrecht, 1994, pp.375-394.

22. J.S.Kim, R.Datta, Supported liquid-phase catalytic membrane reactor-separator for homogeneous catalysis, *AIChE J., 37 (1991) 1657-1667.*

23. R.Krishna, S.T.Sie, Strategies for multiphase reactor selection, *Chem.Eng.Sci., 49:24A (1994) 4029-4065.*

24. S.Chen, H.Fan, Y.-K. Kao, A membrane reactor with two dispersion-free interfaces for homogeneous catalytic reactions, *Chem.Eng.J., 49 (1992) 35-43.*

25. T.J.Stanley, J.A.Quinn, Phase-transfer catalysis in a membrane reactor, *Chem.Eng.Sci., 42 (1987) 2313-2324.*

26. Mentioned without reference in V.Gryaznov, Membrane Catalysis, *Catalysis Today, 51 (1999) 391-395.*

27. J.W.Mellor, A comprehensive treatise on inorganic and theoretical chemistry, vol XV, pp. 616-625, Longmans Green & Co., 1936

28. K.Mohan, R.Govind, Analysis of equilibrium shift in isothermal reactors with a permselective walls, *AIChE Journal, 34:9 (1988) 1493-1503.*

29. A.B.Bindjouli et al, Numerical simulation of catalytic inert membrane reactor, *Comp.Chem.Engng, 18 (1994) S337-S341.*

30. See references in J.N.Armor, Catalysis with permselective inorganic membranes, *Appl.Cat., 49 (1989) 1-26.*

31. E.Kikuchi, Membrane reactor application to hydrogen production, *Catalysis Today, 56 (2000) 97-101.*

32. V.Gryaznov, Membrane Catalysis, *Catalysis Today, 51 (1999) 391-395.*

33. (a) G.Saracco, V.Specchia, Catalytic inorganic membrane reactors: present experience and future opportunities, *Cat.Rev.-Sci.Eng., 36:2 (1994) 305-384.* (b) G.Saracco et al, High-temperature membrane reactors: potential and problems, *Chem.Eng.Sci., 54 (1999) 1997-2017.* (c) J.Coronas, J.Santamaria, Catalytic reactors based on porous ceramic membranes, *Catalysis Today, 51 (1999) 377-389.* (d) J.Zaman, A.Chakma, Inorganic membrane reactors, *J.Membr.Sci., 92 (1994) 1-28.*

34. M.Liu et al., Composite mixed ionic-electronic conductors for oxygen separation and electrocatalysis, *US Patent 5,478,444 (1995).*

35. K.K.Sirkar, P.V.Shanbhag, A.S.Kovvali, Membrane in a reactor: a functional perspective, *Ind.Eng.Chem.Res., 38 (1999) 3715-3737.*

36. R.Vos, V.Hatziantoniou, N.-H.Schoon, The cross-flow catalyst reactor. An alternative for liquid-phase hydrogenations, *Chem.Eng.Sci., 37 (1982) 1719-1726.*

37. S.Wu, C.Bouchard, S.Kaliaguine, Zeolite containing catalytic membranes as interphase contactors, *Res.Chem.Intermed., 24 (1998) 273-289.*

38. A.A.Lapkin and O.M.Ilinitch, unpublished results.

39. G.Langhendries et al, Selective hydrocarbon oxidation using a liquid-phase catalytic membrane reactor, *Catalysis Today, 56 (2000) 131-135.*

40. K.Daub et al, Studies on the use of catalytic membranes for reduction of nitrate in drinking water, *Chem.Eng.Sci., 54 (1999) 1577-1582.*

41. P.Cini, M.P.Harold, Experimental study of the tubular multiphase catalyst, *AIChE J., 37 (1991) 997-1008.*

42. G.Strukul et al, Use of palladium based catalysts in the hydrogenation of nitrates in drinking water: from powders to membranes, *Catalysis Today 55 (2000) 139-149.*

43. O.M.Ilinitch et al, Catalytic membrane in reduction of aqueous nitrates: operational principles and catalytic performance, *Catalysis Today 56 (2000) 137-145.*

44. H.J.Sloot, G.F.Versteeg, W.P.M. van Swaaij, A non-permselective membrane reactor for chemical processes normally requiring strict stoichiometric feed rates of reactants, *Chem.Eng.Sci., 45 (1990) 2415-2421.*

45. O.M.Ilinitch, P.A.Simonov, F.P.Cuperus, Nanosize palladium loaded catalytic membranes: preparation characterisation and cis-trans selectivity in hydrogenation of sunflower oil, *Studies in Surface Science and Catalysis, 118 (1998) 55-61.*

46. A.P.Philipse et al, *Euroceramics, 3 (1989) 600.*

47. Y.Itaya et al, *Int.Chem.Eng., 32:1 (1992) 123.*

48. M.A.Anderson, W.A.Zeltner, C.M.Merritt, Green technology for the 21st century: ceramic membranes, *Mat.Res.Soc.Symp.Proc., 368 (1995) 377-387.*

49. Y.Owobi-Andely et al, Use of electrocatalytic membrane reactor for synthesis of sorbitol, *Catalysis Today, 56 (2000) 173-178.*

50. N.Itoh et al, Electrochemical coupling of benzene hydrogenation and water electrolysis, *Catalysis Today, 56 (2000) 307-314.*

51. Wiggers, A., Ann., 57 (1846) 247. (Reference from "Catalysis", Vol. VII, Ed. P.H.Emmett, Reinhold Pub.Corp., 1960.)

52. Butlerow and Gorianow, Ann., 169 (1873) 147. (Reference from "Catalysis", Vol. VII, Ed. P.H.Emmett, Reinhold Pub.Corp., 1960.)

53. T.C.Carle, D.M.Stewart, Synthetic ethanol production, *Chemistry and Industry, May 12, 1962 830.*

54. Cotelle, USP 41,685 (1861). (Reference from S.A.Miller, Ethylene and its industrial derivatives, Ernest Benn Limited, London, 1969, pp.710-712.)

55. Slade R.E., and ICI Ltd., British Patent 308,859 (1928). (Reference from "Catalysis", Vol. VII, Ed. P.H.Emmett, Reinhold Pub.Corp., 1960.)

56. R.W.Taft, The dependence of the rate of hydration of isobutene on the acidity function, Ho, and the mechanism for olefin hydration in aqueous acids, *J.Am.Chem.Soc., 74 (1952) 5372.*

57. V.J.Nowlan, T.T.Tidwell, Structural effects on the acid-catalyzed hydration of alkenes, *Acc.Chem.Res., 10 (1970) 252-258.*

58. L.F.Fieser, M.Fieser, "Advanced organic chemistry", Reinhold Pub.Co., 1961.

59. Chirkov, N.M., et al, Aspects of chemical kinetics and reactions, Izd. Akademii Nauk SSSR, 1954 (russian). (Чирков Н.М. Вопросы химической кинетики и реакционной способности, Изд. Академии Наук СССР, 1954).

60. B.T.Baliga, E.Whalley, Pressure effect and mechanism in the acid-catalyzed hydration of propylene and isobutylene, *Can.J.Chem., 42 (1964) 1019-1026.*

61. Taft R.W., et al, *J.Am.Chem.Soc., 77 (1955) 1584.*

62. Kazansky V.B., Senchenya I.N., On the real nature of aliphatic carbenium ions as active intermediates of homogeneous and heterogeneous acid catalysis, *J.Mol.Cat., 74 (1992) 257-266.*

63. Gel'bshtein, A.I., Bakshi, Yu.M., Temkin, M.I., Kinetics of vapour phase ethylene hydration over acidic phosphorous catalyst, *Doklady Akademii Nauk SSSR, 132(2) (1960) 384-387.*

64. L.Petrus, R.W.De Roo, E.J.Stamhuis, G.E.H.Joosten, Kinetics and equilibria of the hydration of propene over a strong acid ion-exchange resin as catalyst, *Chem.Eng.Sci., 39 (1984) 433-446.*

65. F.J.Sanders, B.F.Dodge, Catalytic vapour-phase hydration of ethylene, *Ind.Eng.Chem., 26:2 (1934) 208-214.*

66. C.S.Cope, B.F.Dodge, Equilibria in the hydration of ethylene at elevated pressures and temperatures, *AIChE J., 5:1 (1959) 10-16.*

67. C.S.Pope Equilibria in the hydration of propene and of butylenes, *J.Chem.Eng.Data 11 (1966) 379-383.*

68. A.Wyczesany, Nonstoichiometric algorithm of calculation of simultaneous chemical and phase equilibria. 2. High-pressure hydration of propene to 2-propanol, *Ind.Eng.Chem.Res., 33 (1994) 1971-1978.*

69. F.P.Heese, M.E.Dry, K.P.Moller, Single stage synthesis of diisopropyl ether – an alternative octane enhancer for lead-free petrol, *Catalysis Today 49 (1999) 327-335.*

70. Y.K.Kim, J.D.Hatfield, Kinetics and equilibrium data of the dehydration-hydration reaction between diacetone alcohol and mesityl oxide in phosphoric acid, *J.Chem.Eng.Data, 30 (1985) 149-153.*

71. J.R.Kaiser, H.Beuther, L.D.Moore, R.C.Odioso, Direct hydration of propylene over ion-exchange resins, *I&EC Prod.Res.Dev., 1:4 (1962) 296-302.*

72. F.J.Metzger, Manufacture of alcohols, *USP 2,021,564, 1932.*

73. W.H.Shiffler, M.M.Holm, L.F.Brooke, Catalytic hydration of olefins, *Ind.Eng.Chem., 31:9 (1939) 1099-1103.*

74. H.P.Rustamov, N.M.Chirkov, On the absorption of butylene in sulphuric acid, *Russian J.Phys.Chem., 30:2 (1956) 261-268.*

75. P.E.Burton, W.E.Wellman, Process for producing isopropyl alcohol and di-isopropyl ether, *USP 4,471,142, 1984.*

76. F.M.Majewski, L.F.Marek, Hydration of propylene under pressure, *Ind.Eng.Chem., 30:2 (1938) 203-210.*

77. M.A.Dalin, State of the art in production of unsaturated gaseous hydrocarbons and synthesis of ethyl alcohol by direct hydration of ethylene, *Khimicheskaya Nauka Promyshlennost', 1 (1956) 259-272 (in Russian).*

78. BP 1,049,043 (1964); USP 3,340,313 (1967); BP 1,126,206 (1965)

79. M.A.Dalin et al, Study of silicophosphates and their activity in the direct hydration of ethylene, *Khimicheskaya Promyshlennost, 4 (1978) 28-30 (in Russian).*

80. P.A.Obraztsov, V.S.Malinsky, Catalytic dehydration of aliphatic alcohols under homogeneous and heterogeneous conditions, *J.Mol.Cat., 55 (1989) 285-292.*

81. Y.Maki et al, Structures of H_3PO_4/SiO_2 catalysts and catalytic performance in the hydration of ethene, *Appl.Cat., A:Gen., 170 (1998) 269-275.*

82. C.M.Fougret, M.P.Atkins, W.F.Holderich, Influence of the carrier on the catalytic performance of impregnated phosphoric acid in the hydration of ethylene, *Appl.Cat. A: Gen., 181 (1999) 145-156.*

83. Malinsky, V.S., et al, Comparison of catalytic activity of phosphoric acid in aqueous solution and impregnated on porous support, *Kinetica i Kataliz, 28 (1987) 1233-1236 (in Russian).*

84. W.Ester, Process for the production of alcohols by catalytic hydration of olefins, *USP 3,232,997 (1966).*

85. Yusuke Izumi, Yuzo Kawasaki, Mitsuo Tani, Process for the preparation of alcohols, *USP 3,758,615 (1973).*

86. M.P.Atkins, Olefin hydration process, *USP 5,616,815 (1997).*

87. J.Muller, H.I.Waterman, *Brennstoff Chemie, 38 (1957) 357.*

88. Yusuke Izumi, Acid catalysis of heteropoly compounds for industrial organic reactions, *Memoirs of the School of Engineering, Nagoya University, 48:2 (1996) 194-234.*

89. G.I.Kapustin et al, *Kinet. Katal, 31 (1990) 1017 (in Russian).*

90. I.V.Kozhevnikov, Catalysis by heteropoly acids and multicomponent polyoxometalates in liquid-phase reactions, *Chem.Rev., 98 (1998) 171-198.*

91. M.Misono, M.Nojiri, Recent progress in catalytic technology in Japan, *Appl.Cat., 64 (1990) 1-30.*

92. T.Okuhara et al, A pronounced catalytic activity of an acidic cesium salt of 12-tungstophosphoric acid for ester decomposition in solid-liquid system, *Chem.Let., (1990) 1201-1202.*

93. Y.Izumi, K.Urabe, M.Onaka, "Zeolite, clay and heteropoly acid in organic reactions", Kodansha/VCH, Tokyo, 1992, p. 99.

94. I.V.Kozhevnikov, S.Ts.Khankhasaeva, S.M.Kulikov, *Kinet.Katal., 30 (1989) 50.*

95. R.C.Odioso, A.M.Henke, H.C.Stauffer, K.J.Frech, Direct hydration of olefins, *Ind.Eng.Chem., 53:3 (1961) 209-211.*

96. G.Olah, Hydration of propylene to isopropyl alcohol over solid superacidic perfluorinated sulfonic acid catalysts, *USP 4,861,923 (1989).*

97. K.Inoue, M.Iwasaki, N.Ueda, Process for catalytic hydration of olefins, *USP 5,608,123 (1997).*

98. C.V.Mace, C.F.Bonilla, The conversion of ethylene to ethanol, *Chem.Eng.Prog., 50:8 (1954) 385-395.*

99. O.D.Frampton, W.R.Birchall, Process for the hydration of olefins employing slurried catalyst, *USP 4,234,748 (1980).*

100. K.Eguchi, T.Tokiai, H.Arai, High pressure hydration of olefins over various proton-exchanged zeolites, *Appl.Cat., 34 (1987) 275-287.*

101. D.O.Marler, C.M.Sorensen, P.Varghese, Process for the hydration of olefins, *USP 4,967,020 (1990).*

102. S.H.Brown, J.C.Trewella, Gas phase process for the hydration of propylene, *USP 5,488,186 (1996).*

103. E.G.Latimer, Vapour-phase hydration of olefins to alcohols in series reactors with intermediate alcohol removal, *USP 4,956,506 (1990).*

104. R.Carls, G.Osterburg, M.Prezelj, W.Webers, Process for the production of isopropyl alcohol, *USP 4,760,203 (1988).*

105. S.A.Bezman, Diisopropyl ether hydration in isopropanol production, *USP 4,405,822 (1983).*

106. A.Sommer, W.Heitmann,R.Brcker, Method of preparing alcohols having two to four carbon atoms by catalytic hydration of olefins, *USP 4,351,970 (1982).*

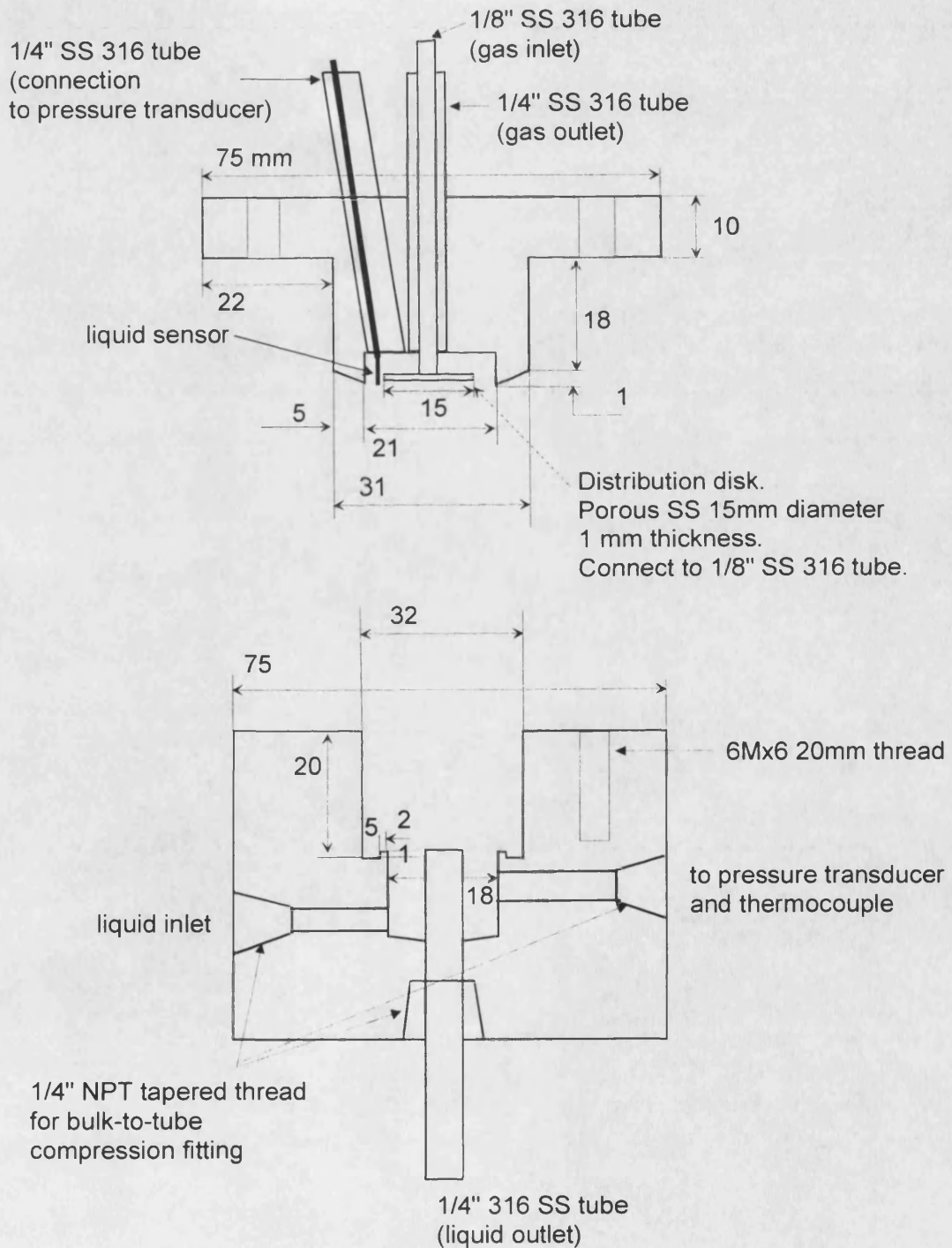107. D.G.Braithwaite, J.D.Pickle, Production of alcohols by hydration of olefins, *USP 4,424,388 (1984).*

108. S.Hirata, S.Ogawa, Process for producing isopropyl alcohol, *USP 5,763,693 (1998)*.

109. A.Sommer, M.Urban, Extractive distillation of isopropyl alcohol with an ether solvent recovered from the initial feed, *USP 3,955,939 (1976)*.

110. W.Webers, L.Sandhack, W.Neier, Process for the production of lower alcohols by direct catalytic hydration lower olefins, *USP 3,994,983 (1976)*.

111. R.J.Schmidt, Process for coproduction of isopropanol and tertiary butyl alcohol, *USP 4,484,013 (1984)*.

112. R.Ramachandran, Process for the production of ethanol and isopropanol, *USP 5,488,185 (1996)*.

113. T.L.Marker et al, Two-stage process for producing diisopropyl ether using catalytic distillation, *USP 5,744,645 (1998)*.

114. J.H.Beech et al., Di-isopropyl ether production, *USP 5,324,865 (1994)*.

115. M.N.Harandi, H.Owen, Two-stage process for production of diisopropyl ether, *USP 5,208,387 (1993)*.

116. W.K.Bell, S.H.Brown, J.C.Trewella, Multistage indirect propylene hydration process for the production of diisopropyl ether and isopropanol, *USP 5,569,789 (1996)*.

117. K.Schneider, W.Holz, R.Wollbeck, Membranes and modules for transmembrane distillation, *J.Membr.Sci., 39 (1988) 25-42*.

118. E.Jakobs, W.J.Koros, Ceramic membrane characterization via the bubble point technique, *J.Membr.Sci., 124 (1997) 149-159*.

119. K.W.Lawson, D.R.Lloyd, Membrane distillation, *J.Membr.Sci., 124 (1997) 1-25*.

120. R.B.Bird, W.E.Stewart, E.N.Lightfoot, "Transport phenomena", J.Wiley & Sons, 1960, pp.199.

121. S.R.Tennison, Phenolic resin derived activated carbons, *App.Cat.A –General, 173:2 (1998) 289-311*.

122. A.W.Adamson, "Physical Chemistry of Surfaces", 2nd Ed., Interscience Pub., 1960.

123. L.R.Radovic, Carbon materials in catalysis, *Chem.Phys.Carbon, 25 (1997) 243-358*.

124. C.N.Satterfield, "Mass Transfer in Heterogeneous Catalysis", M.I.T. Press, 1970.

125. S.Kim, PhD thesis, University of Bath, 2000.

126. S.J.Gregg, K.S.W.Sing, "Adsorption, surface area and porosity", Academic Press, London, 1982.

127. "Propylene and its industrial derivatives", E.G.Hancock Ed., Ernest Benn Ltd, 1973.

128. L.A.Zadeh, Fuzzy Sets, *Information and Control*, 8 (1965) 338-353.

129. S.Menzl, M.Stuhler, R.Benz, A self adaptive computer-based pH measurement and fuzzy-control system, *Water Research, 30:4 (1996) 981-991.*

130. S.Marsili-Libelli, A.Colzi, Fuzzy control of a transport/diffusion system, *Control Engineering Practice, 6 (1998) 707-713.*

131. Y.Yamashita, S.Matsumoto, M.Suzuki, Start-up of a catalytic reactor by fuzzy controller, *J.Chem.Eng.Japan, 21:3 (1988) 277-282.*

132. D.A.Linkens, S.Kandiah, Long-range predictive control using fuzzy process models, *Trans. IChemE, 74:A (1996) 77-88.*

133. J.J.Buckley, Applicability of the fuzzy controller, in "Between mind and computer: fuzzy science and engineering", Ed. P.-Z. Wang, K.-F.Loe, World Scientific Pub., 1993, pp. 47-54.

134. C.L.Karr, S.K.Sharma, W.J.Hatcher, T.R.Harper, Fuzzy control of an exothermic chemical reactor using generic algorithms, *Engng.Applic.Artif.Intell.*, 6 (1993) 575-582.

135. I.A.Ibragimov, I.R.Efindiev, V.T.Kopysitckii, Methods of optimisation of unsteady state reactors complexes in fuzzy environment, *Doklady Akademii Nauk SSSR, 317:3 (1991) 680-683 (in Russian).*

136. T.J.Ross, "Fuzzy logic with engineering applications", McGraw-Hill Inc., 1995.

137. P.R.Bevingston, D.K.Robinson, "Data reduction and error analysis for the physical sciences", 2nd edition, McGraw-Hill Inc, 1992.

138. T.W.G.Solomon, "Fundamentals of organic chemistry", 2nd ed., John Wiley & Sons, 1986

139. H.A.Cassar, Determination of isopropyl alcohol in presence of acetone and methylethylketone in presence of secondary butyl alcohol, *Ind.Eng.Chem., 19 (1927) 1061.*

140. Shmylyakovskii, *Khim.Tekhnol.Topliv i Masel, 4:12 (1959) 46 (in Russian).*

141. L.J.Bruce, A.J.Daugulis, Extractive fermentation by zymomonas mobilis and the use of solvent mixtures, *Biotech.Letters, 14:1 (1992) 71-76.*

142. Denzler, C.G., *J.Phys.Chem., 49 (1945) 358-365.*

143. Smith, A.S. *Ind.Eng.Chem., 42 (1950) 1206-1209.*

144. Vinnik M.I., Acidity function of aqueous solutions of strong acids, *Uspekhi Khimii 35 (1966) 1922-1952 (in Russian).*

145. C.C.Li, J.J.McKetta, *J.Chem.Eng.Data, 8:2 (1963) 271-275.*

146. "Kirk-Othmer Encyclopaedia of Chemical Technology", V18, p.674, 4th edition, Willey Interscience.

147. R.C.Reid, J.M.Prausnitz, B.E.Poling, "The properties of gases and liquids", 4th Edition, McGraw-Hill, 1987.

148. D.Ambrose et al, Thermodynamic properties of organic oxygen compounds. XLVII. Pressure, volume, temperature relations and thermodynamic properties of propane-2-ol, *J.Chem.Thermodynamics, 10 (1978) 1033-1043.*

149. J.M.Coulson, J.F.Richardson, "Chemical Engineering", Pergamon Press, 1979, Vol. 3, p. 80.

150. A.M.Shwartz, J.W.Perry, "Surface active agents", Interscience Publishers, vol 1, p.163, 1966.

151. A.D.King, Solubilisation of gases by polyethoxylated lauryl alcohols, *J.Col.Int.Sci., 148:1 (1992) 142-147.*

152. J.M.Prausnitz, "Molecular thermodynamics of fluid-phase equilibria", Prentice-Hall, Inc., 1969.

153. A.H.Harvey, J.M.Prausnitz, Thermodynamic of high-pressure aqueous systems containing gases and salts, *AIChE J., 35 (1989) 635-644.*

154. H.Lee, G.Thodos, Generalized treatment of self-diffusivity for the gaseous and liquid states of fluids, *Ind.Eng.Chem.Fundam., 22 (1983) 17-26.*

155. W.F.Ames, "Numerical methods for partial differential equations, Nelson, 1969.

Material of construction: stainless steel 316.

1/4" SS 316 tube
(connection
to pressure transducer)

1/8" SS 316 tube
(gas inlet)

1/4" SS 316 tube
(gas outlet)

75 mm

10

22

18

liquid sensor

5

15

1

21

31

Distribution disk.
Porous SS 15mm diameter
1 mm thickness.
Connect to 1/8" SS 316 tube.

32

75

20

6Mx6 20mm thread

5 2

1

18

to pressure transducer
and thermocouple

liquid inlet

1/4" NPT tapered thread
for bulk-to-tube
compression fitting

1/4" 316 SS tube
(liquid outlet)

Photograph of the experimental membrane contactor rig. External view and view of the heated cabinet
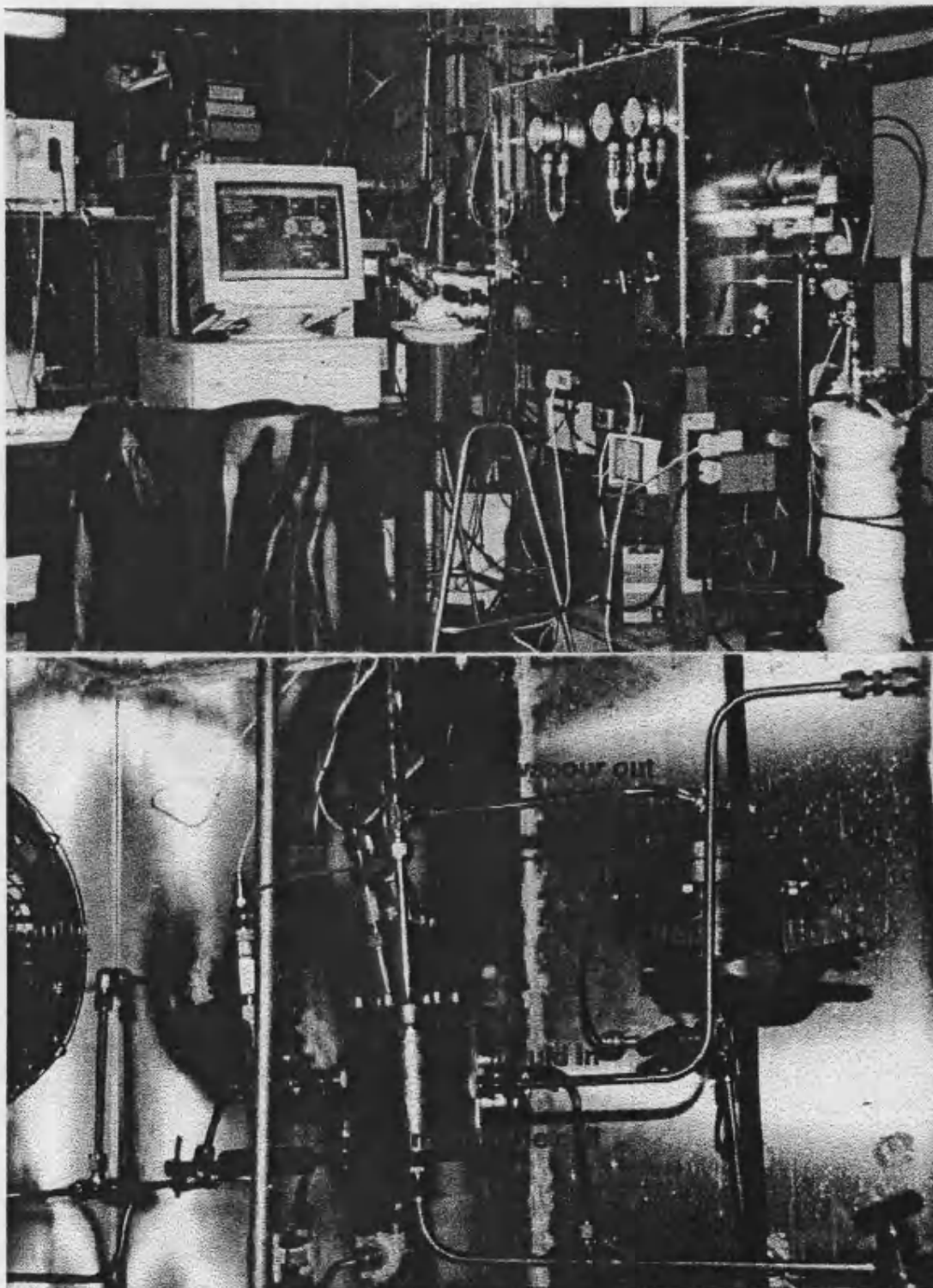
Appendix B. Design of Wicke-Kallenbach cell
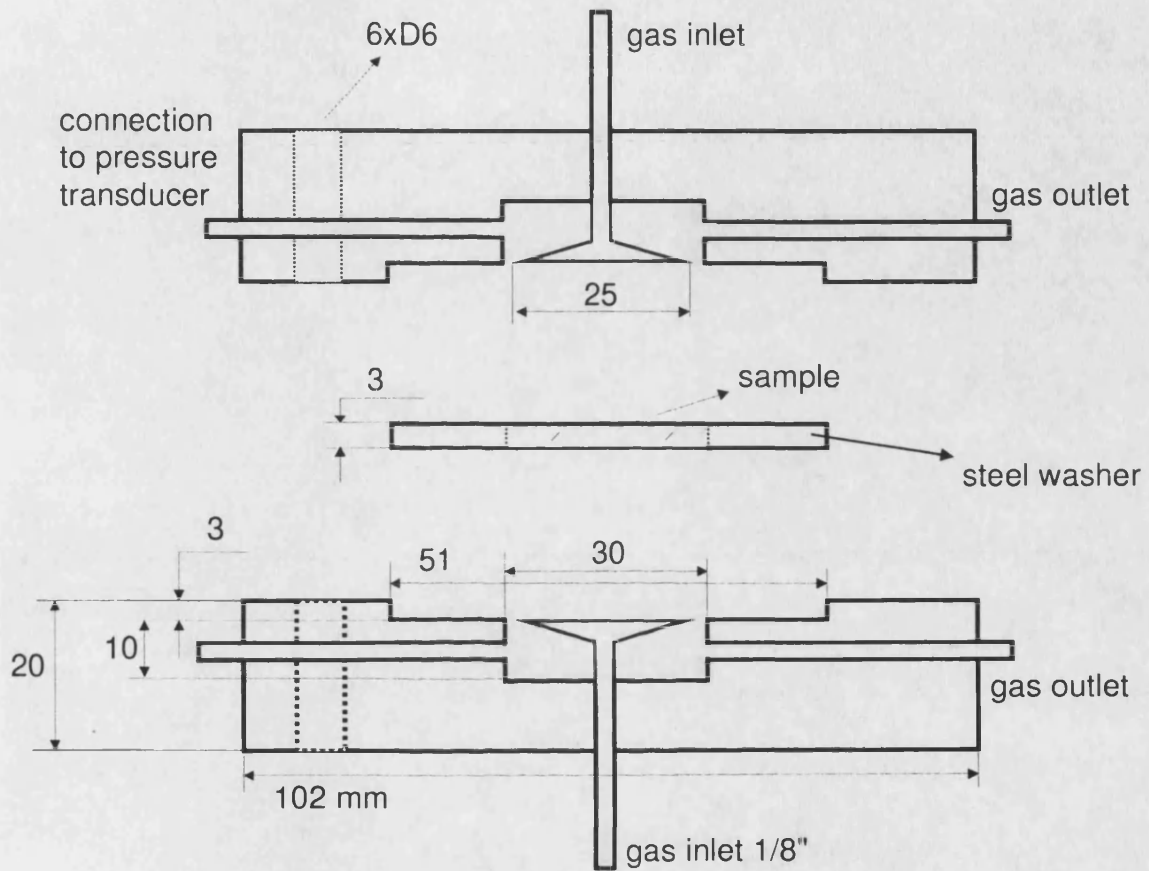
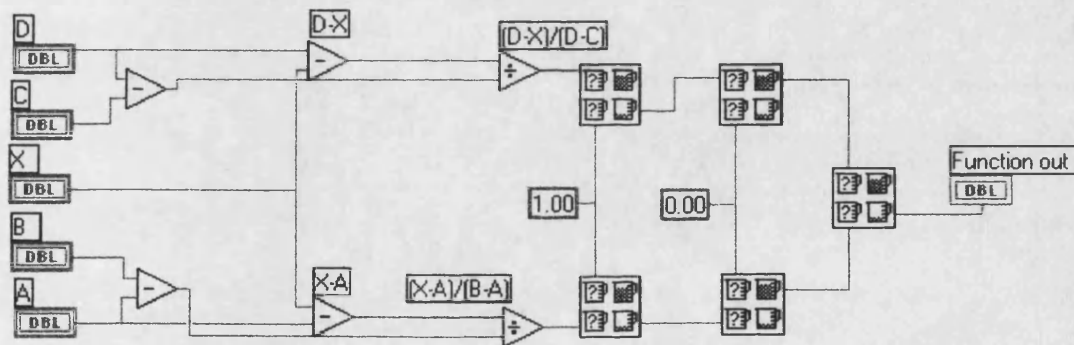Diagram of the asymmetrical triangular membership function subroutine
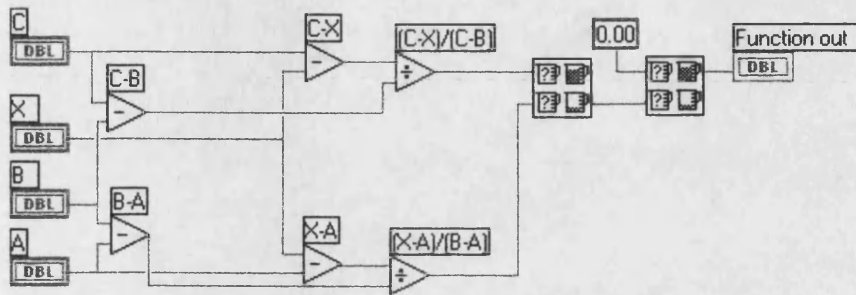
Diagram of the trapezoid membership function subroutine

Main Controls panel
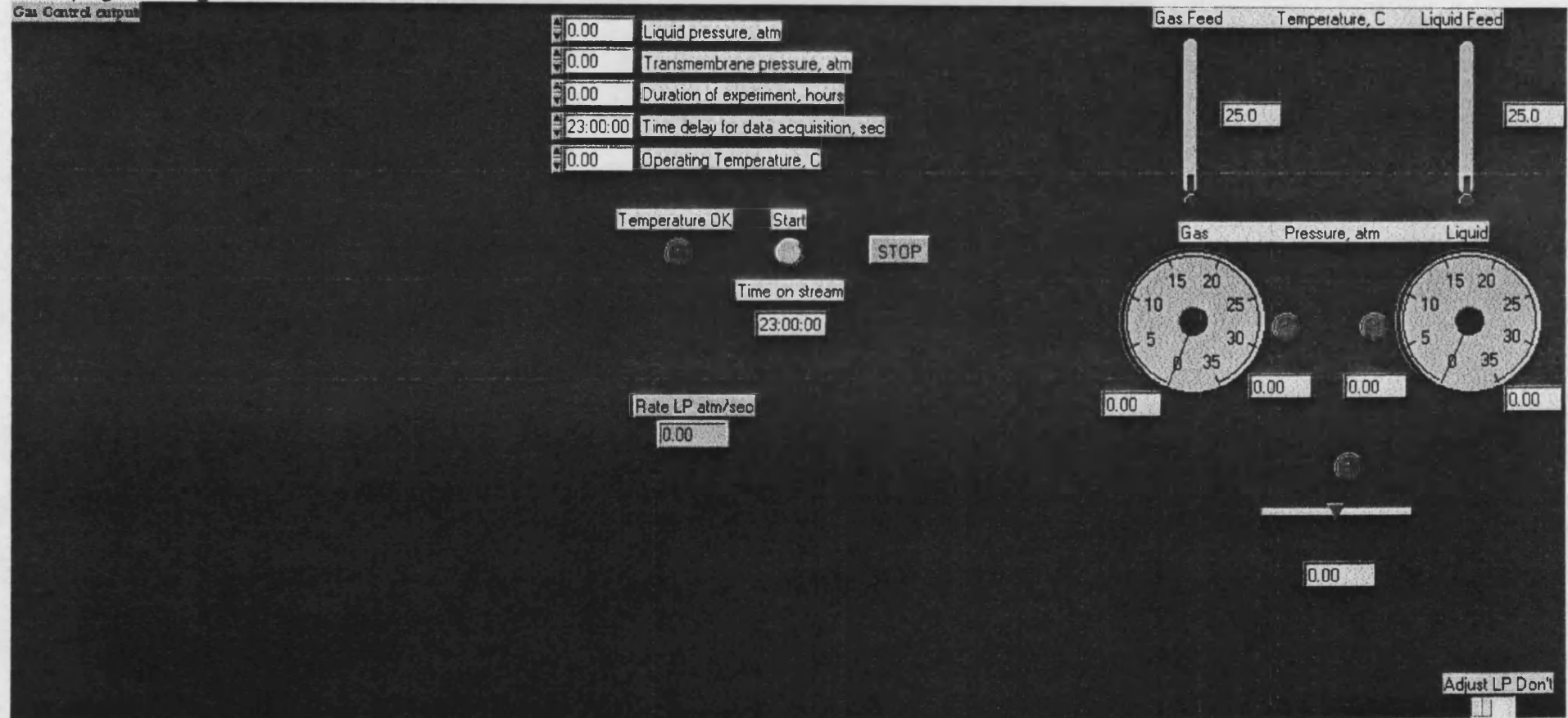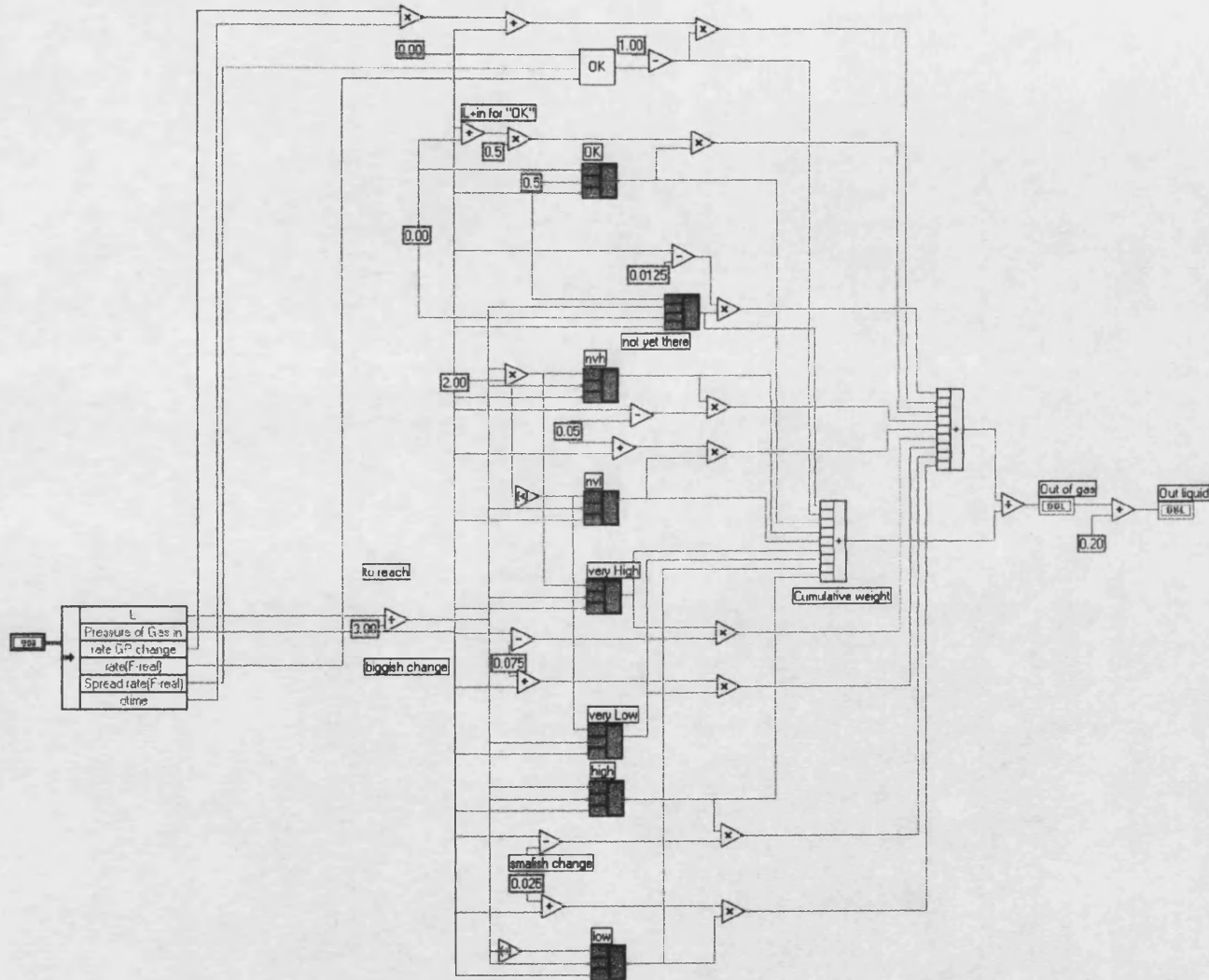
Next page – Diagram of the main module

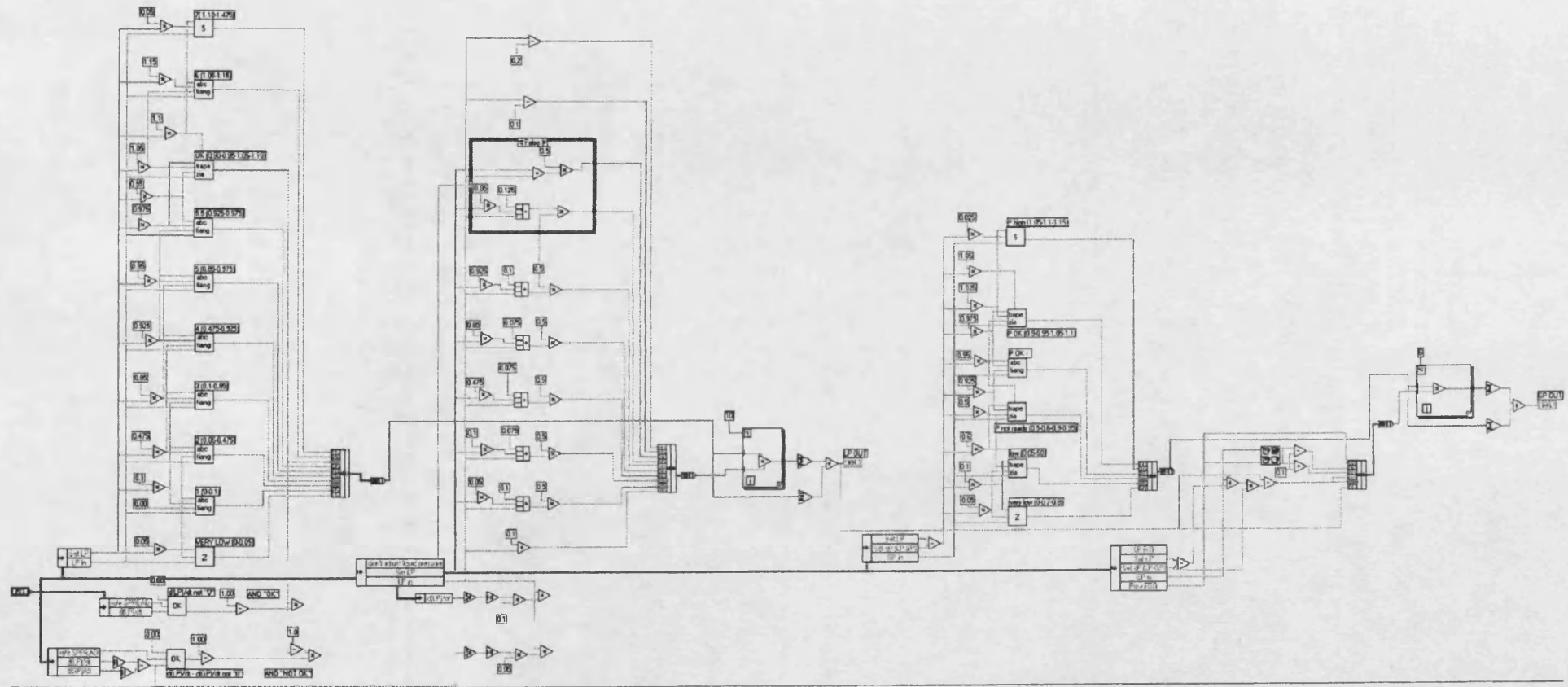# Diagram of the shut-down control module

Start-up and normal operation control module

The general condition of thermodynamic equilibrium in a closed system is the equality of chemical potentials of the components of a mixture in each phase $\mu_i^\alpha = \mu_i^\beta$. Therefore, the condition of equilibrium is the minimum of the total Gibbs energy of a system:

$$\min G = \min\left(\sum_i \sum_j n_{ij}\mu_{ij}\right),$$

Eq. D-1

where subscripts i,j refer to components and phases correspondigly.

Minimisation of the total Gibbs free energy is the general approach to calculation of thermodynamic equilibrium [1,2]. The expression of chemical potential will depend upon the complexity of the system of interest: whether it involves chemical reactions, contains supercritical components or electrolytes.

The system of interest in the present study contains one supercritical component (propene), polar compounds (water and 2-propanol), diisopropyl ether and medium strength electrolyte (concentrated phosphoric acid). Because of the complexity of the system, the presence of electrolytes is ignored in the first approximation of VLE.

Another constraint of the system is the presence of a supercritical component. It was shown in [2] that the presence of supercritical components makes it nearly impossible to use activity coefficient models. The activity coefficient of a component is determined in relation to its standard state, which is unknown in the case of supercritical components. Alternatively, chemical potential may be expressed in terms of fugacity coefficients [2]:

$$\mu_i = \mu_i^0 + RT\ln P + RT\ln n_i - RT\ln n_T + RT\ln\phi_i,$$

Eq. D-2

where P is total pressure; n_T is total number of mols; n_i is number of mols of i-th component.

Fugacity coefficient is defined as $f_i \equiv \phi_i \cdot P_i$ and does not require definition of a standard state. In the case of physical equilibrium, the condition of equilibrium may be written as equality of fugacities of a component in each phase:

$$\phi_{ij} \cdot P_i = \phi_{ik} \cdot P_i \quad \text{or} \quad \phi_{ij} \cdot x_i = \phi_{ik} \cdot y_i$$

Eq. D-3

where P_i is partial pressure of i-th component and x_i, y_i are mole fractions.

In order to calculate the fugacity coefficients the Peng-Robinson-Stryjec-Vera equation of state was used [3]. It has previously been successfully applied to a model mixture containing propene, propane, water and 2-propanol [4]. The EOS, mixing rules and fugacity coefficient calculation formula are given below:

$$P = \frac{RT}{v-b} - \frac{a}{v^2 + 2bv - b^2}$$

$$a_i = (0.477235 R^2 T_{ci}{}^2 / P_{ci})\alpha_i$$

$$\alpha_i = \left[1 + k_i\left(1 - \sqrt{T_{Ri}}\right)\right]^2$$

$$k_i = k_{i0} + k_{i1}\left(1 + \sqrt{T_{Ri}}\right)\left(0.7 - T_{Ri}\right)$$

$$k_{0i} = 0.378893 + 1.4897153\omega_i - 0.17131848\omega_i^2 + 0.0196554\omega_i^3$$

$$b_i = 0.077796 R T_{ci} / P_{ci}$$

$$a_{mix} = x_1^2 a_1 + x_2^2 a_2 + 2x_1 x_2 \sqrt{a_1 a_2}\left(1 - x_1 k_{12} - x_2 k_{21}\right)$$

$$b_{mix} = x_1 b_1 + x_2 b_2$$

$$\ln\phi_i = \frac{b_i}{b_{mix}}(Z-1) - \ln(Z-B) - \frac{A}{2\sqrt{2}B}\left(\frac{\bar{a}_i}{a_{mix}} + 1 - \frac{b_i}{b_{mix}}\right)\ln\left(\frac{Z + \left(1 + \sqrt{2}\right)B}{Z + \left(1 - \sqrt{2}\right)B}\right)$$

$$A = a_{mix}\frac{P}{(RT)^2} \qquad B = b_{mix}\frac{P}{RT}$$

$$\bar{a}_i = 2\sum_j x_j a_{ij} - a_{mix} + 2\sum_{j \neq i} x_i x_j \sqrt{a_i a_j}\left(x_i k_{ij} + x_j k_{ji} - k_{ij}\right) +$$

$$+ 2\sum_{j \neq i} \sum_{m > j} x_j x_m \sqrt{a_j a_m}\left(x_j k_{jm} + x_m k_{mj}\right)$$

$$Z^3 - (1-B)Z^2 + \left(A - 2B - 3B^2\right)Z - AB + B^2 + B^3 = 0$$

It was demonstrated in [4], that PRSV EOS adequately describes simultaneous chemical and vapour-liquid equilibrium in the mixture modelling the propene hydration reaction mixture. In the present study only physical equilibrium needs to be calculated. Diisopropyl ether should be included in calculation, being the main and inevitable side product. It is therefore necessary to obtain binary interaction parameters k_{ij} and k_{ji} for pairs of components containing ether. At the same time the binary coefficients reported in [4] should be evaluated. Binary coefficients are given in the Table D-1 and Table D-2.

Following [4] the temperature dependent binary coefficients are used in this study:

$$k_{ij} = k_{ij}^1 + k_{ij}^2 / T, \qquad k_{ji} = k_{ji}^1 + k_{ji}^2 / T$$

Table D-1. Binary coefficients given in [4]

Components	Δy^*	k_{ij}^1	k_{ij}^2	k_{ji}^1	k_{ji}^2
$C_3H_6 - H_2O$	0.024	-0.4337	243.4	0.4192	-190.5
$C_3H_6 - C_3H_7OH$	0.0007	0.1552	-37.52	0.1630	-39.60
$C_3H_7OH - H_2O$	0.009	0.2291	-128.7	-0.07513	-36.72

Table D-2. Binary coefficients obtained in this work

Components	Δx^*	Δy^*	k_{ij}^1	k_{ij}^2	k_{ji}^1	k_{ji}^2
$C_3H_6 - H_2O$	0.00005	0.006	-0.222437	284.486	0.416899	-190.793
$C_3H_6 - C_6H_{14}O$	0.007	0.017	1.196	-377.184	-0.085037	20.472
$C_3H_6 - C_3H_7OH$	0.013	0.050	0.642807	-30.85	0.130932	-66.713
$C_3H_7OH - H_2O$	0.018	0.012	0.00460	-35.826	-0.089274	-30.522
$C_6H_{14}O - H_2O$	0.027	0.077	-0.055614	-366.407	0.408983	-288.177
$C_6H_{14}O - C_3H_7OH$	0.059	0.019	-0.097019	50.466	0.027233	-19.191

* Δy - in [4] – mean absolute deviation between calculated and experimental mole fractions in **vapour phase**. Δx - mean absolute deviation in mole fractions in **liquid phase**.

Table D-3. Validity region of binary coefficients k_{ij} and k_{ji} (experimental & simulated VLE data)

Components	T, K	P, atm
$C_3H_6 - H_2O$	310-410	2.5-318
$C_3H_6 - C_6H_{14}O$	273-478	1-44
$C_3H_6 - C_3H_7OH$	283-393	1-9
$C_3H_7OH - H_2O$	355-573	1-120
$C_6H_{14}O - H_2O$	341-393	1
$C_6H_{14}O - C_3H_7OH$	341-355	1

The experimental VLE data were available for four out of six pairs of components. For the pairs 2-propanol-propene and diisopropyl ether-propene the VLE data were simulated using the group contribution method UNIQUAC implemented in the

engineering simulation package "HYSYS". A similar approach was used in [4] and was proved to be reasonably accurate.

In this study the UNIQUAC generated VLE data have also been used to extend the temperature-pressure validity region of the binary coefficients. For example, in the case of ether-alcohol pair the experimental data presented in [5,6] were obtained at 1 atmosphere and in the temperature range between 66 and 80°C. UNIQUAC produces VLE data in reasonable agreement with experiment (see Figure D-1). The total error defined as mean absolute deviation between experimental and simulated data

$$err = \frac{\sum \left| x_{i,exp} - x_{i,calc} \right|}{N_{exp}}$$ was 1.7 in molar percent.
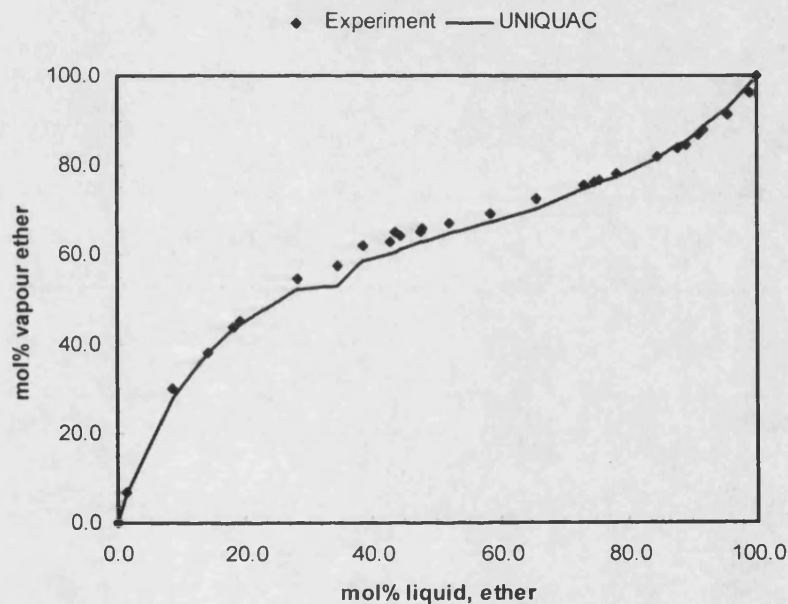
Figure D-1. Comparison of experimental and simulated VLE data for 2-propanol-diisopropyl ether mixture. Experimental data from [6].

Such a good agreement between the experimental and simulated data permitted to use UNIQUAC to generate data over a broader range of temperatures and pressures. The binary coefficients were calculated on the basis of purely experimental data and the combined set of data containing both the experimental and the simulated VLE data.

In order to obtain binary coefficients experimental data were fitted by PRSV EOS equation. Non-linear regression algorithm must be employed to solve this problem. Alternatively, a random value method (simplified analogue of the Monte-Carlo method) can be used. The advantage of the latter method of optimisation is that random value method will always find global optimum regardless of the nature of a function and

number of variables. A multi-step optimisation algorithm was designed and applied in order to improve the performance of the method.

In this algorithm, calculation of mean value of successful trials is performed until deviation between mean values did not exceed 0.5% in the two successive iterations. This condition allows automatic search in the area around the best value of previous iteration until no further improvement achieved.

The values of binary interaction parameters obtained in this study significantly differ from those reported in [4]. These differences may have originated from using the different sets of experimental data as well as using different numerical algorithms. In the case of propene-2-propanol pair, the VLE data were generated by UNIFAC method. It is possible that the data generated in this work and that used in [4] are very different. It was also found in this work that when the binary coefficients reported in the literature were used to fit the experimental VLE, the total error was much bigger than the reported figure. For example, for the pair 2-propanol-water the reported mean error of calculating vapour-phase mole fractions was 0.009, whereas in the program used in this work the same data produced error 0.026. Because binary coefficients bear no physical meaning, it is impossible to cross check the value of these parameters. Therefore, the decision on which set of data to use for further calculations may only be based on the quality of fit. The results of fitting of the experimental and simulated VLE data with the set of binary coefficients generated in this work are presented in Figures 1-7.
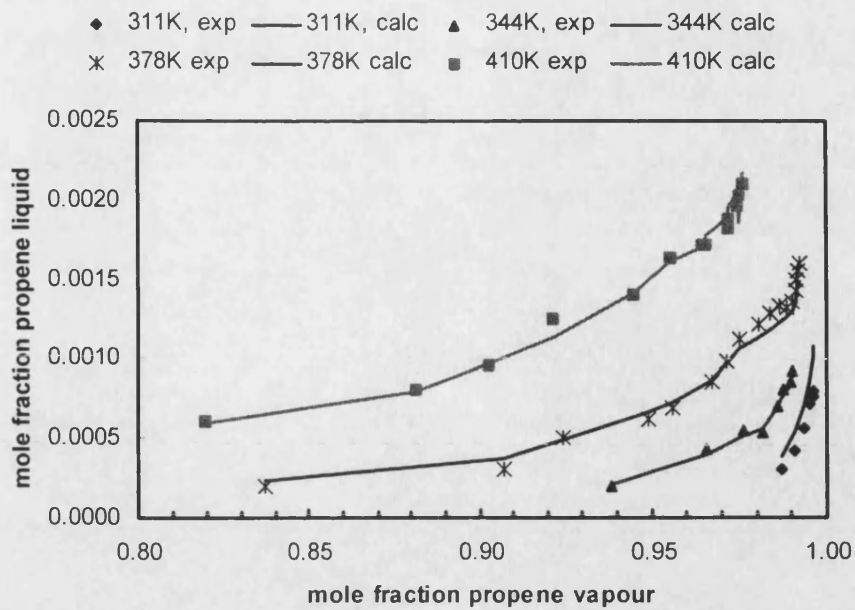
Figure D-2. Propene-water VLE fit by PRSV EOS with binary coefficients given in Table D-2. Experimental data from [7].
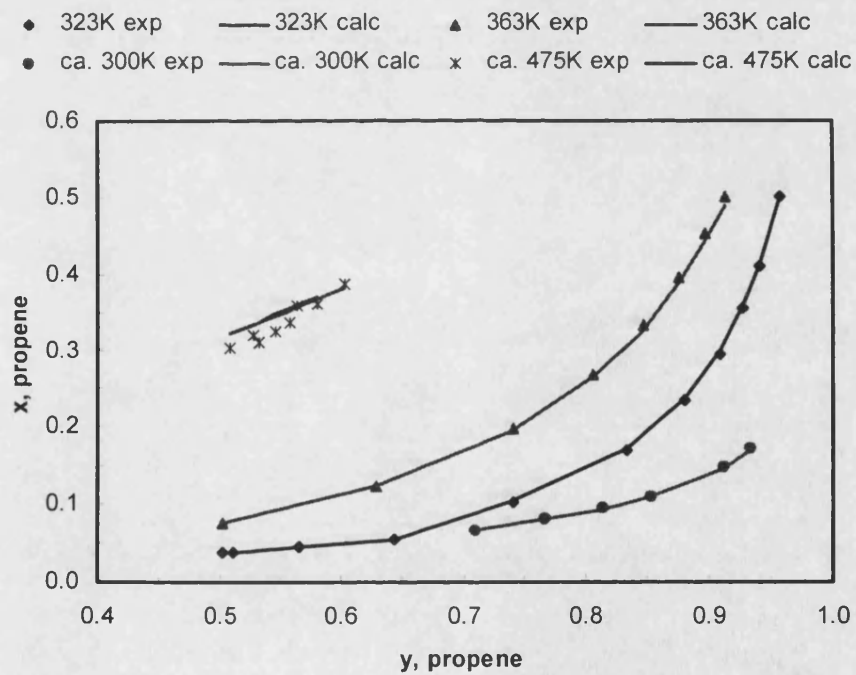

Figure D-3. Propene-diisopropyl ether VLE fit by PRSV EOS with binary coefficients given in Table D-2. "Experimental" data estimated using UNIFAC method in "HYSYS" engineering package.
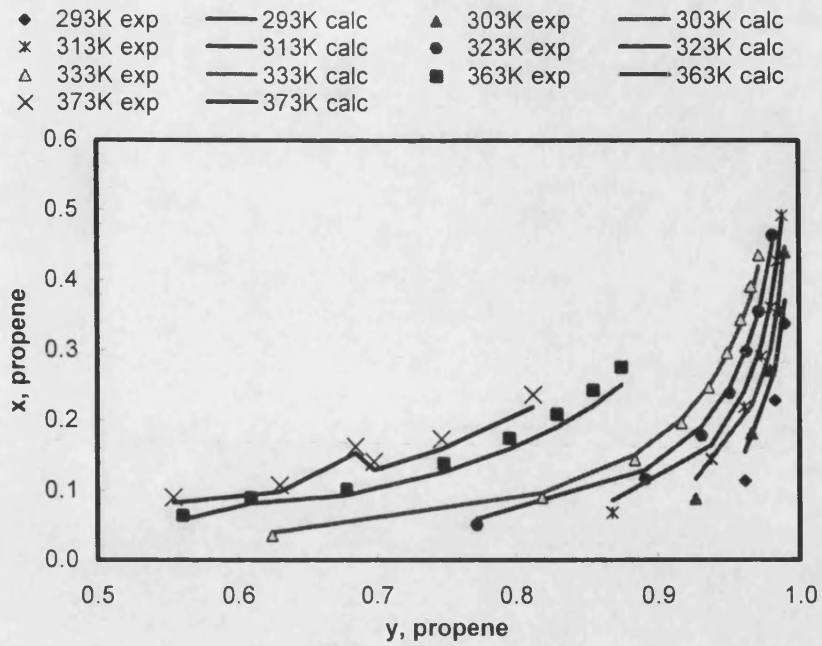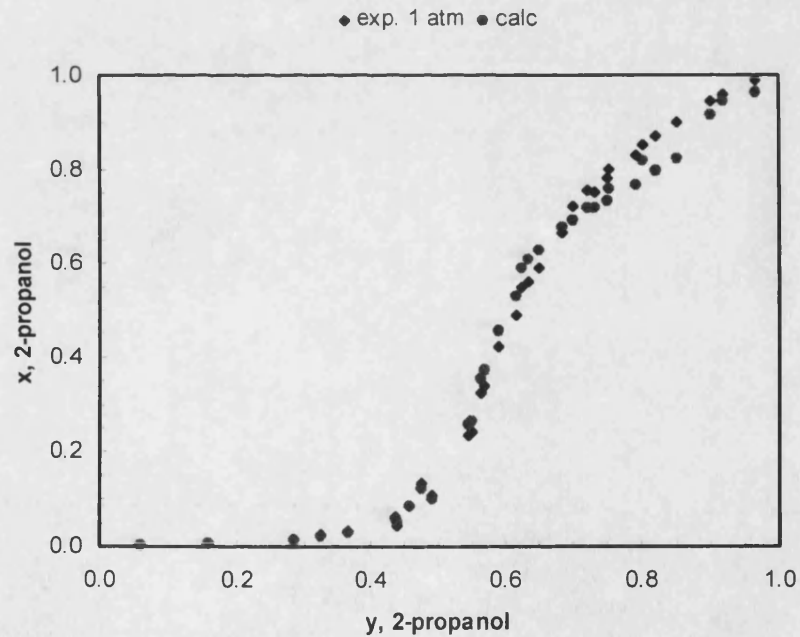
Figure D-4. Propene-2-propanol VLE fit by PRSV EOS with binary coefficients given in Table D-2. "Experimental" data estimated using UNIFAC method in "HYSYS" engineering package.

Figure D-5. 2-propanol-water VLE fit by PRSV EOS with binary coefficients given in Table D-2. Experimental data from [8].
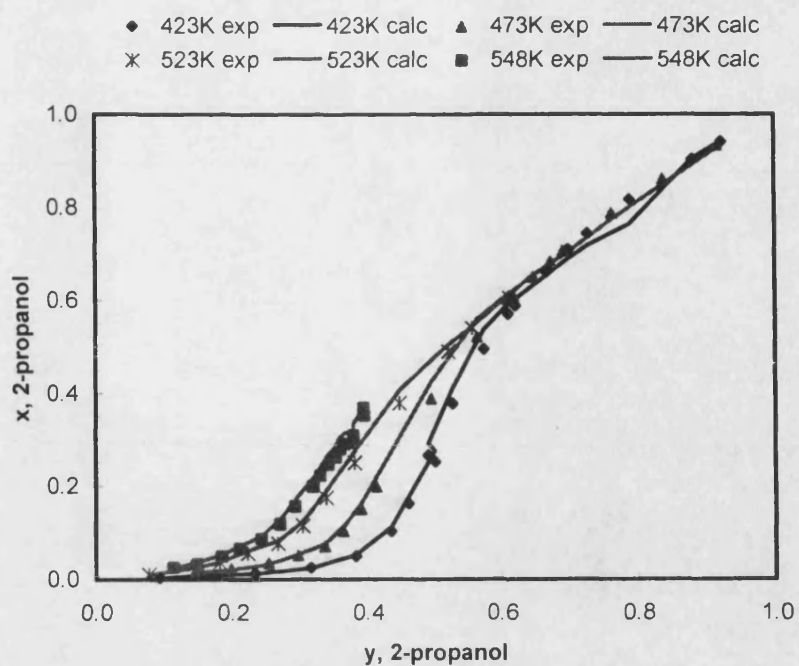
Figure D-6. 2-propanol-water VLE fit by PRSV EOS with binary coefficients given in Table D-2. Experimental data from [9, 10].
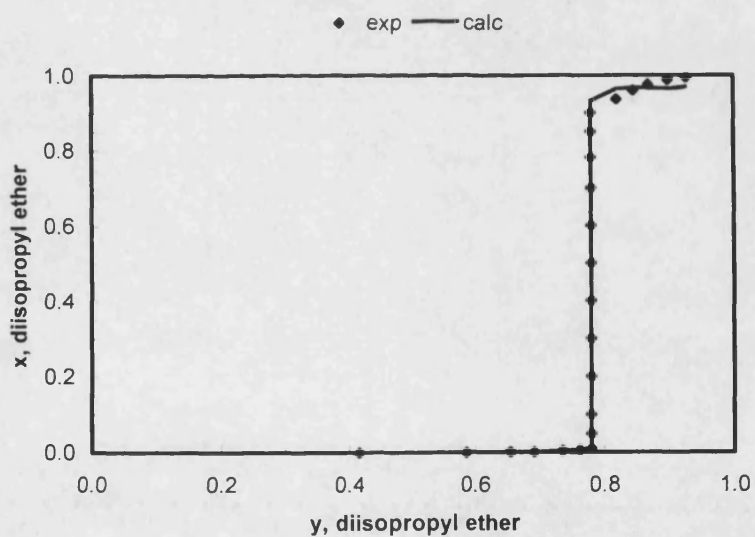

Figure D-7. Diisopropyl ether-water VLE fit by PRSV EOS with binary coefficients given in Table D-2. Experimental data from [8].
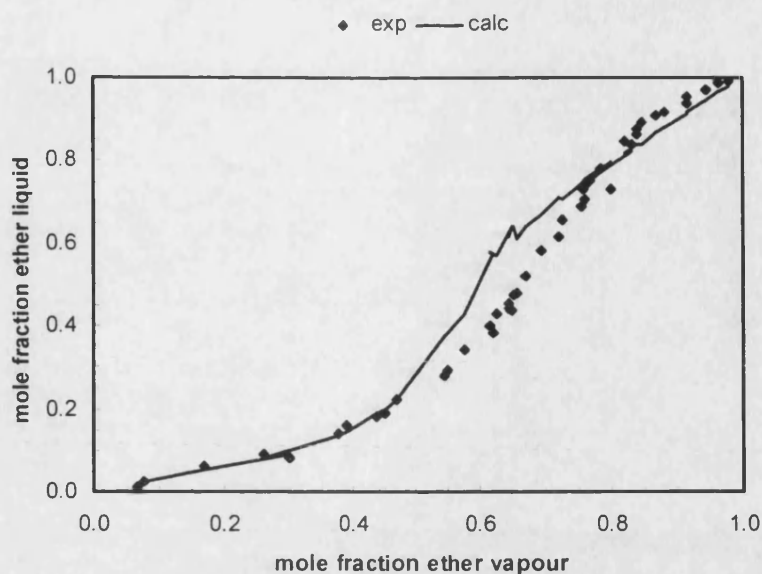
Figure D-8. Diisopropyl ether-2-propanol VLE fit by PRSV EOS with binary coefficients given in Table D-2. Experimental data from [11,8].

[1] W.R.Smith, R.W.Missen "Chemical reaction equilibrium analysis", John Wiley & Sons, 1982.

[2] J.M.Prausnitz, "Molecular thermodynamics of fluid-phase equilibria", Prentice-Hall, Inc., 1969.

[3] R.Stryjek, J.H.Vera, PRSV: An improved Peng-Robinson equation of state with new mixing rules for strongly nonideal mixtures, Can.J.Chem.Eng., 64 (1986) 334-340.

[4] A.Wyczesany, Nonstoichiometric algorithm of calculation of simultaneous chemical and phase equilibriua. 2. High-pressure hydration of propene to 2-propanol, Ind.Eng.Chem.Res., 33 (1994) 1971-1978.

[5] Masahiro Yorizane, S.Yoshimura, T.Yamamoto, Measurement of the ternary vapour-liquid equilibtium (isopropyl alcohol-water-isopropyl ether system), Kogato Kagato, 31 (1967) 451-457.

[6] H.C.Miller, H.Bliss, The system isopropyl ether – isopropanol, Ind.Eng.Chem., 32:1 (1940) 123-125.

[7] C.C.Li, J.J.McKetta, Vapor-liquid equilibrium in the propylene-water system, J.Chem.Eng.Data, 8:2 (1963) 271-275.

[8] Masahiro Yorizane, S.Yoshimura, T.Yamamoto, Measurement of the ternary vapour-liquid equilibtium (isopropyl alcohol-water-isopropyl ether system), Kogato Kagato, 31 (1967) 451-457.

[9] F.Barr-David, B.F.Dodge,J.Chem.Eng.Data, Vapor-liquid equilibrium at high pressures, The systems ethanol-water and 2-propanol-water, 4:2 (1959) 107-121.

[10] B.Khalfaoui, A.H.Meniai, R.Borja, Thermodynamic properties of water + normal alcohols and vapour-liquid equilibria for binary systems of methanol or 2-propanol with water, Fluid Phase Equilibria 127 (1997) 181-190.

[11] H.C.Miller, H.Bliss, The system isopropyl ether – isopropanol, Ind.Eng.Chem., 32:1 (1940) 123-125.